March 2019

Regeneration of Trace Metals During Phytoplankton Decay: An Experimental Study

Adrienne P. Hollister
University of South Florida, hollister@mail.usf.edu

Regeneration of Trace Metals During Phytoplankton Decay:

An Experimental Study

by

Adrienne P. Hollister

A thesis submitted in partial fulfillment
of the requirements for the degree of
Master of Science
College of Marine Science
University of South Florida

Major Professor: Kristen N. Buck, Ph.D.
Mya Breitbart, Ph.D.
Tim Conway, Ph.D.
Katherine Hubbard, Ph.D.

Date of Approval:
March 5, 2019

Keywords: trace metal biogeochemistry, Gulf of Mexico, West Florida Shelf, *Karenia brevis*, *Pseudo-nitzschia dolorosa*, macronutrients

DEDICATION

Mom, Dad, and Luke

ACKNOWLEDGEMENTS

This research was funded by grants from the National Science Foundation Division of Ocean Sciences OCE-1443483 and OCE-1756433, the Florida Institute of Oceanography (FIO) for state funded ship time, the Wells Fargo Fellowship in Marine Science, and the Carl Riggs Fellowship in Marine Science. Thank you to Dr. Celia Villac for her generous help with phytoplankton identification and interpretation, and especially her assistance with Figure 2.1. I would also like to thank the following individuals for assistance with laboratory analyses: Ethan Goddard for POC and PON analysis, Dr. Anthony Greco for SEM operation, Jenifer Cannizzaro for assistance with and use of the fluorometer, Joseph Donnelly for assistance with the environmental incubation chamber, Shannon Burns for seaFAST method development and assistance, Drs. Salvatore Caprara and Kelly Diester for ICP-MS operation and assistance, William Abbott for his training on the use of the Lachat, and Kady Palmer for her assistance with the Berger Leaches. For help with field sampling, I would like to thank the crew of the R/V *Weatherbird II*, the R/V *W. T. Hogarth*, Dr. Brad Seibel and the University of South Florida (USF) OCE 6934 Pelagic Ecology class, and Dr. Chris Stallings and the USF Fish Ecology Lab for assistance in seawater collection. Finally, thank you to my lab mates Shannon Burns, Gabriel Browning, Travis Mellett, and Chelsea Chase for all your support and friendship.

TABLE OF CONTENTS

LIST OF TABLES

LIST OF FIGURES

ABSTRACT

Trace metals act as important nutrients, and sometimes toxins, to phytoplankton and other marine microorganisms. When phytoplankton decay, the elements in their cells are released back into the water column through regeneration (also referred to as remineralization), one of the processes responsible for governing concentrations of dissolved trace metals and macronutrients in depth profiles. In order to experimentally study regeneration, controlled experimental incubations of mixed phytoplankton assemblages from the Gulf of Mexico (GoM) and monocultures of the diatom *Pseudo-nitzschia dolorosa* and the dinoflagellate *Karenia brevis* were placed in the dark and monitored as they decayed with naturally present bacteria. Over six months, samples were collected and analyzed for dissolved trace metals (Mn, Fe, Co, Ni, Cu, Zn, Cd, and Pb), macronutrients (phosphate, silicate, nitrate + nitrite ("N+N"), nitrite, and ammonium), chlorophyll *a* (Chl *a*), and particulate organic carbon and nitrogen (POC and PON) concentrations. In experiments with diatoms present (*P. dolorosa* and mixed assemblages), phosphate and silicate remained closely coupled during regeneration, and no delay in silicate regeneration was observed. Cadmium (Cd) regeneration mirrored that of phosphate, consistent with the nutrient-type distributions of Cd commonly observed in the global oceans. Zn (Zn) followed a similar trend, but was less tightly coupled with any of the macronutrients. Dissolved manganese (Mn), on the other hand, was briefly released at the onset of regeneration but was then drawn down through the remainder of the experiments, which was attributed to the formation of Mn-oxides. Of the other trace elements studied, lead (Pb) and iron (Fe) showed the

most evidence of scavenging to Mn oxides during the regeneration, and a delayed increase in Fe was observed by the end of most of the experiments after Mn stabilized. In M2 and M3, copper (Cu) also followed a similar delayed increase to Fe, but was less pronounced. Cobalt (Co) and nickel (Ni) did not display clear evidence of scavenging to Mn-oxides, and in one of the mixed assemblages (M1), followed a more nutrient-like uptake and regeneration. For the rest of the experiments, Cu, Co, and Ni exhibited more conservative behavior (i.e., little change relative to the overall reservoir), though any biological uptake observed in the grow-out phase was generally returned to the dissolved fraction in the regeneration experiments. The results of these experiments fill an important gap in understanding the important role of regeneration in trace metal cycling and can ultimately be applied to understanding vertical distributions in ocean water columns.

CHAPTER ONE:

INTRODUCTION

Trace metals play a fundamental role in controlling the growth of phytoplankton and other marine organisms, serving as essential nutrients and sometimes toxins. In addition to the macronutrients carbon (C), nitrogen (N), phosphorous (P), and, for diatoms, silicon (Si), a suite of trace metals are also incorporated into cells (Fig. 1.1) and/or scavenged to surfaces. The trace metals of interest in this thesis include manganese (Mn), iron (Fe), cobalt (Co), nickel (Ni), copper (Cu), zinc (Zn), cadmium (Cd), and lead (Pb) (Huntsman and Sunda 1980; Brand et al. 1983; Sunda 1989; Bruland et al. 1991; Coale 1991; Morel et al. 1991; Ho et al. 2003; Morel and Price 2003; Sunda 2012). With the exception of Pb, which has no known nutritive properties, these elements serve roles as important micronutrients and are present in relative cellular abundance of approximately Fe≈Zn>Mn≈Ni≈Cu>Co≈Cd (Twining and Baines 2013).

Iron (Fe) is essential to all life and is arguably the most important trace metal due to its role in limiting primary productivity in oceans worldwide (Martin et al. 1987; Martin and Fitzwater 1988; Martin et al. 1989; Martin et al. 1990; Martin et al. 1991; Hutchins 1995; Coale et al. 1996; Behrenfeld and Kolber 1999; Hutchins et al. 2002; Moore et al. 2002; Tsuda et al. 2003; Coale et al. 2004; Ussher et al. 2004; Jickells et al. 2005; Boyd et al. 2007; Boyd and Ellwood 2010; Schoffman et al. 2016; Tagliabue et al. 2017). As a result, Fe may have even played a role in amplifying glacial-interglacial periods (Martin 1990; Martínez-Garcia et al.

2011). Owing to its ability to switch between redox states and participate in electron-transport chains, Fe is utilized in a variety of cellular processes including photosynthesis, respiration, nitrogen assimilation, denitrification, and detoxification of oxygen radicals (Huntsman and Sunda 1980; Sunda 1989; Raven et al. 1999; Morel and Price 2003; Sunda 2012). In addition to being required by phytoplankton, Fe is also utilized by heterotrophic bacteria, driving a process known as the "microbial ferrous wheel" (Kirchman 1996), and this recycling provides an important source of dissolved Fe to other microorganisms (Hutchins et al. 1993). Interestingly, even though Fe and N are closely coupled in phytoplankton physiology, the ferricline does not always follow the nitrocline (Johnson et al. 1997; Boyd et al. 2017). It remains unknown whether this decoupling is due to the low solubility of Fe(III) in seawater and Fe-scavenging, or to the differential timing of regeneration.

Dissolved Fe concentrations are influenced by a variety of processes including biogenic uptake, deposition of sediment and dust, precipitation as Fe-(oxyhydr)oxides, and particle scavenging (Duce and Tindale 1991; Johnson et al. 1997; Elrod et al. 2004; Moore and Braucher 2008; Bowie et al. 2009; Boyd and Ellwood 2010; Conway and John 2014; Hatta et al. 2015; Tagliabue et al. 2017). Although Fe is highly abundant on earth, it is poorly soluble in seawater in its stable Fe(III) oxidized state (Kuma et al. 1996; Liu and Millero 2002). Thus, dissolved Fe in large portions of the surface ocean is often present in low, growth-limiting concentrations in otherwise nutrient-rich regions of upwelling. These so-called "High Nutrient-Low Chlorophyll" (HNLC) zones occur in ~40% of the global surface ocean (Moore et al. 2002), making Fe a critical driver of the phytoplankton community, global biogeochemical cycles, and climate.

Importantly, dissolved Fe is extensively complexed by strong organic ligands (>99.9%), which can serve to increase solubility and bioavailability (Gledhill and van den Berg 1994; Rue

and Bruland 1995; Kuma et al. 1996; Rue and Bruland 1997; Hutchins et al. 1999; Maldonado and Price 1999; Chen et al. 2004; Buck and Bruland 2007; Vraspir and Butler 2009; Gledhill and Buck 2012). Furthermore, ligand production in response to Fe limitation has been observed in incubation experiments (Rue and Bruland 1997; Buck et al. 2010; King et al. 2012; Mellett et al. 2017), providing support to the importance of organic ligands in Fe acquisition by organisms.

Zinc (Zn) displays a nutrient-type profile (Bruland 1980; Bruland and Franks 1983; Bruland et al. 1994; Ellwood and Van den Berg 2000). Notably however, Zn is more closely coupled with silicate than with phosphate in the water column (Croot et al. 2011; Wyatt et al. 2014), despite the lack of Zn present in opal (Ellwood and Hunter 2000). It remains unclear whether this so-called "Zn-paradox" is the result of cellular incorporation and regeneration of these elements, ocean circulation patterns in the Southern Ocean (Vance et al. 2017), or scavenging (John and Conway 2014).

Zinc (Zn) is an essential micronutrient utilized in a variety of enzymes (Sinoir et al. 2012), including carbonic anhydrase (Badger and Price 1994) and alkaline phosphatase (Plocke et al. 1962). Additionally, Zn can substitute for Co requirements in some phytoplankton (Sunda and Huntsman 1995a; Jakuba et al. 2008). Like Cd and Cu, Zn is toxic at high enough concentrations and can stimulate phytochelatin production (Stauber and Florence 1990; Ahner and Morel 1995; Dupont and Ahner 2005). However, toxic levels are not generally present in the open ocean, and Zn can also serve to decrease the toxicity of other metals such as Cu (Ahner et al. 1997) or Cd (Ahner et al. 1998). Finally, dissolved Zn is dominated by organic ligand-complexes (>97 – 98%) (Bruland 1989; Ellwood and Van den Berg 2000), although the function of these ligands also remains unclear, and they may result from phytoplankton degradation (Ellwood and Van den Berg 2000).

Manganese (Mn) is widely utilized in photosynthesis (Raven et al. 1999) and in superoxide dismutases (SODs) (Peers and Price 2004; Wolfe‑Simon et al. 2005; Wolfe-Simon et al. 2006). These SODs serve to protect against oxygen radicals produced during photosynthesis and other metabolic processes, and can incorporate either Fe, Mn, Cu and Zn, or Ni as a metal cofactor. As a result of shared functionality in these SODs, Mn may co-limit phytoplankton growth with Fe (Peers and Price 2004). Additionally, Mn is utilized by Mn-oxidizing bacteria at depth and precipitates as insoluble Mn-oxides (Tebo et al. 1984; Sunda and Huntsman 1987; Sunda and Huntsman 1988; Sunda and Huntsman 1990; Tebo et al. 2004). In surface waters, Mn-oxidizing bacteria are photoinhibited (Sunda and Huntsman 1988), and Mn-oxides can undergo photoreduction (Sunda and Huntsman 1994). This combination of surface uptake, regeneration, and redox chemistry results in a profile that generally decreases with depth but may have subsurface maxima (Landing and Bruland 1987; Jickells and Burton 1988; Bruland et al. 1994; Sunda 2012; Hatta et al. 2015).

Nickel (Ni), Zn, and Cd generally display the most classic nutrient-type profiles of the trace metals in the water column. Like nitrate, phosphate, and silicate, these elements generally exhibit the lowest concentrations at the surface and increase at depth (Sclater et al. 1976; Bruland et al. 1978; Bruland 1980; Bruland and Franks 1983; Jickells and Burton 1988; Bruland et al. 1991; Bruland et al. 1994; de Baar et al. 1994), although Ni is not always fully utilized in surface waters (Sclater et al. 1976; Bruland 1980; Bruland and Franks 1983; Bruland et al. 1991). Nickel (Ni) is utilized by urease and may co-limit phytoplankton growth with nitrogen (Price and Morel 1991). Additionally, Ni can serve as a cofactor in some SODs (Dupont et al. 2008a; Dupont et al. 2008b). Dissolved Ni can also be scavenged to Mn-oxides (Balistrieri and Murray 1986; Tani et al. 2004), and a previous dark incubation experiment showed coupling between the two

elements, which was attributed to possible scavenging or incorporation into Mn-SODs (Mellett et al. 2017).

Copper (Cu) displays a "hybrid-type" water column profile and is influenced by both scavenging and biogenic processes (Bruland 1980; Bruland and Franks 1983; Jickells and Burton 1988; Sunda and Huntsman 1995b). In some cases, Cu and Fe may co-limit phytoplankton growth (Peers et al. 2005; Annett et al. 2008; Semeniuk et al. 2009). Additionally, a diatom species in an Fe-limited region was shown to utilize the Cu-containing enzyme plastocyanin instead of the more common Fe-containing cytochrome for photosynthesis (Peers and Price 2006). However, Cu can also be toxic (Brand et al. 1986). In response, a variety of phytoplankton have developed adaptations to protect against toxicity, including the production of phytochelatins, metal-binding organic ligands that regulate toxicity of Cu and other potentially toxic metals (Ahner and Morel 1995; Ahner et al. 1997; Ahner et al. 1998; Ahner and Wei 2005; Dupont and Ahner 2005). In fact, dissolved Cu is also extensively complexed (>99%) by strong organic ligands in global oceans (Coale and Bruland 1990; Moffett 1995; Moffett and Dupont 2007; Buck et al. 2010; Buck et al. 2012; Bundy et al. 2013), although the role of this ligand pool is not fully understood.

Cobalt (Co) is widely known to be coupled with Mn in the water column (Knauer et al. 1982; Jickells and Burton 1988; Sunda 2012) as a result of scavenging to Mn-oxides (Tebo et al. 1984; Balistrieri and Murray 1986; Johnson et al. 1988; Lee and Fisher 1993; Tani et al. 2004; Hawco et al. 2018) and/or co-oxidation of Co and Mn by a shared microbial pathway (Moffett and Ho 1996). Additionally, Co sometimes displays a minimum at the oxygen minimum zone (OMZ) in ocean water columns (Noble et al. 2012; Hawco et al. 2016), which is attributed partly to suppression of Mn-oxide formation and subsequent Co scavenging (Hawco et al. 2016).

Cobalt (Co) may also co-limit growth with Fe (Saito et al. 2005; Browning et al. 2017; Browning et al. 2018) or Zn (Saito and Goepfert 2008). Cobalt (Co) and Zn may substitute for each other in some enzymes (e.g. carbonic anhydrase) in eukaryotic phytoplankton (Price and Morel 1990; Sunda and Huntsman 1995a; Yee and Morel 1996; Lane and Morel 2000b; Saito and Goepfert 2008), although cyanobacteria have been shown to have an obligate Co requirement (Sunda and Huntsman 1995a; Saito et al. 2002). Importantly, cobalt serves as a cofactor for vitamin B_{12}, a micronutrient known to be important for controlling marine primary productivity (Menzel and Spaeth 1962), which is acquired by a wide variety of eukaryotic phytoplankton through a symbiotic relationship with bacteria (Croft et al. 2005). Finally, Co is also extensively complexed by organic ligands (Ellwood and Van den Berg 2001; Saito and Moffett 2001; Saito et al. 2005; Bown et al. 2012). Although the structure of these ligands remains largely unknown, studies show that at least some may be synthesized by cyanobacteria and increase Co bioavailability in some specialized cells (Saito et al. 2005; Bown et al. 2012).

Cadmium (Cd) also displays a nutrient-type profile similar to phosphate (Bruland et al. 1978; Bruland et al. 1994; de Baar et al. 1994) and can be incorporated into carbonic anhydrases (Park et al. 2007; Xu et al. 2008; Xu and Morel 2013). Moreover, Cd and Zn may sometimes substitute for each other in diatoms (Price and Morel 1990; Xu et al. 2008; Xu and Morel 2013) and may co-limit phytoplankton growth (Lane and Morel 2000a). However, given the relatively limited biological roles of Cd, non-specific uptake may also explain its nutrient-like distribution (Horner et al. 2013). Cd can also be toxic for phytoplankton (Brand et al. 1986), although concentrations in the open ocean are generally below toxic levels. As a buffer against toxicity, phytoplankton can produce phytochelatins in response to elevated Cd (Ahner and Morel 1995; Ahner et al. 1998; Ahner and Wei 2005; Dupont and Ahner 2005; Xu and Morel 2013). Thus, Cd

is susceptible to organic ligand complexation: ~67% in North Pacific surface waters (Bruland 1992), 86 – 96% in the South Atlantic Sub-Antarctic zone (SAZ) (Baars et al. 2014), 87 – 99% in the East Pacific SAZ (Ellwood 2004), and 45 – 75% in the Southern Ocean (Baars et al. 2014).

Unlike the other trace metals discussed, Pb has no known nutritive properties and is commonly used a tracer for anthropogenic inputs such as gasoline emissions (Wu and Boyle 1997a; Boyle et al. 2014). Early studies noted a disequilibrium between ^{210}Pb and its parent radionuclide ^{226}Ra in the ocean water column, indicating a scavenging process influencing dissolved Pb concentrations (Craig et al. 1973; Krishnaswami et al. 1975; Bacon et al. 1976; Somayajulu and Craig 1976). The scavenged-type profile of Pb has now been well-documented across ocean basins: Pb is deposited at the ocean surface, and dissolved concentrations then decrease with depth due to particle scavenging (Nozaki et al. 1980; Chung et al. 1983; Chung and Craig 1983; Boyle et al. 2014). Particles which scavenge Pb may be organic (e.g. phytoplankton and fecal pellets from grazers) (Fisher et al. 1983; Fisher et al. 1987; Moore and Dymondt 1988) or inorganic (e.g. Mn or Fe oxides) (Takahashi et al. 2007). Thus, even though Pb is not expected to be biologically utilized by phytoplankton, it provides a representative abiotic analog for scavenging-type behavior.

Historically, trace metals have been difficult to quantify as a result of exceedingly low concentrations in seawater and the propensity for contamination. Some of the earliest efforts to quantify trace metal distributions in global oceans were with the GEOSECS program in the 1970s (Spencer et al. 1970; Brewer et al. 1972). Improvements in trace metal clean sampling and techniques enabled increasingly more accurate quantification of the concentrations of these elements in seawater across ocean basins (Bruland 1980; Boyle et al. 1981; Bruland and Franks

1983). In 2007, global trace metal data collection was standardized through the GEOTRACES program, an international collaboration with the goal of quantifying trace metal and isotope (TEI) distributions in global oceans (Henderson et al. 2007).

More recently, trace metal preconcentration on a chelating column coupled with Inductively Coupled Plasma Mass Spectrometry (ICP-MS) has allowed for faster quantification of trace metals at nano- to picomolar concentrations (Sohrin et al. 2008; Milne et al. 2010; Lee et al. 2011; Sohrin and Bruland 2011; Biller and Bruland 2012; Lagerström et al. 2013; Rapp et al. 2017). In the research conducted for this thesis, dissolved trace metals were preconcentrated by adapting previous methods (Biller and Bruland 2012) to an automated seaFAST system (Lagerström et al. 2013), quantified on an ICP-MS, and assessed for accuracy and precision using GEOTRACES intercalibration standards (Sohrin et al. 2008).

Acquisition of trace metals and macronutrients by phytoplankton, followed by regeneration from sinking cells, are major drivers of their concentrations in ocean water columns. In the euphotic zone, phytoplankton and other organisms utilize trace metals and macronutrients, which are then released as organic matter sinks and decays at depth, a process mediated in part by bacteria and grazers (Caron et al. 1988; Hutchins et al. 1993; Hutchins and Bruland 1994; Lee and Fisher 1994; Bidle and Azam 1999; Barbeau et al. 2001; Strzepek et al. 2005; Sato et al. 2007; Sarthou et al. 2008; Burkhardt et al. 2014), as well as viruses (Poorvin et al. 2004).

Macronutrient regeneration has been well studied. Early laboratory regeneration experiments of decaying phytoplankton established the progression of particulate organic nitrogen to ammonium, nitrite, and nitrate (Von Brand et al. 1937; Von Brand et al. 1939; Von Brand and Rakestraw 1941; Von Brand et al. 1942; Grill 1964; Kamatani 1969; Garber 1984),

demonstrating a process that occurs naturally in the water column as phytoplankton sink and decay at depth. (Fig. 1.2). A classic nutrient-type water column depth profile for phosphate, nitrate, or silicate shows depletion at the surface followed by an increase at depth and has been well-documented (e.g., Sverdrup et al. 1942; Sunda 2012) (Fig. 1.3a – c). Silicate generally displays the deepest maximum, which has been attributed to slower regeneration of silicate diatom frustules due to a protective organic coating (Bidle and Azam 1999). However, diatom frustule dissolution can also be influenced by a variety of other factors, including temperature (Hurd 1972; Kamatani 1982), saturation state (Hurd 1972; Rickert et al. 2002), turbulence (Hurd 1972), surface area (Hurd 1972; Dixit et al. 2001; Van Cappellen et al. 2002), incorporation of aluminum (Al) into the frustules (Gehlen et al. 2002; Van Cappellen et al. 2002), trace metal limitation during growth (Boutorh et al. 2016), and the presence of grazers (Hurd 1972; Schultes et al. 2010). Additionally, entrainment of deep water from the Southern Ocean also plays a role in elevating silicate at depth, further complicating the observed distributions (Sarmiento et al. 2004).

Trace metal regeneration is more complex. Water column profiles for the trace metals (Mn, Fe, Co, Ni, Cu, Zn, Cd, and Pb) are influenced by a combination of abiotic and biotic factors and often deviate from those of macronutrients (Fig. 1.2d – h) (Johnson et al. 1997; Twining et al. 2014; Boyd et al. 2017). Because trace metals are essential for life, they are influenced by cellular uptake and subsequent regeneration of sinking particles (Twining et al. 2014; Boyd et al. 2017). Additional abiotic factors include physical mixing and upwelling, particle scavenging (Balistrieri and Murray 1986; Fowler and Knauer 1986; Bruland et al. 1994; Jannasch et al. 1996), and/or precipitation as Mn-oxides (Tebo et al. 1984; Sunda and Huntsman

1987; Sunda and Huntsman 1988; Sunda and Huntsman 1990; Bruland et al. 1994; Tebo et al. 2004) or Fe-(oxyhydr)oxides (Liu and Millero 2002; Tang and Morel 2006; Yoshida et al. 2006; Boyd and Ellwood 2010; Tagliabue et al. 2017). Additionally, Fe, Cu, Zn, Cd, and Co are predominantly chelated by organic ligands (Bruland 1989; Coale and Bruland 1990; Bruland 1992; Gledhill and van den Berg 1994; Rue and Bruland 1995; Kuma et al. 1996; Rue and Bruland 1997; Ellwood and Van den Berg 2000; Ellwood and Van den Berg 2001; Morel and Price 2003; Chen et al. 2004; Buck and Bruland 2005; Saito et al. 2005; Boyd and Ellwood 2010; Buck et al. 2012; Gledhill and Buck 2012; Bundy et al. 2013), and such ligands can either increase bioavailability (e.g. Fe siderophores) or decrease it (e.g. phytochelatins for Cu, Zn, or Cd).

The goal of this thesis research was to experimentally study the regeneration of trace metals and macronutrients from decaying phytoplankton blooms in the laboratory. The research conducted for this thesis was conducted on phytoplankton relevant to the Gulf of Mexico (GoM) by monitoring regeneration from (1) mixed phytoplankton assemblages collected from natural GoM waters and (2) monocultures of the diatom *Pseudo-nitzschia dolorosa* and the dinoflagellate *Karenia brevis*. Bloom conditions were induced in carboys, and these carboys were then placed in the dark in order to simulate regeneration conditions that naturally occur in the water column. Over the course of six months, samples were collected and analyzed for dissolved trace metal concentrations (Mn, Fe, Co, Ni, Cu, Zn, Cd, Pb), macronutrient concentrations (phosphate, silicate, nitrate + nitrite ["N+N"], nitrite, and ammonium)), chlorophyll *a* (Chl *a*), particulate organic carbon and nitrogen concentrations (POC and PON), and electron microscopy. This research is presented in Chapter 2.

Chapter 1 Figures

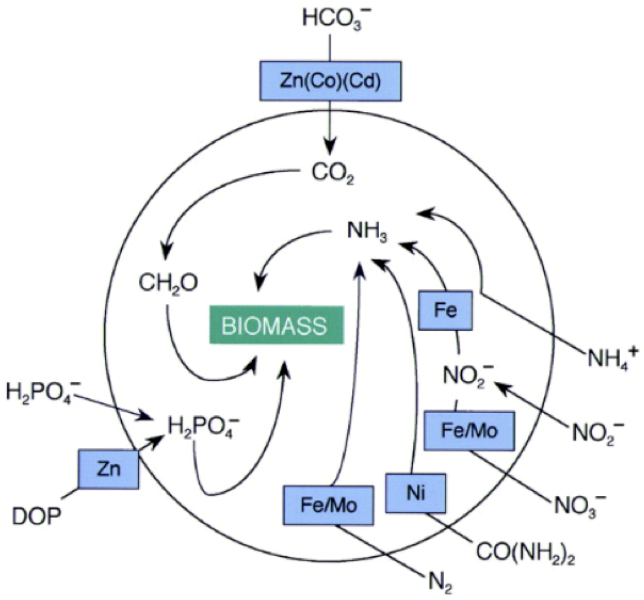

Fig. 1.1. Some of the biological functions of trace metals in phytoplankton. The roles of trace metals are discussed in more detail below. (Morel and Price 2003)

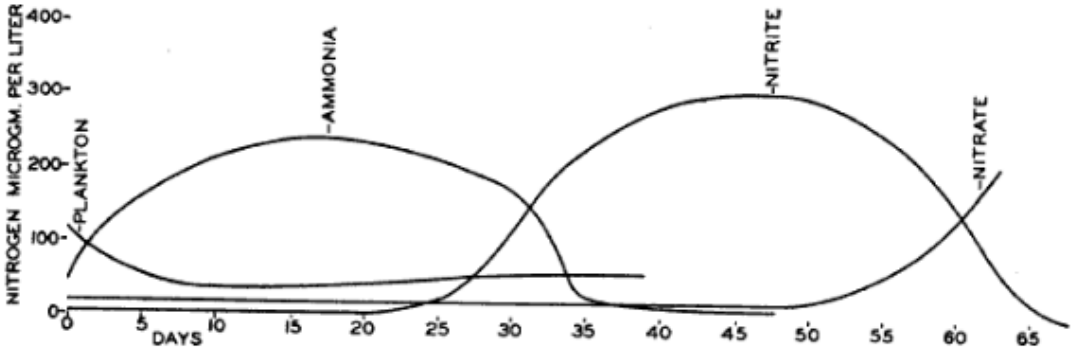

Fig. 1.2. Regeneration of nitrogen as ammonium, nitrite, and nitrate from phytoplankton assemblages. (Von Brand et al. 1937)

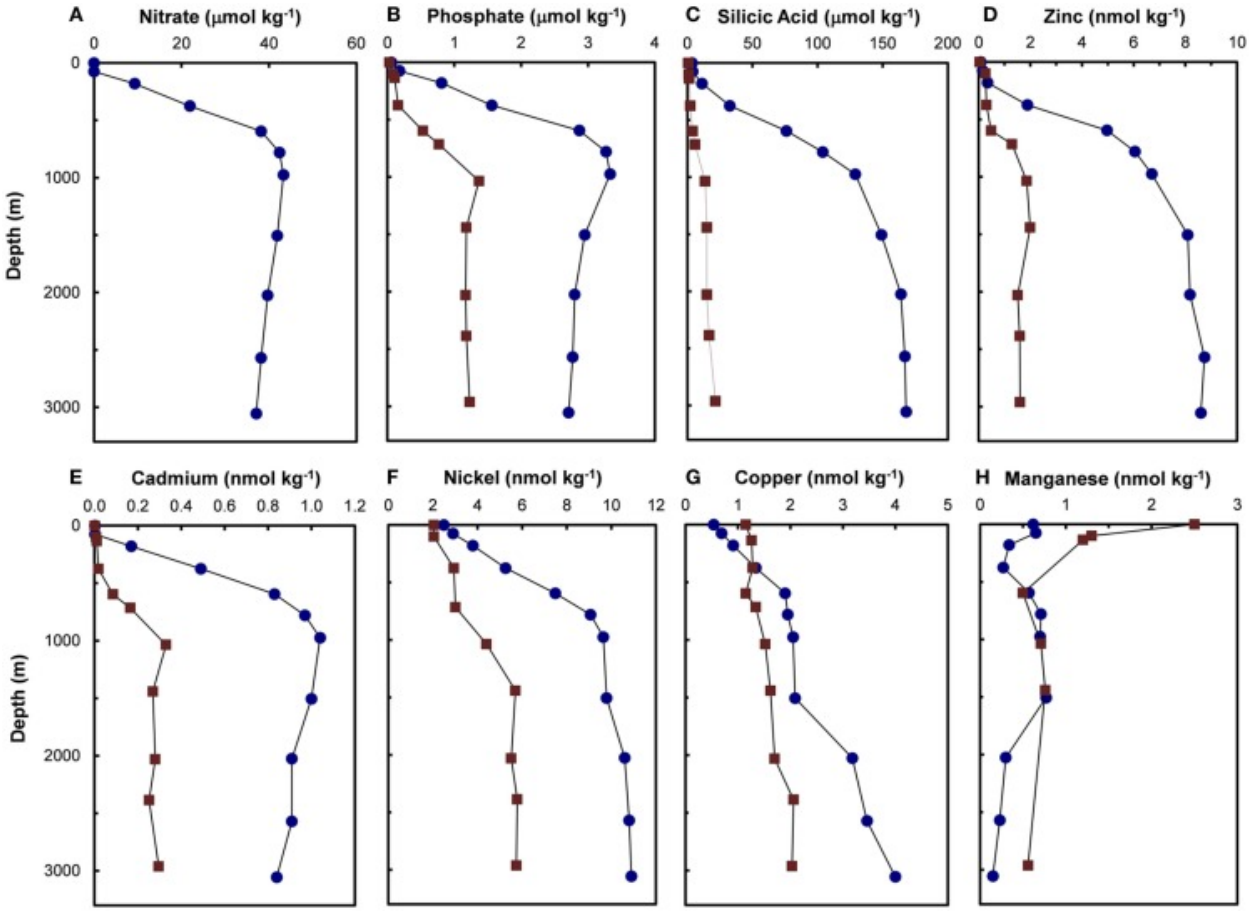

Fig. 1.3. Depth profiles for dissolved concentrations of nitrate (A), phosphate (B), and silicic acid (C), zinc (Zn; D), cadmium (Cd; E), nickel (Ni; f), copper (Cu; G), and manganese (Mn; H) in the North Pacific (blue circles) and North Atlantic (red squares). (Sunda 2012)

CHAPTER TWO:

REGENERATION OF TRACE METALS DURING PHYTOPLANKTON DECAY: AN EXPERIMENTAL STUDY

Adrienne P. Hollister[1,2], Katherine Hubbard[3], Maya Robert[3], Charles L. Tilney[3], Kristen N. Buck[1]

[1]University of South Florida, College of Marine Science, St. Petersburg, FL, USA

[2]hollister@mail.usf.edu

[3]Fish and Wildlife Research Institute, St. Petersburg, FL, USA

Keywords: biogeochemistry, diatom, dinoflagellate, Gulf of Mexico, *Karenia brevis*, macronutrients, phytoplankton, *Pseudo-nitzschia dolorosa*, regeneration, trace metals

Introduction

At the base of the marine food web, phytoplankton require the macronutrients carbon (C), nitrogen (N), and phosphorous (P) to build cellular organic matter, and, for diatoms, silicon (Si) to build cellular frustules (Redfield 1934; Brzezinski 1985). In addition, a suite of trace metals are also incorporated into cells and/or scavenged to cell surfaces, including manganese (Mn), iron (Fe), cobalt (Co), nickel (Ni), copper (Cu), zinc (Zn), cadmium (Cd), and lead (Pb) (Brand et al. 1983; Sunda 1989; Bruland et al. 1991; Morel and Price 2003; Sunda 2012). With the exception of Pb, these trace metals act as micronutrients, required for the function of various enzymes (Brand et al. 1986), and have been found in phytoplankton with a general relative cellular abundance in phytoplankton of Fe≈Zn>Mn≈Ni≈Cu>Co≈Cd (Twining and Baines 2013).

As macronutrients and many trace metals are essential for phytoplankton growth, phytoplankton and bacteria are major drivers in the vertical cycling of these elements. In the oceanic water column, trace metals and macronutrients are incorporated into phytoplankton in the euphotic zone, exported to depth and liberated from decaying cells via regeneration. This process, mediated in part by bacteria and grazers (Caron et al. 1988; Hutchins and Bruland 1994; Lee and Fisher 1994; Bidle and Azam 1999; Burkhardt et al. 2014), has been well documented for macronutrients (Martin et al. 1987; Anderson and Sarmiento 1994; Boyd and Trull 2007). However, the timing and speciation of the regeneration of trace metals remains poorly understood. In particular, despite their role as important micronutrients, depth profiles of essential trace metals often deviate from the classic nutrient-type profiles of macronutrients (Johnson et al. 1997; Twining et al. 2014; Boyd et al. 2017; Tagliabue et al. 2017), reflecting the complicated combination of abiotic and biotic factors that influence trace metal cycling in seawater.

In the oceans, Mn concentrations are controlled by a combination of biogenic uptake by phytoplankton, subsequent regeneration, and precipitation at depth by Mn-oxidizing bacteria (Tebo et al. 1984; Sunda and Huntsman 1987; Sunda and Huntsman 1988; Sunda and Huntsman 1990; Bruland et al. 1991; Tebo et al. 2004). Coupling between Mn and Co may occur as a result of either scavenging of Co to Mn-oxides or co-oxidation of these elements via a shared pathway (Tebo et al. 1984; Lee and Fisher 1993; Moffett and Ho 1996). The formation of Mn-oxides may also result in the scavenging of Ni and other bioactive trace metals (Balistrieri and Murray 1986; Tani et al. 2004; Mellett et al. 2017). Iron (Fe) plays a central role in controlling ocean primary productivity (Martin and Fitzwater 1988; Hutchins 1995; Coale et al. 1996; Coale et al. 2004; Boyd et al. 2007; Boyd et al. 2017). Iron (Fe) concentrations are influenced by a variety of processes including nutritive uptake, aeolian dust deposition, oxidation, and particle scavenging (Johnson et al. 1997; Tagliabue et al. 2017). Copper (Cu), which also has a hybrid-type profile in the oceans, is influenced by a combination of nutritive uptake and scavenging (Bruland 1980; Bruland and Franks 1983; Bruland et al. 1991). Lead (Pb) is deposited at the ocean surface and its water column profile is influenced primarily by particle scavenging (Fisher et al. 1983; Fisher et al. 1987; Moore and Dymondt 1988; Boyle et al. 2014). Nickel (Ni), Zn, and Cd, on the other hand, generally display the most classic nutrient-type profiles of the trace metals in the water column; these elements exhibit depletion at the surface and increased concentrations at depth (Sclater et al. 1976; Bruland et al. 1978; Bruland 1980; Bruland and Franks 1983; Bruland et al. 1991; Bruland et al. 1994; de Baar et al. 1994), although Ni is often not fully depleted in surface waters (Sclater et al. 1976; Bruland 1980; Bruland and Franks 1983; Bruland et al. 1991).

The aim of this study was to characterize the regeneration of both macronutrient and trace metal concentrations during phytoplankton decay. Using controlled incubation experiments,

dissolved macronutrients (phosphate, silicate, nitrate + nitrite ["N+N], nitrite, and ammonium) and trace metals (Mn, Fe, Co, Ni, Cu, Zn, Cd and Pb) were monitored over six months in darkness in order to observe the decay of blooms of natural (mixed) assemblages of phytoplankton from the Gulf of Mexico (GoM) and of monocultures of two GoM isolates: the diatom *Pseudo-nitzschia dolorosa* and the dinoflagellate *Karenia brevis*.

Methods

Incubation setup

Five regeneration experiments were performed. In order to induce phytoplankton death and observe the regeneration process that occurs naturally in oceanic water columns, all incubations were subjected to complete darkness for six months and monitored as they decayed. Three of these experiments were conducted with natural, mixed GoM phytoplankton assemblages (M1, M2, and M3), and two with monocultures of either the GoM-isolated phytoplankton species *Pseudo-nitzschia dolorosa* (P1) or *Karenia brevis* (K1) as described below.

Natural assemblages, M1

Gulf of Mexico (GoM) surface seawater was collected from the West Florida Shelf, ~33 km offshore (28°51'N, 83°11'W), on 7 September, 2016 from a small vessel. Seawater was collected by submersion-filling a 50 L polypropylene (PP) carboy that had been acid-cleaned with 10% trace metal grade (TMG) hydrochloric acid (HCl; Fisher), rinsed with Milli-Q water (> 18.2 MΩ cm), and rinsed with sample seawater prior to filling. After filling, 20 L of this water was then divided into 1 L polycarbonate (PC) incubation bottles that had been acid-cleaned with 10% HCl (Fisher, TMG), rinsed with Milli-Q (> 18.2 MΩ cm), and triple-rinsed with experimental seawater prior to filling. A bloom was induced in the 1 L incubation bottles with

the addition of 4 nM of $FeCl_3$, 50 µM nitrate, 50 µM silicate, and 3.1 µM phosphate, and incubation in a temperature-controlled environmental chamber at 20 °C for 13 days under blue lights (Philips 36 W; 10 – 15 µmol photons m^{-2} sec^{-1}) on 12 h light/dark cycles. Separate triplicate bottles incubated in a heavy-duty black garbage bag served as a dark control. Prior to carboy amendments, all macronutrient stocks were chelexed (Bio-Rad) to remove trace metals, and the silicate solution was maintained at pH ~13 to prevent polymerization. After 13 days in the incubator, a bloom had occurred, and dark controls were sampled. The contents of the light bottles were combined into a single acid-cleaned and Milli-Q (> 18.2 MΩ cm) rinsed 20 L PC carboy and placed in an enclosed dark container at room temperature for the remainder of the regeneration experiment. All samples for the grow-out and regeneration were collected following standard trace metal clean techniques in a class-100 clean air environment.

Natural assemblages, M2–M3

Surface GoM seawater was collected from the West Florida Shelf ~8 km offshore (27°59'N, 82°55'W), on 1 March 2018, on the R/V *W. T. Hogarth*. A trace metal clean tow-fish system with a Teflon diaphragm pump was utilized to collect seawater. Seawater was homogenized in a 50 L PP carboy that had been acid-cleaned with 10% HCl (Fisher, TMG), rinsed with Milli-Q water (> 18.2 MΩ cm), and triple-rinsed with sample seawater prior to filling. After filling, 40 L of this water was then distributed into two 20 L PP incubation carboys ("M2" and "M3") that had been acid-cleaned with 10% HCl (Fisher, TMG) and rinsed with Milli-Q (> 18.2 MΩ cm) and experimental seawater prior to filling. In this experiment, a ^{57}Fe spike solution was added as a source of Fe. A bloom was induced in the incubation carboys by adding 4 nM of $^{57}FeCl_3$, 50 µM nitrate, 50 µM silicate, and 3.1 µM phosphate, using the same macronutrient stocks as described above (refer to *Natural assemblages, M1*). Following the

macronutrient and ^{57}Fe addition, the 20 L carboys were incubated in a temperature-controlled environmental chamber at 25 °C under white lights (Sylvania 40 W 47.78" T12 cool white fluorescent bulbs; 80–120 µmol photons m^{-2} sec^{-1}) on 14 h light/10 h dark cycles. Carboys were shaken daily and rotated periodically in order to maintain even light exposure. After 14 days in the incubator, carboys were placed in darkness at room temperature by enclosing each in two heavy-duty black garbage bags, and compressed air was bubbled into both carboys to prevent oxygen depletion. Oxygen levels in all experiments tested (M2, M3, P1, and K1) remained ≥97%, and the persistence of ammonium without nitrification in P1 and K1 may reflect an absence of nitrifying bacteria in these experiments.

Monocultures of* P. dolorosa *and* K. brevis*, P1 and K1

Filtered low-nutrient seawater (< LOD N+N, phosphate, and silicate; Table S3 "P1 and K1 Matrix") was collected ~270 km offshore (27°32'N, 85°35'W) on the R/V *Weatherbird II* on 2 November 2017. An in-line pumping system with a Teflon diaphragm pump was used to collect seawater through a 0.45 µm Teflon membrane (GE Osmonic) that had been rinsed with methanol (Fisher, ACS grade), acid-cleaned with 10% HCl (Fisher, TMG), and thoroughly flushed with sample seawater prior to use. The filtered seawater was homogenized in two 50 L PP carboys that had been acid-cleaned with 10% HCl (Fisher, TMG), rinsed with Milli-Q water (> 18.2 MΩ cm), and triple-rinsed with filtered seawater prior to filling. Filtered seawater from the combined carboys was distributed into two 20 L PP incubation carboys that had been acid-cleaned with 10% HCl (Fisher, TMG), rinsed with Milli-Q (> 18.2 MΩ cm), and rinsed with experimental seawater prior to filling.

Cell cultures of *P. dolorosa* (P1) and *K. brevis* (K1) were maintained at Florida Fish and Wildlife Research Institute's (FWRI) Harmful Algal Bloom (HAB) lab. *Pseudo-nitzschia*

dolorosa was cultured to stationary phase in f/2 media. Cells were gradually acclimated to filtered GoM seawater amended with 4 nM of $FeCl_3$, 50 μM nitrate, 50 μM silicate, and 3.1 μM phosphate over the course of three successive weekly transfers. Cells were then concentrated by vacuum filtration and rinsed with distilled water to remove the medium, and 50 mL of the resulting culture was added to 15 L seawater.

Karenia brevis was grown to stationary phase in GSe/20 media (Table S1) and soil extract in treated tissue culture flasks according to previously described methods (Blackburn et al. 2001). The soil extract contained an additional unknown quantity of nutrients, trace metals, and ligands and was prepared by autoclaving 100 g in 1 L Milli-Q (> 18.2 MΩ cm) and filtering (< 0.2 um) and added to the GSe/20 to reach 5 – 20 mg/L. Because the cells were too fragile to be concentrated by vacuum filtration, 750 mL of culture was added directly to 10 L seawater to reach a starting cell density of 428 ± 44 cells/mL. Carboys for P1 and K1 were placed immediately in darkness at room temperature by enclosing each in two heavy-duty black garbage bags, and compressed air was bubbled into both carboys to prevent oxygen depletion. Oxygen levels and pH were monitored every ~1 month (refer to *Natural assemblages, M2 – M3* above).

Sampling and Analyses

***Chlorophyll* a**

Samples for Chlorophyll *a* (Chl *a*) were filtered onto 0.7 μm GF/F glass microfiber filters (Whatman®), frozen (-20 °C) in foil-wrapped 15 mL acid-cleaned PP Falcon tubes, and extracted in methanol (Fisher, HPLC) overnight at -20 °C. The extracts were then measured fluorometrically before and after acidification with 1 – 2 drops of 10% HCl (Fisher, TMG) (Holm-Hansen and Riemann 1978). A Turner 10-AU solid secondary standard was run daily to

account for instrument drift. The fluorometer was calibrated prior to use with a Chl *a* standard (Sigma, *Anacystis nidulans*) dissolved in methanol (Fisher, HPLC).

Particulate organic carbon and nitrogen (POC and PON)

Samples for particulate organic carbon (POC) and particulate organic nitrogen (PON) and stable isotope analysis ($\delta^{13}C$, $\delta^{15}N$) were collected by vacuum filtration (100 mL each) on a 12-port Millipore filtration rig onto pre-combusted GF/F Whatman® glass microfiber filters (0.7 μm), rinsed with 100 mL Milli-Q (> 18.2 MΩ cm), wrapped loosely in aluminum foil, and stored at -20 °C according to the Bermuda Atlantic Time-series Study (BATS) protocol *(Gundersen 1989).* Filters were then prepared for analysis by drying overnight at 50 °C and encapsulating in 50x50 mm tin foil squares (EA Consumables), which gave no detectible carbon blank. Samples were analyzed for bulk elemental composition, carbon isotopes, and nitrogen isotopes using a Continuous Flow Elemental Analyzer Isotope Ratio Mass Spectrometry (CF-EA-IRMS) at the University of South Florida College of Marine Science (USF-CMS) Stable Isotope Biogeochemistry laboratory using standard methods (Werner et al. 1999). Isotopic compositions, expressed as per mil (‰) were measured on a ThermoFinnigan Delta^{PLUS} XL IRMS (Isotope Ratio Mass Spectrometer) and normalized to Vienna Pee Dee Belemnite (VPDB; $\delta^{13}C$) and atmospheric air (AT-Air; $\delta^{15}N$). Each set of 19 samples was accompanied with a 6-point calibration curve prepared with NIST 8573 and NIST 8574, and 1570a standards. For $\delta^{13}C$ and $\delta^{15}N$, NIST 8573 and 8574 were used as the primary reference materials (Werner and Brand 2001; Qi et al. 2003; Coplen et al. 2006), and NIST 1570 was used as a calibration check; for POC and PON, all three standards were used in the calibration curve. A mid-run standard (NIST 1570a) and end-of-run 4-point calibration check served as additional QCs to monitor uncertainty.

Macronutrients

Samples for macronutrient concentrations (phosphate, silicate, N+N, nitrite, and ammonium) in experiments M2, M3, P1, and K1 were vacuum filtered through sequential acid-cleaned 3 µm and 0.2 or 0.4 µm polycarbonate track-etched (PCTE; Whatman®) filters (refer to *Dissolved trace metals (Mn, Fe, Co, Ni, Cu, Zn, Cd, Pb)* below) into 50 mL acid-cleaned, sample-rinsed PP Falcon tubes. Samples for M1 were vacuum filtered through 0.7 µm GF/F glass microfiber filters (Whatman®) into 60 – 125 mL acid-cleaned high-density polyethylene (HDPE) bottles. A previous study showed that samples filtered through PCTE and GF/F filters did not differ significantly for any of the macronutrient concentrations measured (Knefelkamp et al. 2007). All samples were analyzed on a Lachat 8500 QuickChem Flow Injection Analysis System using standard colorimetric methods (Parsons 1984). The samples for phosphate, N+N, nitrite, and ammonium were stored at -20 °C, thawed, and equilibrated to room temperature before analysis unless otherwise indicated. Ammonium was measured immediately after uncapping to minimize atmospheric exchange. The samples for silicate were either refrigerated or frozen and thawed 24 h in the refrigerator prior to equilibrating at room temperature, which gave comparable values across frozen and refrigerated samples (data not shown). A daily 5-point calibration curve in GoM low nutrient seawater (LNSW) was made from three mixed nutrient stocks of silicate, nitrate plus phosphate, and nitrite plus ammonium prepared according to standard methods (Parsons 1984). Limits of detection (LODs) were determined for each nutrient by taking three times the standard deviation of the seawater blank. An additional mid-curve calibration standard was run every seventh sample as a quality control (QC), and the standard curve was re-analyzed at the end of every run to monitor instrument drift.

Electron microscopy

Unfiltered seawater for M2 and M3 was collected in 15 mL acid cleaned PP Falcon tubes, fixed with iodine ("Lugol's solution"), and stored in the dark at room temperature. Selected samples were analyzed by Scanning Electron Microscopy (SEM) in the USF-CMS Electron Microscopy laboratory after 3 – 7 months of storage. Fixed samples (4 – 10 mL) were filtered onto a 25 mm, 0.2 μm PC filter (Millipore) using a hand held vacuum pump. Filters were dried 2 – 3 h or overnight in a desiccator. Dried filters were attached at the edges to a 25 mm aluminum stub using double stick glue tabs and secured at the edges using Cu-tape. Aluminum stubs with attached filter were then coated with a thin film of gold palladium (AuPd) in a Hummer 6.2 sputter coater. Samples were examined on a Hitachi S-3500-N variable pressure scanning electron microscope at high vacuum using an accelerating voltage of 15 kV.

Dissolved trace metals (Mn, Fe, Co, Ni, Cu, Zn, Cd, Pb)

Samples for dissolved trace metal concentrations were vacuum filtered through sequential acid-cleaned 3 μm and either 0.2 or 0.4 μm PCTE (Whatman®) filters (Table S4). The vacuum filtration was conducted using a Teflon dual stage filter holder (Savillex) fitted with a custom acrylic base, and filtrate was collected in acid-cleaned and sample-rinsed 125 mL low-density polyethylene (LDPE; Nalgene) bottles. Bottles were acidified with 0.5 mL of 6 M HCl (Fisher, Optima) to 0.024 M HCl (pH ~1.8) (Johnson et al. 1997) and stored at room temperature for a minimum of 1 – 2 weeks prior to analysis. All sample processing was conducted in a class-100 laminar flow work station (AirClean Systems).

Prior to analysis, dissolved trace metals were preconcentrated by adapting previously described methods (Biller and Bruland 2012) to an Elemental Scientific Inc. (ESI) seaFAST system (seaFAST-pico^{TM}) (Lagerström et al. 2013). Briefly, the sample preparation, reagents,

and resin followed Biller and Bruland (2012), but an automated seaFAST-pico^{TM} manifold was utilized. To ensure complete recovery of Cu and Co, all samples were first UV-oxidized in a UV box (Jelight Company Inc., Model 342) for 90 minutes (Biller and Bruland 2012) in 30 mL acid-cleaned Teflon vials (Savillex) capped with Teflon lids custom-fitted with quartz windows prior to preconcentration. Teflon vials and caps were cleaned in concentrated aqua regia prior to initial use and in heated 10% HCl (Fisher, TMG) between uses thereafter. Trace metals were preconcentrated by a factor of 25 on a Nobias Chelate-PA 1 resin (Sohrin et al. 2008; Sohrin and Bruland 2011) using the automated seaFAST system (ESI). The sample (10 mL) was mixed with a 5.4 M acetate acid-ammonium acetate buffer to obtain a pH of 6.4 ± 0.2 (NBS scale) before loading onto the chelating resin. The buffer was prepared in Milli-Q (> 18.2 MΩ cm) with 320 g acetic acid (Fisher, TMG) and 460 g concentrated ammonium hydroxide (Fisher, Optima^{TM}) per 1 L and adjusted to a pH 7.6 ± 0.1 with HCl and/or additional ammonium hydroxide. The concentrated acetic acid and ammonium hydroxide were weighed as prepared by the manufacturer without further dilution prior to making the buffer. Once loaded, the column was rinsed with Milli-Q (> 18.2 MΩ cm), and trace metals were eluted from the resin with 0.4 mL of 5% triple-distilled nitric acid (HNO_3) in Milli-Q (> 18.2 MΩ cm) with 10 ng/g indium (In) and rhodium (Rh) added as internal standards. All NHO_3 used for the elution acid was triple-distilled on a trace metal clean quartz distillation apparatus for optimal trace metal purity. The column was rinsed with 2% HNO_3 (Fisher, TMG) between each sample.

Each seaFAST sample set (~150 samples) was accompanied by a minimum of eight GoM QC samples, six GEOTRACES and/or SAFe reference samples, six manifold (air) blanks, and six procedural (Milli-Q) blanks dispersed throughout the run (Table 1). A 6-point GoM seawater calibration curve was run at the beginning and end of each set; calibration curve samples were

spiked with mixed metal standards to encompass the expected sample concentration range. All calibration samples, QCs, and Milli-Q blanks were acidified and UV-treated as described above. Quality control samples were prepared from a 50 L carboy of filtered (<0.2 μm) seawater previously collected in the GoM. The SAFe 1000-m reference sample D1 from the 2004 SAFe Intercalibration Cruise, in addition to GEOTRACES surface water reference standards GSP 230 (central North Pacific) and GSC 207 (coastal North Pacific) from the 2009 GEOTRACES Intercalibration Cruise (Johnson et al. 2007; Sohrin et al. 2008) served as additional QCs. Manifold (air) blanks were obtained by drawing ambient HEPA-filtered air into seaFAST with the autosampler and treating it as a sample. These air blanks accounted for contributions from the seaFAST manifold, elution acid, buffer, and Thermo-Scientific Element XR inductively coupled-plasma mass spectrometer (ICP-MS) system. Procedural blanks were also prepared using Milli-Q (> 18.2 MΩ cm) spiked with 0.1% QC seawater, and accounted for the sources listed above for air blanks in addition to contributions from the Milli-Q and 0.1% QC seawater, sample preparation (acidification in LDPE bottles, transfer to Teflon vials, and UV treatment), and seaFAST tubing. The seawater spike contribution and air blank averages were subtracted from these values to yield the final procedural blank values, which assessed additional sources of contamination. Mixed metal calibration curves were prepared in GoM QC seawater from mixed metal stock solutions of Mn, Fe, Co, Ni, Cu, Zn, Cd, and Pb in 10% HNO_3 (Fisher, Optima).

Trace metals in the preconcentrated samples were analyzed on a Thermo Element XR-ICP-MS. Counts for ^{55}Mn, ^{56}Fe, ^{57}Fe, ^{59}Co, ^{60}Ni, ^{63}Cu, ^{65}Zn, ^{95}Mo, ^{98}Mo, ^{110}Cd, ^{111}Cd, ^{115}In, and ^{208}Pb were measured and normalized to the In internal standard. A 6-point elution acid calibration curve and three elution acid blanks were prepared without seaFAST preconcentration, and recovery from the Nobias Chelate-PA 1 resin was calculated from the quotient of the

preconcentrated seawater calibration curve and the elution acid calibration curve. An elution acid blank or calibration standard was run after every 10 samples on the XR-ICP-MS, and the elution acid calibration curve was re-run at the end of the run to monitor instrument drift. A Mo standard curve was applied to correct ^{110}Cd and ^{111}Cd for possible Mo-oxide interferences (Wu and Boyle 1997b).

Trace metal concentrations for the preconcentrated samples were determined by standard addition as follows. First, raw counts for all metals were normalized to the In internal standard counts. The slope of the six-point seawater calibration curve, after preconcentration on seaFAST, was then calculated for each metal. Finally, the trace metal concentrations in each sample were calculated by dividing the In-normalized counts by the slope by the seawater calibration curve, subtracting the air blank average, and dividing by the preconcentration factor. Limits of detection (LODs) were assessed as three times the standard deviation of the air blank, after dividing by the preconcentration factor (Table 1).

Results and discussion

Grow-out: mixed assemblages (M1, M2, M3)

Prior to the onset of regeneration experiments for the unfiltered GoM surface water, it was necessary to promote biomass growth of natural mixed phytoplankton assemblages. This was accomplished by amending two separate batches of unfiltered GoM seawater with macronutrients and Fe and incubating in temperature- and light-controlled environments (refer to *Incubation setup* in Methods for details).

Scanning electron microscopy (SEM) confirmed that diatoms were the dominant phytoplankton group at the end of the grow-out phase in M2 – M3 (Fig. 2.1a,b). No SEM samples were collected for M1, but a similar Chl *a* response and silicate drawdown in this

experiment suggests that the growth in M1 was also dominated by diatom communities. In M2, the most commonly observed diatoms were small pennates (5 – 10 μm width, 10 – 15 μm length). In M3, both larger (150 – 300 μm) needle-shaped diatoms and smaller (5 – 20 μm width) diatoms were present. Some erosion of diatoms was also noted on day 0, likely a result of storage in neutral Lugol's solution over several months.

In all three of these experiments, significant increases in biomass were achieved over the 13 – 14 day grow-out periods (Fig. 2.2a, Table S2). Initial Chl *a* concentrations were low: 1.1 μg/L for M1 waters and below the limit of quantification (< LOQ) for M2 and M3 (Table S2). After macronutrient and Fe enrichment and 13 days in the incubator, M1 Chl *a* increased to 23.3 μg/L. No POC or PON samples were collected for M1. In M2 and M3, Chl *a* concentrations reached 11.9 μg/L and 27.0 μg/L, respectively, after 14 days in the incubator (Fig. 2.2a, Table S2). Over these 14 days, POC increased from 53 μM to 112 μM in M2 and from 45 μM to 219 μM in M3 (Fig 2c, Table S2). Similarly, PON increased from < LOQ in both experiments to 14 μM in M2 and 23 μM in M3 (Fig. S1, Table S2). An increase in $\delta^{13}C$ (Fig. 2.2e, Table S2) and $\delta^{15}N$ (Fig. S1, Table S2) corresponded with the observed increases in biomass for these experiments. The presence of POC and PON pre-grow out, despite low Chl *a* suggests the presence of non-phytoplankton organic particles in the initial seawater, which was collected in a coastal setting.

Macronutrient (phosphate, silicate, and N+N) drawdown in the grow-out experiments generally tracked with patterns of biomass accumulation (Fig. 2.3, Table S3). In M1, much less N+N was drawn down relative to silicate by the end of the 13 day incubation, which can suggest Fe limitation of diatoms (Hutchins and Bruland 1998). However, given the 4 nM Fe amendment, such limitation is unexpected; thus, the reason for the persistence of N+N is unclear. Nitrate +

nitrite (N+N) also continued to decrease for the first 1 – 2 days in the dark, indicating possible residual growth in the dark, and ultimately reached roughly silicate levels of drawdown. The M2 and M3 experiments had higher initial macronutrient and Fe concentrations than M1 (Fig. 2.3 – 4a, Table S3 – S4), consistent with the further inshore coastal waters used for these experiments relative to M1. Yet even though there was less accumulation of biomass in M2 than M1, both M2 and M3 exhibited much greater drawdown of macronutrients through the grow-out than M1, and the ratio of N+N:silicate drawdown in M2 and M3 was roughly 1:1, consistent with nutrient-replete diatom growth (Hutchins and Bruland 1998). Complete drawdown of N+N and phosphate was only observed in M3. In M1 and M2, residual macronutrients remained at the end of the grow-out phase. Interestingly, in M2, which also had the lowest biomass accumulation of the three experiments (Fig. 2.2a,c, Table S2), elevated levels of nitrite (0.87 μM) and ammonium (2.6 μM) were detected by the end of the grow-out (Fig. 2.3g,i, Table S3), suggesting that regeneration had begun to dominate in this experiment despite residual N+N and phosphate.

Dissolved Mn, Fe, Co, Ni, Cu, Zn, Cd, and Pb were measured before and after the grow-out phases of the M1, M2 and M3 experiments. With the exception of Pb, initial concentrations of all trace metals were higher in the M2 and M3 experiments compared to M1 (Fig 2.4 – 2.6, Table 4), reflecting the more inshore water used for M2 and M3. All dissolved trace metals decreased by a detectable amount in the three experiments (Fig. 2.4, Table S4). For Fe, some of this decrease can be attributed to wall loss (Fischer et al. 2007; Buck et al. 2010; Fitzsimmons and Boyle 2012; King et al. 2012; Bundy et al. 2016; Mellett et al. 2017). Although a prior incubation experiment suggested that Mn, Zn, and Cu may also experience wall loss (Coale 1991), other studies observed no wall loss of trace metals other than Fe (Fitzwater et al. 1982;

Mellett et al. 2017), and the drawdown of metals other than Fe during the grow-out in this study is thus likely attributable primarily to biogenic uptake and scavenging.

Regeneration

Electron microscopy

Scanning electron microscopy (SEM) samples collected from the M2 and M3 experiments showed that diatoms dominated the phytoplankton at the start of the regeneration (Fig. 2.1a,b; refer to *Grow-out: mixed assemblages (M1, M2, M3)* above). As noted previously, erosion of diatom frustules was apparent in the samples from day 0 (Fig. 2.1a,b), which was attributed possibly to aging in the neutral Lugol's solution. Thus, the preserved samples were likely at least partly biased toward morphologies more resistant to dissolution, and may not be fully representative of all species.

While the assemblages in M2 and M3 displayed some differences in phytoplankton composition, commonalities over time were also apparent. Both experiments were dominated by diatoms from days 0 – 20 and contained spores and pennates, including chain forming ones (Fig. 2.1a – f). In M3, there was a large centric (*Odontella*) not detected in M2 (Fig. 2.1d). Overall, M3 showed greater diatom preservation over time compared to M2, although it is not known whether this was caused by a difference in species composition or the higher overall biomass. In M2, no intact diatoms were observed by day 124 (Fig 2.1g). On the other hand, heavily silicified diatoms were preserved through day 124 in M3 (Fig. 2.1h). Nevertheless, both experiments showed abundant diatom fragments on day 124 (Fig 2.1g – h), which is consistent with the observed increase in silicate (Fig 2.2).

In addition to diatom frustules, numerous placoliths from the coccolithophore *Gephyrocapsa oceanica* were also observed on day 124 in both the M2 and M3 carboys (Fig.

2.1g – h). Surprisingly, no evidence of *G. oceanica* or other coccolithophores was observed at earlier time points. Although this appearance on day 124 may be a result of uneven sampling or overshadowing by diatom higher abundances in previous samples, evidence for mixotrophy in coccolithophores has also been reported (Poulton et al. 2017). If *G. oceanica* can engage in mixotrophy under these conditions, it would have had little competition after the diatoms died, giving it an opportunity for proliferation. The preservation of coccoliths and mildly alkaline environment throughout the regeneration (pH = 7.9 – 8.4) indicates conditions amenable to calcite preservation. In M2, small (1–2 µm) oval-shaped particles were also abundant, and an X-ray spectrum (data not shown) identified the presence of calcium (Ca), indicating that dissolution of the placoliths followed by re-precipitation took place.

Chlorophyll a, POC, PON, and macronutrients

On day 0 of the regeneration, the highest levels of Chl *a* were observed in the mixed assemblage experiments M3 (27.0 µg/L), M1 (23.3 µg/L), and M2 (11.9 µg/L) (Fig. 2.2a, Table S2). Chlorophyll *a* (Chl *a*) levels were lower for monocultures P1 (9.7 µg/L) and K1 (4.6 µg/L), which were diluted in a carboy of filtered seawater for regeneration without an initial grow-out (Fig. 2.2b, Table S2). Particulate organic carbon (POC) on day 0 of the regeneration reflected the relative levels of Chl *a* between the experiments, although P1 displayed high error between early sample replicates (Fig. 2.2c,d, Table S2). By days 20–22 in the dark, Chl *a* had declined to either < LOQ or < 1 µg/L for M2, M3, P1, and K1 (Fig. 2.2a,b, Table S2). In M1, Chl *a* did not reach < 1 µg/L until after 54 days. The reason for the slower decline in M1 is unknown, although it may indicate that complete darkness was insufficiently achieved. Particulate organic carbon (POC) corresponded with Chl *a* for M2, M3, and P1, decreasing primarily within the first 20 days (Fig. 2.2c,d, Table S2). By day 7 in M2 and M3, PON had also declined to below the limit of

quantification (LOQ) (Fig. S1, Table S2). For P1 and K1, which had lower biomass, PON remained below LOQ for the entirety of the experiments (Table S2). Surprisingly, POC for experiment K1 increased initially during the regeneration and did not decrease to day 0 levels until day 86, despite the rapid decrease in Chl *a*, reflecting possible heterotrophic activity, although the identity of such remains unclear.

Phosphate was detected on day 0 of the regeneration in experiments M1 (1.87 μM) and M2 (0.84 μM), but was below the limit of detection in M3, P1, and K1 (Fig. 2.3a,b, Table S3). Silicate concentrations on day 0 of the regeneration were highest in M2 (28.2 μM), followed by M1 and M3 (both 11.2 μM), K1 (3.4 μM), and P1(< LOD) (Fig. 2.3c,d, Table S3). Phosphate and silicate followed similar timing to each other, with the exception of K1. *Karenia brevis*, a dinoflagellate, which therefore does not require silicate to build frustules, showed comparatively little change in silicate, with only minor increases likely attributable to debris in the initial seawater.

Because these regeneration experiments attempted to simulate the processes governing depth distributions, it is instructive to compare them to known depth profiles. In ocean water columns, a deeper silicate maximum relative to phosphate has been widely observed (Bruland et al. 1994; Twining et al. 2014; Vance et al. 2017), and is attributed to slow dissolution of the silicate frustules of diatoms due to the protective organic coating (Bidle and Azam 1999). Additionally, mixing with deep water formed in the Southern Ocean can cause additional Si decoupling at lower latitudes (Sarmiento et al. 2004). On the other hand, silicate and phosphate regeneration remained coupled for P1 and the mixed diatom-dominated experiments (M1–M3) (Fig. 2.3a – d; Table S3), and this silicate regeneration was also reflected in the observed erosion of diatom frustules in the first 20 days for M2 and M3 (Fig. 2.1e,f).

Dissolution rates of diatom frustules are known to be influenced by a variety of factors, including pH, temperature (Hurd 1972; Kamatani 1982), Si saturation state (Hurd 1972; Rickert et al. 2002), turbulence (Hurd 1972), surface area (Hurd 1972; Dixit et al. 2001; Van Cappellen et al. 2002), incorporation of Al into frustules (Gehlen et al. 2002; Van Cappellen et al. 2002), and the presence of grazers (Hurd 1972; Schultes et al. 2010). In addition, trace metal and/or macronutrient limitation during growth can affect morphology and degree of silicification (Marchetti and Cassar 2009; Boutorh et al. 2016). A combination of several of these factors accounts for an observed order-of-magnitude faster dissolution rate of silicate frustules in the surface ocean compared to sediments at depth, which include both changes in the diatoms themselves (e.g. removal of the organic coating and Al incorporation), as well as decreased temperature and increased Si saturation state as they sink (Van Cappellen et al. 2002). Thus, the observed lack of decoupling in our silicate and phosphate data may reflect the inability to perfectly replicate water column conditions at depth in the laboratory, but also suggests that the deeper silicate maxima observed in ocean water columns may be a result of factors other than absolute regeneration rates, including physical processes such as deep water mixing.

Nitrate + nitrite ("N+N") was present on day 0 of the regeneration in experiments M1 (27.6–30.3 μM) and M2 (20.7 μM), but was depleted to < LOD in M3, P1, and K1 (Fig. 2.3e,f, Table S3). During the initial stages of the regeneration, all experiments showed a regeneration of nitrogen in the form of ammonium (Fig. 2.3i,j, Table S3). In M2, ammonium reached a maximum of 25.8 μM after 40 days of regeneration and declined to near baseline levels (1.47 μM) after 97 days, corresponding to an increase in N+N to near pre-incubation levels (43.1 μM) (Fig. 2.3e,i, Table S3). For the remainder of the regeneration, N+N continued to increase to 51.5 μM, while ammonium and nitrite remained negligible. In M3, the decline in ammonium was

more delayed, and a distinct nitrite maximum was observed. Ammonium reached a maximum of 44.5 μM on day 97 of the regeneration and declined to 0.5 μM on day 156 (Fig. 2.3e, Table S3). This same 156-day time point corresponded to a complete regeneration of N+N (68.7 μM), which was primarily in the form of nitrite (53.5 μM) (Fig. 2.3e,g, Table S3). On day 176, nitrite began to decrease again (33.9 μM), while N+N continued to slowly increase (75.9 μM), indicating conversion to nitrate. In both M2 and M3, N+N ultimately surpassed pre grow-out levels, suggesting that regeneration of existing organic particles in the initial seawater beyond those generated in the grow-out had occurred. This is plausible, given the eventual decrease of both POC and PON to below pre-grow out levels (Fig. 2.2c, Fig. S1a). In P1 and K1, ammonium remained elevated throughout the duration of the experiment, and N+N was not regenerated (Fig. 2.3f,j, Table S3). Surprisingly, a low level of nitrite (<0.4 μM) was also observed from in P1 and K1 until day 110 (Fig. 2.3h, Table S3), despite the presence of ammonium, although this nitrite remained undetected as N+N as a result of the higher limits of detection inherent for N+N measurements.

The initial increase in ammonium in all experiments (Fig. 2.3i,j) is consistent with the well-established nitrogen regeneration pathway from ammonium to nitrite and then to nitrate (e.g. Fig. 1.2), although the rate and timing of this process in laboratory regeneration experiments has been shown to be highly variable (Von Brand et al. 1937; Von Brand et al. 1939; Von Brand and Rakestraw 1941; Von Brand et al. 1942; Grill 1964; Garber 1984). Oxygen levels in all experiments tested (M2, M3, P1, and K1) remained at ≥97%. Thus, there was no indication that suboxic conditions led to the persistence of ammonium without nitrification observed in P1 and K1. Instead, the variable timing of nitrification is likely a reflection of other factors such as the presence of nitrifying bacteria.

Dissolved trace metals

Dissolved Cd has been commonly observed to follow a nutrient-type distribution in ocean profiles (Bruland et al. 1978; Bruland et al. 1994; de Baar et al. 1994). The regeneration of Cd in these experiments was consistent with this pattern, and remained closely coupled with the macronutrients phosphate and silicate (Fig. 2.3a – d, Table S3). Despite the different concentrations of dissolved Cd at the start of the regeneration for the five experiments, its regeneration trajectory followed predictable timing in each: the dissolved Cd minimum occurred on days 0 – 1 in the dark, followed by an increase and gradual attenuation (Fig. 2.6c,d, Table S4). By day 68 of M2 and M3, Cd had nearly completely regenerated (> 90%) to pre grow-out concentrations (Fig. 2.6c,d, Table S4), while Cd regeneration in M1 was somewhat more gradual (Fig. 2.6c Table S4), reflecting the comparative trends observed in phosphate and silicate (Fig. 2.3a,c, Table S3). Because Cd showed no scavenging or wall loss, it thus served as a baseline for "nutrient-type" regeneration in these experiments.

Zinc (Zn), an important micronutrient, is also known to display a nutrient-type profile (Bruland 1980; Bruland and Franks 1983; Bruland et al. 1994), although is more closely coupled with silicate than with phosphate (Croot et al. 2011; Wyatt et al. 2014). Like Cd, dissolved Zn increased over time in all five regeneration experiments (Fig. 2.6a,b, Table S4). In K1 and P1, Zn regeneration followed a trend of increase and attenuation similar to Cd (Fig. 2.6,b,d, Table S4). In experiments M1, M2, and M3, however, dissolved Zn was much more variable and increased beyond pre-incubation levels (Fig. 2.6a, Table S4), suggesting a source of a source of Zn beyond the regeneration of the phytoplankton generated during the grow-out. Because the seawater was collected in a coastal setting, it is possible that Zn-containing particles were present in the initial seawater, which added to the regenerated Zn. This explanation is consistent with the presence of

POC in the initial waters (Fig. 2.2c, Table S2) and the observation that N+N, phosphate, and silicate also exceeding pre grow-out levels in M2 and M3 (Fig. 2.3a,c,e, Table S3). However, although stringent trace metal clean protocols were followed, we also acknowledge that Zn contamination from repeat carboy sampling may have contributed to these results as well.

Manganese (Mn) serves not only an important nutrient to phytoplankton (Brand et al. 1983; Sunda 1989; Bruland et al. 1991; Morel and Price 2003; Sunda 2012), but is also utilized by Mn-oxidizing bacteria at depth (Tebo et al. 1984; Sunda and Huntsman 1987; Sunda and Huntsman 1988; Sunda and Huntsman 1990; Bruland et al. 1991; Tebo et al. 2004), which can result in a subsurface maximum in ocean water columns (Landing and Bruland 1987; Bruland et al. 1994; Sunda 2012). Thus, Mn was expected to be influenced by both regeneration and Mn-oxidation in these dark incubation experiments. Consistent with observed water column behavior, dissolved Mn showed a slight initial regeneration signal for M1, M3, and P1, but was then drawn down to near baseline levels (< 1 nM) within the first 20 – 64 days (Fig. 2.4a,b, Table S4). In M1, dissolved Mn increased from day 1 (1.6 nM) to day 6 (4.3 nM), decreased again until day 54 (0.33 nM), and stabilized at < 1 nM for the remainder of the regeneration (Fig. 2.4a, Table S4). Dissolved Mn displayed a similar pattern of an early increase followed by a decline in M3 and P1. In M3, dissolved Mn increased from day 0 (6.3 nM) to day 3 (10.7 nM) and in P1 from day 0 (4.0 nM average) to day 20 (4.5 nM average) (Fig. 2.4a,b, Table S4). In M2 and K1, the Mn drawdown was immediate, and no increase in dissolved Mn was observed (Fig. 2.4a,b, Table S4), suggesting that oxidation was dominant throughout the duration of the experiments. The early increase in dissolved Mn for M1, M3, and P1 indicates regeneration, which was followed by decline attributed to Mn-oxidation in all five experiments. Similar trends in dissolved Mn were observed in a previous sediment remineralization experiment (Cheize et al.

in press), which reported Mn-oxidizing bacteria. Thus, our experiments suggest the presence of Mn-oxidizing bacteria, which are photoinhibited in surface waters (Sunda and Huntsman 1988).

Iron (Fe) can be expected to be influenced by a combination of biogenic uptake and regeneration, scavenging, and precipitation as Fe oxy-hydroxides (Johnson et al. 1997; Tagliabue et al. 2017), as well as wall loss (Fischer et al. 2007; Buck et al. 2010; Mellett et al. 2017). Despite being an essential nutrient, dissolved Fe deviated from phosphate in all experiments and instead displayed an initial drawdown (Fig. 2.4c,d, Table S4), suggesting a predominant scavenging influence from the Mn-oxides (Tebo et al. 2004; Cheize et al. in press). In M1, dissolved Fe remained low (< 2.0 nM) until day 116, when it increased to exceed pre-incubation levels (7.0 nM). In M2 and M3, dissolved Fe also displayed an early decrease similar to Mn, followed by a delayed increase starting on day 68 for M3 and on day 156 for M2, though complete recovery of initial concentrations was never achieved (Fig. 2.4c, Table S4). The stable isotope ^{57}Fe, which was added as a tracer to M2 and M3 at the start of the grow-out, displayed similar timing, supporting the idea that the observed Fe trends were a result of delayed regeneration from biogenic particles, although the magnitude of the changes was smaller (Fig. 2.4e, Table S4). Notably, the trends and timing of Fe and Mn followed similar timing to a prior regeneration experiment conducted with natural Si sediments (Cheize et al. in press). In Cheize et al, Fe decreased initially as a result of scavenging to Mn-oxides, and a regeneration signal was only observed after levels of dissolved Mn stabilized. Thus, the apparently delayed Fe regeneration in our experiments was likely also a result of an initial predominance of scavenging, followed by a delayed increase after Mn-oxidation reached equilibrium and dissolved Mn stopped decreasing.

In P1, dissolved Fe also followed a similar regeneration to Mn, also consistent with scavenging to Mn-oxides (Fig. 2.4b,d, Table S4), although no delayed increase was observed. In contrast, dissolved Fe actually increased throughout the duration of the experiment in K1 and corresponded more closely with the macronutrients (Fig. 2.4d, Table S4). This may indicate that Fe was being released from decaying biogenic particles with little apparent scavenging, despite the drawdown of Mn observed (Fig. 2.4b, Table S4). One explanation for this could be the presence of EDTA or other organic ligands from the soil extract in the culture medium (Table S1), which likely solubilized at least some of the Fe as it was regenerated. However, based on the apparent Fe drawdown from the initial growth media (Table S1), the regenerated Fe was predicted to be far higher: ~17 nmol/L, discounting wall loss. Thus, it is likely that a major portion of the Fe was indeed being removed from the dissolved phase as soon as it was regenerated through processes such as scavenging, an idea supported by the apparent production of Mn-oxides (Fig. 5b).

Lead (Pb) is known to be primarily influenced by particle scavenging (Fisher et al. 1983; Fisher et al. 1987; Moore and Dymondt 1988; Boyle et al. 2014). Like Fe, the trajectory of dissolved Pb was consistent with scavenging to Mn-oxides for all experiments except possibly K1 (Fig. 2.4f,g, Table S4), but unlike Fe, no delayed regeneration was apparent. In experiment K1 displayed more of a nutrient-type profile similar phosphate: Pb decreased only from day 0 (0.14 nM) to day 1 (0.04 nM), which was followed by a gradual increase to 0.10 nM by day 176 (Fig. 2.4g, Table S4). Thus, as with Fe, Pb in K1 appeared to be solubilized and not heavily influenced by scavenging. As with Fe, the cause of this remains unknown, though it is likely at least partially a result of the culture media.

Cobalt (Co), Ni, and Cu were largely conservative relative to the total reservoir in all regeneration experiments (Fig. 6a – f). However, a few noteworthy trends were apparent. In M2 and M3, Cu and possibly Ni displayed a delayed regeneration similar to Fe (Fig. 2.4c), reaching initial concentrations only on day 176 for M3 and on days 97 – 124 for M2 (Fig. 2.6c,e, Table S4). Like Fe, Cu can be influenced by both scavenging and nutritive processes and is known to display "hybrid-type" water column profiles (Bruland 1980; Bruland and Franks 1983; Bruland et al. 1991; Jacquot and Moffett 2015), although previous laboratory studies have demonstrated relatively little change in Cu concentrations over the course of an incubation (Buck et al. 2010; Mellett et al. 2017). In M2 and M3, however, Cu and Fe appeared to be influenced similarly by scavenging to Mn-oxides followed by a delayed regeneration signal.

Cobalt (Co) and Ni remained relatively stable in all experiments except M1, which displayed an initial drawdown Co and Ni, followed by a nutrient-like increase (Fig. 6a,c). However, no apparent Mn-coupling was observed. Cobalt (Co) is also widely known to be coupled with Mn in the water column and susceptible to scavenging to Mn-oxides (Tebo et al. 1984; Balistrieri and Murray 1986; Lee and Fisher 1994; Moffett and Ho 1996; Tani et al. 2004). Nickel (Ni), an important nutrient for phytoplankton (Price and Morel 1991) may also be scavenged to Mn-oxides (Tani et al. 2004), and a previous dark incubation experiment showed coupling between the two elements, attributed to possible scavenging or incorporation into Mn-superoxide dismutases (SODs) (Mellett et al. 2017). However, despite the apparent presence of Mn-oxides in all five regeneration experiments (Fig. 5a,b), dissolved Co and Ni, unlike Mn, remained relatively constant throughout the duration of most of the experiments (Fig. 6a,b), with the possible exception of M1.

Conclusions

Experiments reported here shed light on the regeneration of dissolved macronutrients and trace metals observed through laboratory incubations of naturally diatom-dominated GoM mixed phytoplankton assemblages (M1 – M3) and monocultures of the diatom *P. dolorosa* (P1) and the dinoflagellate *K. brevis* (K1). In all experiments, Cd regeneration was closely coupled with phosphate, mirroring the nutrient-type profile observed in ocean water columns (Bruland et al. 1978; Bruland et al. 1994; de Baar et al. 1994). Zinc (Zn) also increased over time, but was more weakly coupled with either phosphate or silicate and exceeded initial concentrations in the mixed experiments, although this may have been partly a result of contamination. On the other hand, Mn was drawn down in all regeneration experiments, consistent with the formation of Mn-oxides. In M1, M3, and P1, an initial Mn regeneration signal was also observed prior to this decrease. Cobalt (Co), Ni, and Cu remained largely conservative in all experiments relative to the overall reservoir with a few exceptions. In M1, Co and Ni both displayed more nutrient-type trends. In M2 and M3, Cu followed a similarly trend to Fe for M2 and M3, displaying an apparently delayed regeneration. Lead (Pb), which is known to be heavily scavenged in the ocean water column (Fisher et al. 1983; Fisher et al. 1987; Moore and Dymondt 1988; Boyle et al. 2014) displayed primarily scavenging behavior with little evidence of a regeneration signal except possibly in K1.

Iron (Fe), an essential and growth-limiting nutrient (Martin and Fitzwater 1988; Hutchins 1995; Coale et al. 1996; Coale et al. 2004; Boyd et al. 2007; Boyd et al. 2017), which is known to also be influenced by scavenging (Johnson et al. 1997; Tagliabue et al. 2017), displayed unique behavior compared to the other trace metals. Notably, these Fe and Mn data showed very similar trends to a previous sediment regeneration study (Cheize et al. in press). In both studies,

dissolved Fe and Mn both decreased initially, followed by a delayed increase for Fe. Thus, rather than having a delayed in regeneration, Fe was likely instead scavenged to Mn-oxides until Mn stabilized.

Several unexplored facets of regeneration are suggested as intriguing future areas of study. For example, a corresponding analysis of size-fractionated particulate trace metals would be useful to provide a mass balance and distinguish the trace metals present in labile and refractory phases. Additionally, a genomic analysis of bacterial assemblages in these same size fractions would provide additional insight into the biological drivers of regeneration (e.g. Mn-oxidizing bacteria or nitrifying bacteria) over time. Finally, measuring the evolution of dissolved organic matter (DOM) and organic speciation of Fe and/or Cu would provide further insight into the role of ligands in trace metal bioavailability during regeneration.

Taken together, these experiments provide novel insight into the combined influences of scavenging and regeneration from decaying phytoplankton on the dissolved trace metals in ocean water columns. If the processes demonstrated in the lab can be extrapolated to the water column, a dataset emerges with global implications. For example, harmful algal blooms (HABs) caused by either *Karenia* or *Pseudo-nitzschia* spp., will be expected to affect trace metal distributions in unique ways. Additionally, changes in phytoplankton species distributions caused by ocean warming (Winder and Sommer 2012) may also alter trace metal distributions. Finally, these data can aid in understanding the effects of 1-dimensional export processes and 3-dimensional mixing processes in determining ocean depth profiles.

Chapter 2 Tables

Table 1. Dissolved trace metal averages and standard deviations for Milli-Q blanks, Gulf of Mexico (GoM) quality controls (QCs), GEOTRACES intercalibration standards (GSP and GSC),

and SAFe reference standard D1 (1000 m). Limit of detections (LOD) were determined as three times the standard deviation of the air blanks and evaluated separately for each seaFAST sample run; a representative sample set of air blanks and corresponding LOD values is reported. All other values for Milli-Q blanks, QCs, and GEOTRACES and SAFe samples are averaged across datasets. All samples were divided by the preconcentration factor after subtracting the air blank average (except the air blank itself, which was only divided by the preconcentration factor). Values excluded by Grubb's test ($p > 0.05$) are not reported. Up-to-date consensus values for SAFe samples can be found on the GEOTRACES website (http://www.geotraces.org/sic/intercalibrate-a-lab/standards-and-reference-materials). No consensus values exist for any GSC or GSP metals, or for D1 Mn as of this writing.

	Mn (nM)	Fe (nM)	Co (pM)	Ni (nM)	Cu (nM)	Zn (nM)	Cd (pM)	Pb (pM)
Air blanks	0.0020 ± 0.0001 (n=3)	0.13 ± 0.01 (n=3)	0.7 ± 0.2 (n=3)	0.031 ± 0.009 (n=3)	0.007 ± 0.001 (n=3)	0.086 ± 0.003 (n=3)	1 ± 1 (n=3)	1 ± 1 (n=3)
LOD	0.0003	0.031	0.6	0.03	0.004	0.009	2	4
MQ blanks	0.005 ± 0.002 (n = 6)	0.03 ± 0.03 (n = 6)	5 ± 6 (n = 6)	0.020 ± 0.008 (n = 6)	0.02 ± 0.02 (n = 6)	0.2 ± 0.2 (n = 7)	0 ± 1 (n = 7)	1 ± 1 (n = 6)
GoM QC	1.1 ± 0.2 (n = 8)	0.6 ± 0.1 (n = 9)	86 ± 9 (n = 8)	2.81 ± 0.05 (n = 8)	1.76 ± 0.05 (n = 9)	2.7 ± 0.3 (n = 9)	27 ± 3 (n = 9)	26 ± 3 (n = 9)
GSP 230	0.83 ± 0.02 (n = 4)	0.4 ± 0.2 (n = 4)	8 ± 1 (n = 2)	2.7 ± 0.2 (n = 4)	0.70 ± 0.03 (n = 4)	0.347 ± 0.007 (n = 3)	< LOD (n = 4)	76 ± 4 (n = 4)
GSC 207	2.2 ± 0.1 (n = 5)	1.7 ± 0.2 (n = 4)	115 ± 18 (n = 4)	4.3 ± 0.3 (n = 5)	1.3 ± 0.1 (n = 5)	1.9 ± 0.6 (n = 5)	350 ± 18 (n = 5)	47 ± 1 (n = 4)
SAFe D1	0.39 ± 0.05 (n = 2)	0.54 ± 0.06 (n = 2)	43 ± 4 (n = 2)	8.6 ± 0.8 (n = 2)	2.2 ± 0.3 (n = 2)	7.2 ± 0.8 (n = 2)	950 ± 116 (n = 2)	25 ± 5 (n = 2)
SAFe D1, consensus	Not available	0.67 ± 0.04	45.4 ± 4.7	8.58 ± 0.26	2.27 ± 0.11	7.4 ± 0.35	991 ± 31	27.7 ± 2.6

Chapter 2 Figures

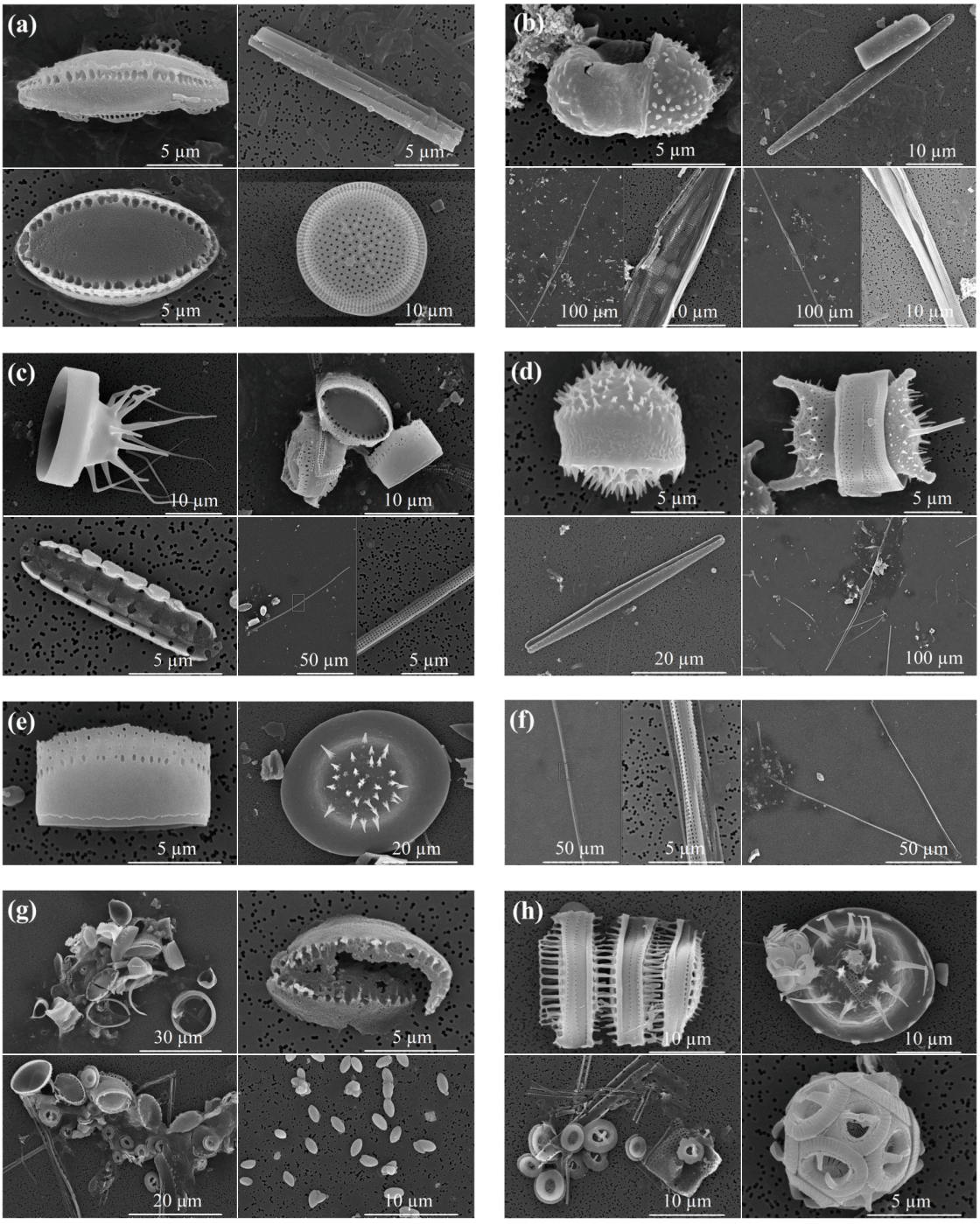

Fig. 2.1. Scanning electron microscopy (SEM) images of mixed assemblages M2 (left) and M3 (right) for regeneration days 0 (a – b), 7 (c – d), 20 (e – f), and 124 (g – h).

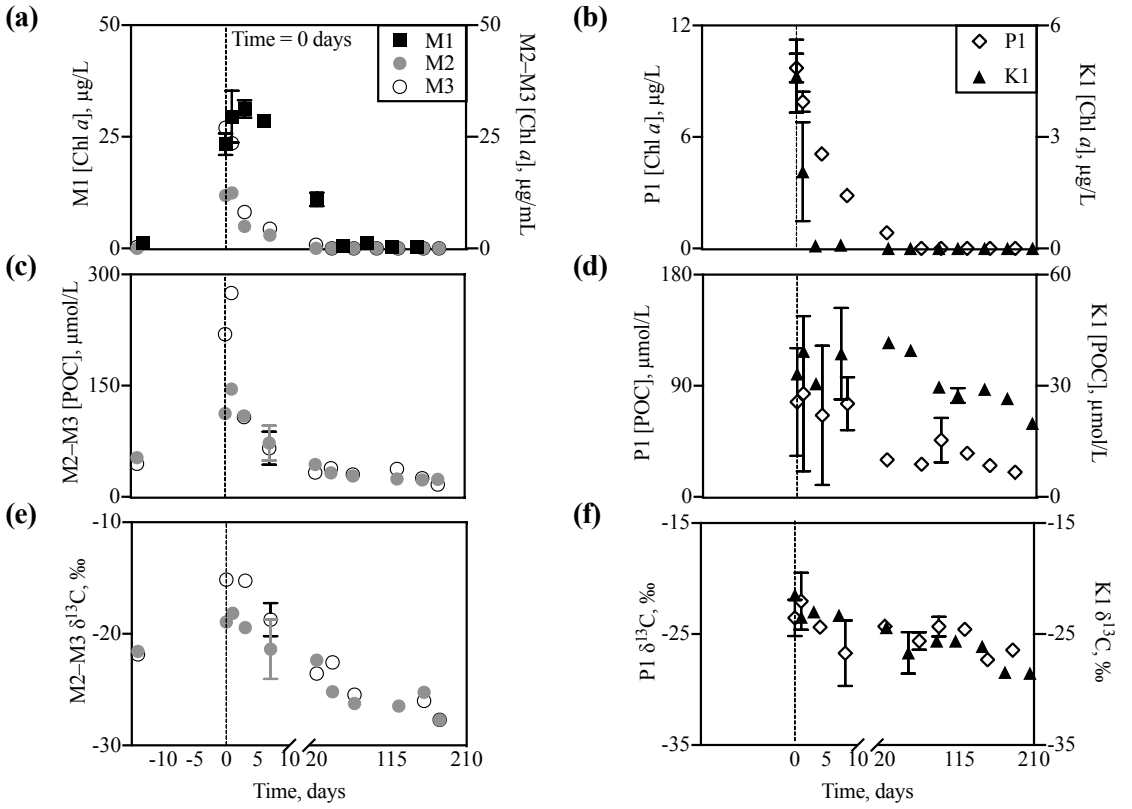

Fig. 2.2. Chlorophyll *a* (Chl *a*, µg/L; a – b), particulate organic carbon (POC, µM; c – d), and ^{13}C isotopic composition ($\delta^{13}C$, ‰; e – f) where available for mixed assemblages (M1 – M3; left) and monocultures of *Pseudo-nitzschia dolorosa* (P1) and *Karenia brevis* (K1) (right). Day 0 (dashed line) represents the start of regeneration; the grow-out is indicated by negative values. For clarity, the x-axis is split at 10 days. Error bars represent the standard deviation of sample replicates where available. Samples below the limit of quantification (LOQ) are plotted as zero.

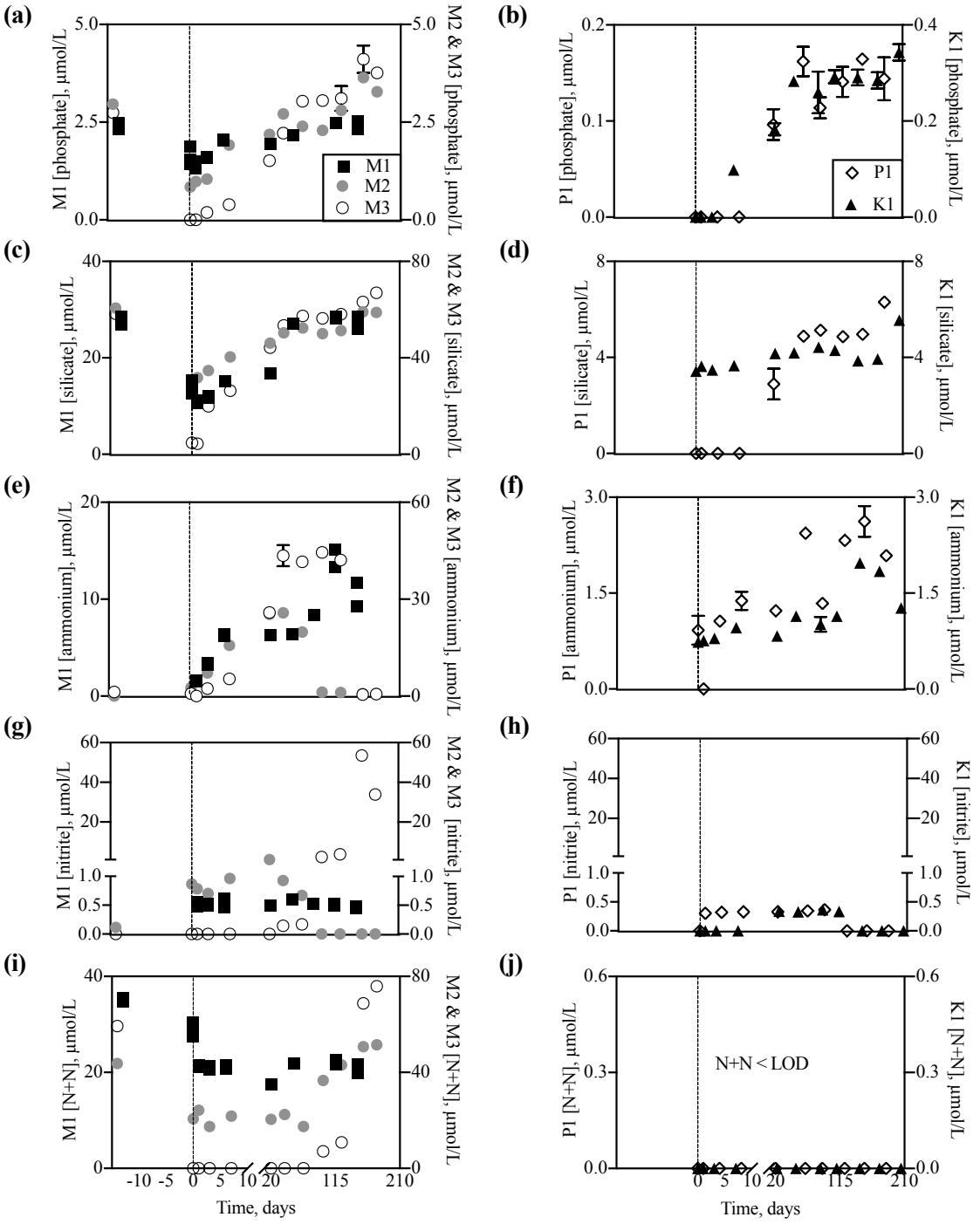

Fig. 2.3. Macronutrients (µM) phosphate (a – b), silicate (c – d), nitrate + nitrite ("N+N"; e – f), nitrite (g – h), and ammonium (i – j) where available for mixed assemblages (M1 – M3; left) and monocultures of *Pseudo-nitzschia dolorosa* (P1) and *Karenia brevis* (K1) (right). Day 0 (dashed

line) represents the start of regeneration; the grow-out is indicated by negative values. For clarity, the x-axis is split at 10 days. The y-axis on nitrite is also split at 1 μM for M1 – M3 to show resolution for both low and high values. Error bars represent the standard deviation of analytical replicates. Samples below the limit of detection (LOD) are plotted as zero.

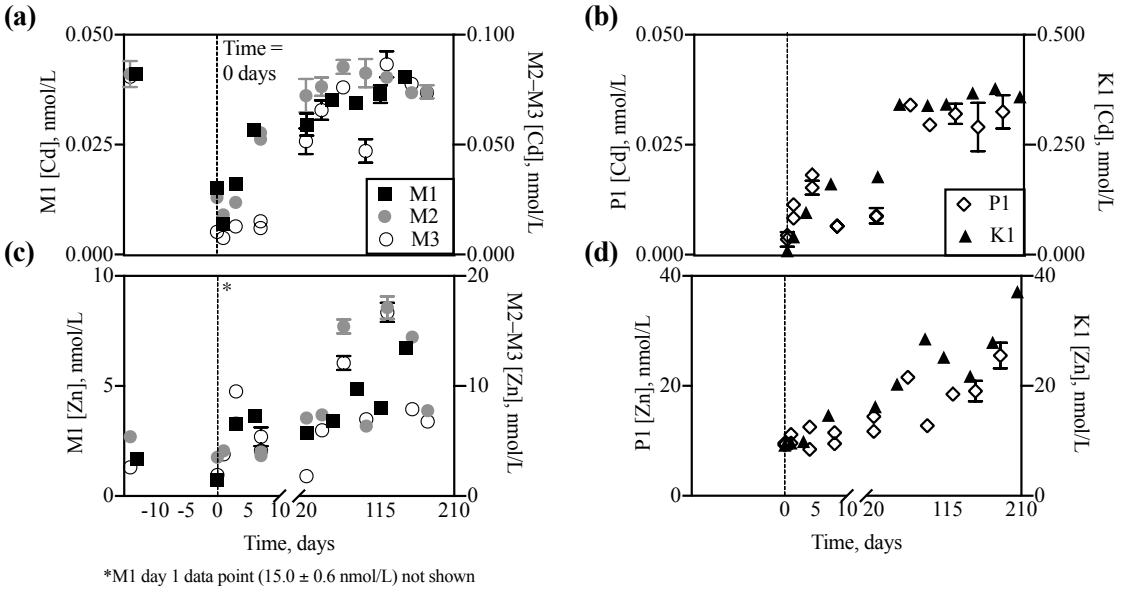

Fig. 2.4. Trace metals (nM) manganese (Mn; a – b), iron (Fe; c – d), iron-57 (^{57}Fe; e), and lead (Pb; f – g) for mixed assemblages (M1 – M3; left) and monocultures of *Pseudo-nitzschia dolorosa* (P1) and *Karenia brevis* (K1) (right). Day 0 (dashed line) represents the start of regeneration; the grow-out is indicated by negative values. For clarity, the x-axis is split at 10 days. Error bars represent the standard deviation of analytical replicates. Samples below the limit of detection (LOD) are plotted as zero. Data for ^{57}Fe were collected only for M2 and M3. For these samples, ^{57}Fe was calculated by subtracting 2.119% natural abundance ^{57}Fe present in the total Fe measured; if Fe < LOD, no subtraction was performed.

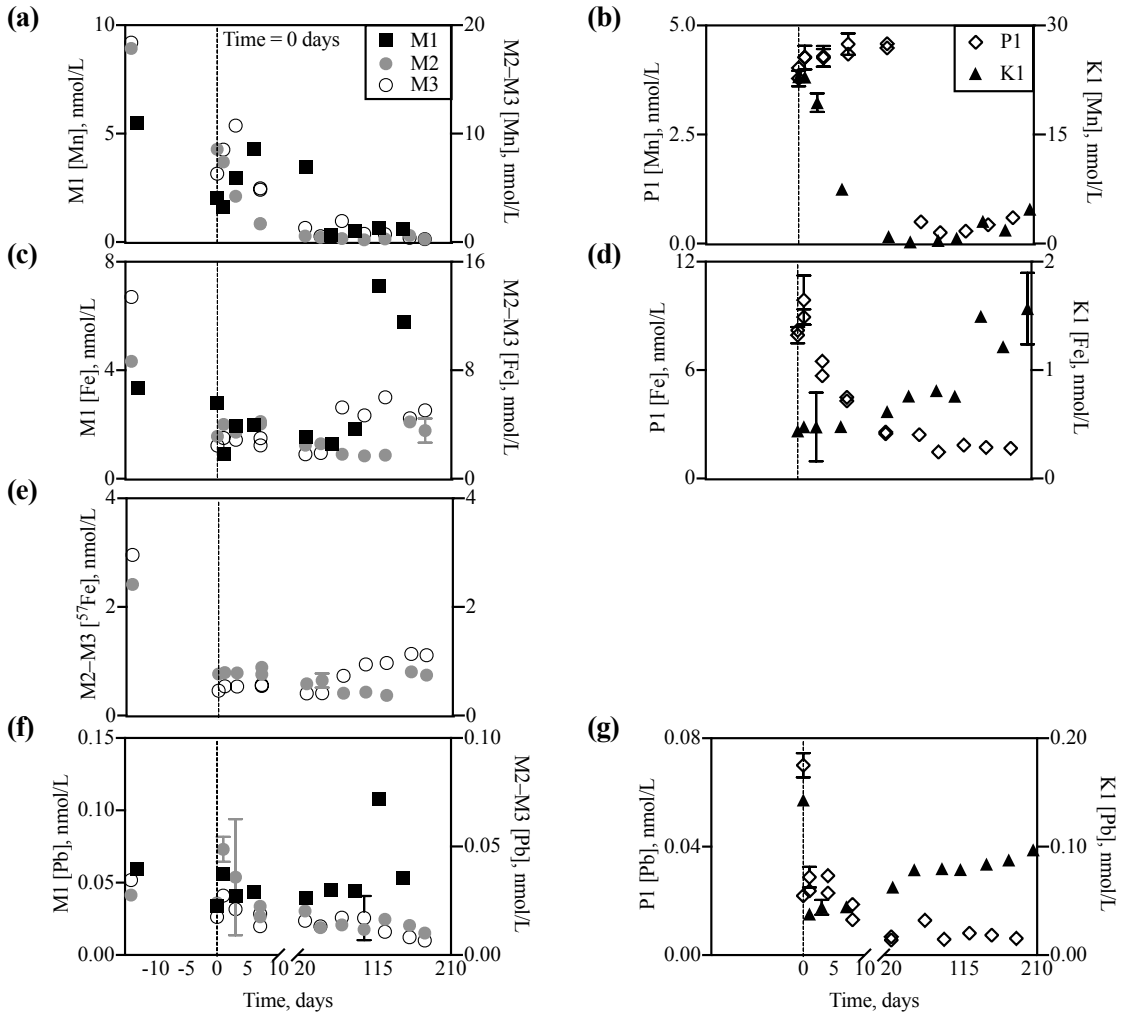

Fig. 2.5. Trace metals (nM) cobalt (Co; a – b), nickel (Ni; c – d), and copper (Cu; e – f) for mixed assemblages (M1 – M3; left) and monocultures of *Pseudo-nitzschia dolorosa* (P1) and *Karenia brevis* (K1) (right). Day 0 (dashed line) represents the start of regeneration; the grow-out is indicated by negative values. For clarity, the x-axis is split at 10 days. Error bars represent the standard deviation of analytical replicates. Samples below the limit of detection (LOD) are plotted as zero.

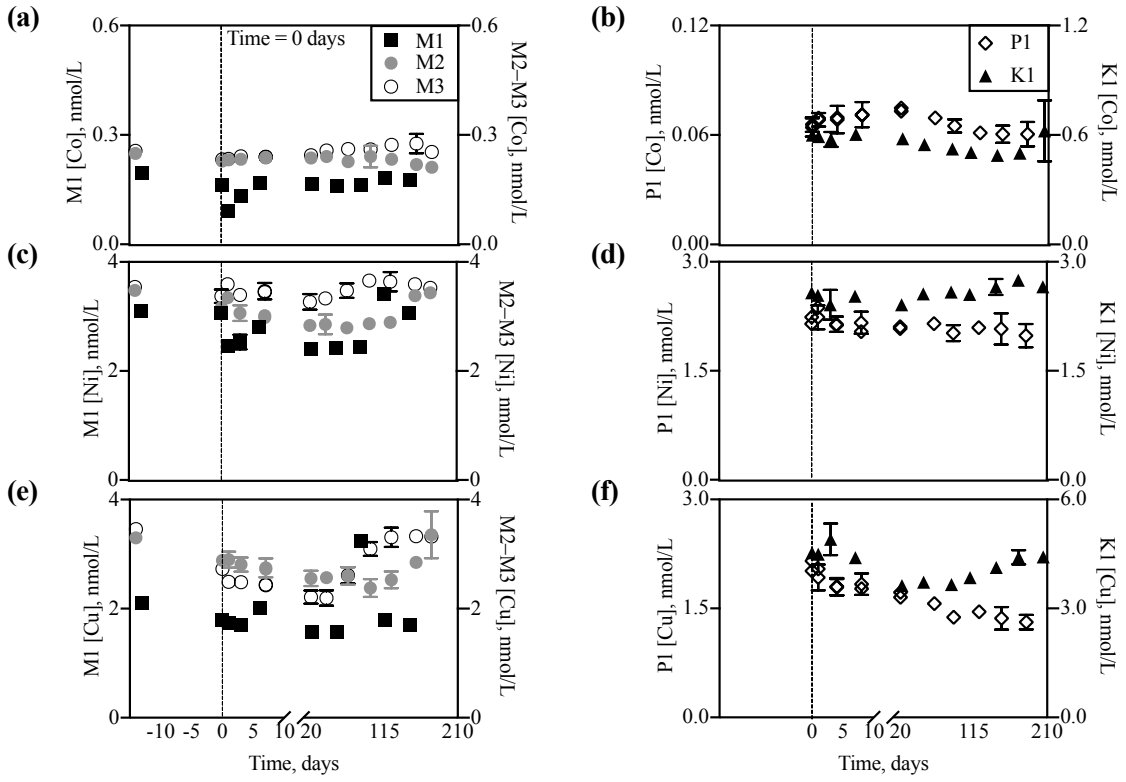

Fig. 2.6. Trace metals (nM) zinc (Zn; a – b) and cadmium (Cd; c – d) for mixed assemblages (M1 – M3; left) and monocultures of *Pseudo-nitzschia dolorosa* (P1) and *Karenia brevis* (K1) (right). Day 0 (dashed line) represents the start of regeneration; the grow-out is indicated by negative values. For clarity, the x-axis is split at 10 days. Error bars represent the standard deviation of analytical replicates. Samples below the limit of detection (LOD) are plotted as zero.

CHAPTER THREE:

CONCLUSION

This thesis research provided novel insight into the timing and chemistry of trace metal regeneration in a controlled laboratory environment. Dissolved trace metals, macronutrients, Chl *a*, POC, and PON were successfully measured over the course of six months using decaying incubations of naturally diatom-dominated mixed phytoplankton assemblages and monocultures of the diatom *P. dolorosa* (P1) and the dinoflagellate *K. brevis* (K1). Distinct behavior was observed among the trace metals. Dissolved Cd displayed the most classic nutrient-type regeneration, reflecting the commonly observed Cd depth profile in ocean water columns (Bruland et al. 1978; Bruland et al. 1994; de Baar et al. 1994). Zinc (Zn) also increased over time during the regeneration experiments, although it was less tightly coupled to either phosphate or silicate, possibly as a result of contamination. Manganese (Mn), Fe, and Pb, on the other hand, showed clear evidence of scavenging. In all experiments, Mn was drawn down in the first 0 – 64 days in the dark and remained low throughout the duration of the experiment, consistent with the formation of Mn-oxides. Lead (Pb) also displayed little regeneration signal in all experiments except K1. Iron (Fe), on the other hand, was initially drawn down by scavenging, but this was generally followed by a delayed increase as Mn stabilized. These Fe and Mn data align very closely with trends observed in a previous regeneration study of biogenic silicate sediments (Cheize et al. in press), indicating that the behavior of Fe can likely be attributed to scavenging to Mn-oxides. Finally, Co, Cu, and Ni remained relatively conservative relative to the overall

reservoirs in most experiments. However, Cu displayed a delayed increase to Fe, which is consistent with the hybrid behavior of both elements, which can be influenced by both biogenic uptake and particle scavenging. In M1, Ni and Co also followed a nutrient-type trend. Taken together, these experiments provide novel insight into the influences of regeneration and scavenging on the dissolved trace metals by isolating the regeneration process to the laboratory and experimentally monitoring a suite of biologically relevant trace metals over the course of six months.

Several unexplored opportunities remain for future study. First, an analysis of size-fractionated particulate trace metals, corresponding to the dissolved time points of the regeneration and initial (day 0) samples, would serve to provide a mass balance and distinguish the trace metals present in leachable and refractory particulate phases. This analysis would also provide insight into the processes governing trace metal concentration and size fractionation, such as adsorption to Mn-oxides or incorporation into larger phytoplankton (>3 μm fraction) or bacteria (0.2 – 3 μm fraction). Isotopic analysis of the dissolved and particulate fractions would provide further information on processes that influence isotopic fractionation, such as uptake and scavenging.

In fact, leachable particulate trace metals were collected and analyzed in both size fractions (Appendix B), but are not reported here as a result of an expired hydroxylamine hydrochloride reagent that compromised the results. Nevertheless, the preliminary leachable particulate data suggest interesting trends, such as possible Mn-Co coupling. Leaching these samples again with new reagents, followed by bomb digestion to obtain refractory particulate metal data, would be a useful additional study.

Additionally, a genomic analysis of bacterial diversity by16S ribosomal RNA (rRNA) gene analysis in these size fractions would provide additional insight into the biological drivers of regeneration over time. For example, the detection of Mn-oxidizing bacteria or nitrifying bacteria throughout the regenerations would help to explain the timing and behavior of dissolved Mn and N+N, respectively. Additionally, genetic analysis of the phytoplankton by18S ribosomal RNA gene analysis would provide insight into the community of the mixed phytoplankton assemblages.

Finally, measuring the evolution of DOM and organic ligand speciation of would provide further insight into the role of the ligand environment in trace metal bioavailability during regeneration. It is well-established that dissolved Fe and Cu are influenced by extensive organic ligand complexation (Coale and Bruland 1990; Gledhill and Buck 2012), although the structure and function of much of this ligand pool remains unclear. Using analytical resources available, such as competitive ligand exchange-adsorptive cathodic stripping voltammetry (CLE-ACSV), the degree of complexation for these elements could be measured over time as cells decay, providing further insight into marine ligand production.

Despite the remaining questions, these results provide unique insight into trace metal cycling. Ultimately, this study aimed to understand the role of regeneration in controlling distributions of trace metals in ocean water columns. If the regeneration trends in these experiments are viewed with respect to distributions at depth instead of time, a valuable dataset can be obtained.

For example, these regeneration experiments can help differentiate the roles of 1-dimensional processes and the 3-dimensional processes in controlling the concentrations of trace metals and macronutrients in the ocean water column. Remineralization is a process that largely

takes place during the vertical export of organic particles; thus, decoupling between these regeneration experiments and water column depth profiles may suggest additional 3-dimensional processes such as physical mixing. For example, the deeper silicate maximum relative to phosphate in the ocean water column has been attributed both to the slower dissolution of silicate frustules (Bidle and Azam 1999) and mixing of deep water masses transported from the Southern Ocean (Sarmiento et al. 2004). Although 3-dimensional circulation is beyond the scope of this experiment, the lack of decoupling of silicate and phosphate during these regeneration experiments suggests a mixing influence.

Additionally, these experiments demonstrated the crucial role of phytoplankton regeneration in controlling marine trace metal concentrations. Phytoplankton distributions can be expected to change in response to environmental disruptions such as climate change (Winder and Sommer 2012) or eutrophication, which can contribute to harmful algal blooms (Anderson et al. 2008). Thus, the regeneration of phytoplankton, and in turn, trace metal concentrations, will also be altered. This study and the future research to follow will provide valuable data for modeling how a changing environment will affect trace metal and macronutrient distributions in the water column.

REFERENCES

Ahner, B., F. Morel, and J. Moffett. 1997. Trace metal control of phytochelatin production in coastal waters. Limnol. Oceanogr. **42:** 601-608.

Ahner, B. A., J. G. Lee, N. M. Price, and F. M. Morel. 1998. Phytochelatin concentrations in the equatorial Pacific. Deep Sea Res. Part 1 Oceanogr. Res. Papers **45:** 1779-1796.

Ahner, B. A., and F. M. Morel. 1995. Phytochelatin production in marine algae. 2. Induction by various metals. Limnol. Oceanogr. **40:** 658-665.

Ahner, B. A., and L. Wei. 2005. Sources and sinks of dissolved phytochelatin in natural seawater. Limnol. Oceanogr. **50:** 13-22.

Anderson, D. M., J. M. Burkholder, W. P. Cochlan, P. M. Glibert, C. J. Gobler, C. A. Heil, R. M. Kudela, M. L. Parsons, J. J. Rensel, and D. W. Townsend. 2008. Harmful algal blooms and eutrophication: examining linkages from selected coastal regions of the United States. Harmful Algae **8:** 39-53.

Anderson, L. A., and J. L. Sarmiento. 1994. Redfield ratios of remineralization determined by nutrient data analysis. Global Biogeochem. Cy. **8:** 65-80.

Annett, A. L., S. Lapi, T. J. Ruth, and M. T. Maldonado. 2008. The effects of Cu and Fe availability on the growth and Cu: C ratios of marine diatoms. Limnol. Oceanogr. **53:** 2451-2461.

Baars, O., W. Abouchami, S. J. Galer, M. Boye, and P. L. Croot. 2014. Dissolved cadmium in the Southern Ocean: distribution, speciation, and relation to phosphate. Limnol. Oceanogr. **59:** 385-399.

Bacon, M., D. Spencer, and P. Brewer. 1976. $^{210}Pb/^{226}Ra$ and $^{210}Po/^{210}Pb$ disequilibria in seawater and suspended particulate matter. Earth Planet Sci. Lett. **32:** 277-296.

Badger, M. R., and G. D. Price. 1994. The role of carbonic anhydrase in photosynthesis. Annu. Rev. Plant. Biol. **45:** 369-392.

Balistrieri, L. S., and J. W. Murray. 1986. The surface chemistry of sediments from the Panama Basin: The influence of Mn-oxides on metal adsorption. Geochim. Cosmochim. Ac. **50:** 2235-2243.

Barbeau, K., E. Kujawinski, and J. Moffett. 2001. Remineralization and recycling of iron, thorium and organic carbon by heterotrophic marine protists in culture. Aquat. Microb. Ecol. **24:** 69-81.

Behrenfeld, M. J., and Z. S. Kolber. 1999. Widespread iron limitation of phytoplankton in the South Pacific Ocean. Science **283:** 840-843.

Berger, C. J., S. M. Lippiatt, M. G. Lawrence, and K. W. Bruland. 2008. Application of a chemical leach technique for estimating labile particulate aluminum, iron, and manganese in the Columbia River plume and coastal waters off Oregon and Washington. J. Geophys. Res. Oceans **113:** C00B01.

Bidle, K. D., and F. Azam. 1999. Accelerated dissolution of diatom silica by marine bacterial assemblages. Nature **397:** 508-512.

Biller, D. V., and K. W. Bruland. 2012. Analysis of Mn, Fe, Co, Ni, Cu, Zn, Cd, and Pb in seawater using the Nobias-chelate PA1 resin and magnetic sector inductively coupled plasma mass spectrometry (ICP-MS). Mar. Chem. **130:** 12-20.

Blackburn, S. I., C. J. Bolch, K. A. Haskard, and G. M. Hallegraeff. 2001. Reproductive compatibility among four global populations of the toxic dinoflagellate *Gymnodinium catenatum* (*Dinophyceae*). Phycologia **40:** 78-87.

Boutorh, J., B. Moriceau, M. Gallinari, O. Ragueneau, and E. Bucciarelli. 2016. Effect of trace metal‐limited growth on the postmortem dissolution of the marine diatom *Pseudo‐nitzschia delicatissima*. Global Biogeochem. Cycles **30:** 57-69.

Bowie, A. R., D. Lannuzel, T. A. Remenyi, T. Wagener, P. J. Lam, P. W. Boyd, C. Guieu, A. T. Townsend, and T. W. Trull. 2009. Biogeochemical iron budgets of the Southern Ocean south of Australia: Decoupling of iron and nutrient cycles in the subantarctic zone by the summertime supply. Global Biogeochem. Cycles **23**.

Bown, J., M. Boye, and D. M. Nelson. 2012. New insights on the role of organic speciation in the biogeochemical cycle of dissolved cobalt in the southeastern Atlantic and the Southern Ocean. Biogeosciences **9:** 2719-2736.

Boyd, P., and M. Ellwood. 2010. The biogeochemical cycle of iron in the ocean. Nature Geosci. **3:** 675.

Boyd, P., and T. Trull. 2007. Understanding the export of biogenic particles in oceanic waters: is there consensus? Prog. Oceanogr. **72:** 276-312.

Boyd, P. W., M. J. Ellwood, A. Tagliabue, and B. S. Twining. 2017. Biotic and abiotic retention, recycling and remineralization of metals in the ocean. Nat. Geosci. **10:** 167-173.

Boyd, P. W., T. Jickells, C. Law, S. Blain, E. Boyle, K. Buesseler, K. Coale, J. Cullen, H. J. De Baar, and M. Follows. 2007. Mesoscale iron enrichment experiments 1993-2005: Synthesis and future directions. Science **315:** 612-617.

Boyle, E. A., S. S. Huested, and S. P. Jones. 1981. On the distribution of copper, nickel, and cadmium in the surface waters of the North Atlantic and North Pacific Ocean. J. Geophys. Res. Oceans **86:** 8048-8066.

Boyle, E. A., J.-M. Lee, Y. Echegoyen, A. Noble, S. Moos, G. Carrasco, N. Zhao, R. Kayser, J. Zhang, and T. Gamo. 2014. Anthropogenic lead emissions in the ocean: The evolving global experiment. Oceanography **27:** 69-75.

Brand, L. E., W. G. Sunda, and R. R. Guillard. 1983. Limitation of marine phytoplankton reproductive rates by zinc, manganese, and iron. Limnol. Oceanogr. **28:** 1182-1198.

---. 1986. Reduction of marine phytoplankton reproduction rates by copper and cadmium. J. Exp. Mar. Bio. Ecol. **96:** 225-250.

Brewer, P., D. Spencer, and D. Robertson. 1972. Trace element profiles from the GEOSECS-II test station in the Sargasso Sea. Earth Planet Sci. Lett. **16:** 111-116.

Browning, T. J., E. P. Achterberg, I. Rapp, A. Engel, E. M. Bertrand, A. Tagliabue, and C. M. Moore. 2017. Nutrient co-limitation at the boundary of an oceanic gyre. Nature **551:** 242.

Browning, T. J., I. Rapp, C. Schlosser, M. Gledhill, E. P. Achterberg, A. Bracher, and F. A. Le Moigne. 2018. Influence of iron, cobalt, and vitamin B12 supply on phytoplankton growth in the tropical East Pacific during the 2015 El Niño. Geophys. Res. Lett.

Bruland, K. W. 1980. Oceanographic distributions of cadmium, zinc, nickel, and copper in the North Pacific. Earth Planet Sci. Lett. **47:** 176-198.

---. 1989. Complexation of zinc by natural organic ligands in the central North Pacific. Limnol. Oceanogr. **34:** 269-285.

---. 1992. Complexation of cadmium by natural organic ligands in the central North Pacific. Limnol. Oceanogr. **37:** 1008-1017.
Bruland, K. W., J. R. Donat, and D. A. Hutchins. 1991. Interactive influences of bioactive trace metals on biological production in oceanic waters. Limnol. Oceanogr. **36:** 1555-1577.
Bruland, K. W., and R. P. Franks. 1983. Mn, Ni, Cu, Zn and Cd in the western North Atlantic, p. 395-414. Trace Metals in Sea Water. Springer.
Bruland, K. W., G. A. Knauer, and J. H. Martin. 1978. Cadmium in northeast Pacific waters Limnol. Oceanogr. **23:** 618-625.
Bruland, K. W., K. J. Orians, and J. P. Cowen. 1994. Reactive trace metals in the stratified central North Pacific. Geochim. Cosmochim. Ac. **58:** 3171-3182.
Brzezinski, M. A. 1985. The Si: C: N ratio of marine diatoms: interspecific variability and the effect of some environmental variables. J. Phycol. **21:** 347-357.
Buck, K. N., and K. W. Bruland. 2005. Copper speciation in San Francisco Bay: a novel approach using multiple analytical windows. Mar. Chem. **96:** 185-198.
---. 2007. The physicochemical speciation of dissolved iron in the Bering Sea, Alaska. Limnol. Oceanogr. **52:** 1800.
Buck, K. N., J. Moffett, K. A. Barbeau, R. M. Bundy, Y. Kondo, and J. Wu. 2012. The organic complexation of iron and copper: an intercomparison of competitive ligand exchange-adsorptive cathodic stripping voltammetry (CLE-ACSV) techniques. Limnol. Oceanogr-Meth. **10:** 496-515.
Buck, K. N., K. E. Selph, and K. A. Barbeau. 2010. Iron-binding ligand production and copper speciation in an incubation experiment of Antarctic Peninsula shelf waters from the Bransfield Strait, Southern Ocean. Mar. Chem. **122:** 148-159.
Bundy, R. M., K. A. Barbeau, and K. N. Buck. 2013. Sources of strong copper-binding ligands in Antarctic Peninsula surface waters. Deep Sea Res. Part 2 Top. Stud. Oceanogr. **90:** 134-146.
Bundy, R. M., M. Jiang, M. Carter, and K. A. Barbeau. 2016. Iron-binding ligands in the southern California current system: mechanistic studies. Frontiers in Marine Science **3:** 27.
Burkhardt, B. G., K. S. Watkins-Brandt, D. Defforey, A. Paytan, and A. E. White. 2014. Remineralization of phytoplankton-derived organic matter by natural populations of heterotrophic bacteria. Mar. Chem. **163:** 1-9.
Caron, D. A., J. C. Goldman, and M. R. Dennett. 1988. Experimental demonstration of the roles of bacteria and bacterivorous protozoa in plankton nutrient cycles. Hydrobiologia **159:** 27-40.
Cheize, M., H. Planquette, J. Fitzsimmons, E. Pelleter, R. Sherrell, C. Lambert, E. Bucciarelli, G. Sarthou, M. Le Goff, and C. Liorzou. in press. Contribution of resuspended sedimentary particles to dissolved iron and manganese in the ocean: An experimental study. Chem. Geol.
Chen, M., W. X. Wang, and L. Guo. 2004. Phase partitioning and solubility of iron in natural seawater controlled by dissolved organic matter. Global Biogeochem. Cycles **18**.
Chung, Y., R. Finkel, M. Bacon, J. Cochran, and S. Krishnaswami. 1983. Intercomparison of 210Pb measurements at GEOSECS station 500 in the northeast Pacific. Earth Planet Sci. Lett. **65:** 393-405.
Chung, Y.-j., and H. Craig. 1983. ^{210}Pb in the Pacific: the GEOSECS measurements of particulate and dissolved concentrations. Earth Planet Sci. Lett. **65:** 406-432.

Coale, K. H. 1991. Effects of iron, manganese, copper, and zinc enrichments on productivity and biomass in the subarctic Pacific. Limnol. Oceanogr. **36:** 1851-1864.
Coale, K. H., and K. W. Bruland. 1990. Spatial and temporal variability in copper complexation in the North Pacific. Deep Sea Res. Part 1 Oceanogr. Res. Papers **37:** 317-336.
Coale, K. H., K. S. Johnson, F. P. Chavez, K. O. Buesseler, R. T. Barber, M. A. Brzezinski, W. P. Cochlan, F. J. Millero, P. G. Falkowski, and J. E. Bauer. 2004. Southern Ocean iron enrichment experiment: carbon cycling in high-and low-Si waters. Science **304:** 408-414.
Coale, K. H., K. S. Johnson, S. E. Fitzwater, R. M. Gordon, S. Tanner, F. P. Chavez, L. Ferioli, C. Sakamoto, P. Rogers, and F. Millero. 1996. A massive phytoplankton bloom induced by an ecosystem-scale iron fertilization experiment in the equatorial Pacific Ocean. Nature **383:** 495-501.
Conway, T. M., and S. G. John. 2014. Quantification of dissolved iron sources to the North Atlantic Ocean. Nature **511:** 212-215.
Coplen, T. B., W. A. Brand, M. Gehre, M. Gröning, H. A. Meijer, B. Toman, and R. M. Verkouteren. 2006. New guidelines for δ 13C measurements. Anal. Chem. **78:** 2439-2441.
Craig, H., S. Krishnaswami, and B. Somayajulu. 1973. 210Pb226Ra: radioactive disequilibrium in the deep sea. Earth Planet Sci. Lett. **17:** 295-305.
Croft, M. T., A. D. Lawrence, E. Raux-Deery, M. J. Warren, and A. G. Smith. 2005. Algae acquire vitamin B12 through a symbiotic relationship with bacteria. Nature **438:** 90.
Croot, P. L., O. Baars, and P. Streu. 2011. The distribution of dissolved zinc in the Atlantic sector of the Southern Ocean. Deep Sea Res. Part 2 Top. Stud. Oceanogr. **58:** 2707-2719.
de Baar, H. J., P. M. Saager, R. F. Nolting, and J. van der Meer. 1994. Cadmium versus phosphate in the world ocean. Mar. Chem. **46:** 261-281.
Dixit, S., P. Van Cappellen, and A. J. van Bennekom. 2001. Processes controlling solubility of biogenic silica and pore water build-up of silicic acid in marine sediments. Mar. Chem. **73:** 333-352.
Duce, R. A., and N. W. Tindale. 1991. Atmospheric transport of iron and its deposition in the ocean. Limnol. Oceanogr. **36:** 1715-1726.
Dupont, C., K. Neupane, J. Shearer, and B. Palenik. 2008a. Diversity, function and evolution of genes coding for putative Ni‐containing superoxide dismutases. Environ. Microbiol. **10:** 1831-1843.
Dupont, C. L., and B. A. Ahner. 2005. Effects of copper, cadmium, and zinc on the production and exudation of thiols by *Emiliania huxleyi*. Limnol. Oceanogr. **50:** 508-515.
Dupont, C. L., K. Barbeau, and B. Palenik. 2008b. Ni uptake and limitation in marine *Synechococcus* strains. Appl. Environ. Microbiol. **74:** 23-31.
Ellwood, M. J. 2004. Zinc and cadmium speciation in subantarctic waters east of New Zealand. Mar. Chem. **87:** 37-58.
Ellwood, M. J., and K. A. Hunter. 2000. The incorporation of zinc and iron into the frustule of the marine diatom *Thalassiosira pseudonana*. Limnol. Oceanogr. **45:** 1517-1524.
Ellwood, M. J., and C. M. Van den Berg. 2000. Zinc speciation in the northeastern Atlantic Ocean. Mar. Chem. **68:** 295-306.
---. 2001. Determination of organic complexation of cobalt in seawater by cathodic stripping voltammetry. Mar. Chem. **75:** 33-47.
Elrod, V. A., W. M. Berelson, K. H. Coale, and K. S. Johnson. 2004. The flux of iron from continental shelf sediments: A missing source for global budgets. Geophys. Res. Lett. **31**.

Fischer, A., J. Kroon, T. Verburg, T. Teunissen, and H. T. Wolterbeek. 2007. On the relevance of iron adsorption to container materials in small-volume experiments on iron marine chemistry: ^{55}Fe-aided assessment of capacity, affinity and kinetics. Mar. Chem. **107:** 533-546.

Fisher, N., J. L. Teyssie, S. Krishnaswami, and M. Baskaran. 1987. Accumulation of Th, Pb, U, and Ra in marine phytoplankton and its geochemical significance. Limnol. Oceanogr. **32:** 131-142.

Fisher, N. S., K. A. Burns, R. Cherry, and M. Heyraud. 1983. Accumulation and cellular distribution of ^{241}Am, ^{210}Po, and ^{210}Pb in two marine algae. Mar. Ecol. Prog. Ser. **11:** 233-237.

Fitzsimmons, J. N., and E. A. Boyle. 2012. An intercalibration between the GEOTRACES GO-FLO and the MITESS/Vanes sampling systems for dissolved iron concentration analyses (and a closer look at adsorption effects). Limnol. Oceanogr-Meth. **10:** 437-450.

Fitzwater, S. E., G. A. Knauer, and J. H. Martin. 1982. Metal contamination and its effect on primary production measurements. Limnol. Oceanogr. **27:** 544-551.

Fowler, S. W., and G. A. Knauer. 1986. Role of large particles in the transport of elements and organic compounds through the oceanic water column. Prog. Oceanogr. **16:** 147-194.

Garber, J. H. 1984. Laboratory study of nitrogen and phosphorus remineralization during the decomposition of coastal plankton and seston. Estuar. Coast. Shelf Sci. **18:** 685-702.

Gehlen, M., L. Beck, G. Calas, A.-M. Flank, A. Van Bennekom, and J. Van Beusekom. 2002. Unraveling the atomic structure of biogenic silica: evidence of the structural association of Al and Si in diatom frustules. Geochim. Cosmochim. Ac. **66:** 1601-1609.

Gledhill, M., and K. N. Buck. 2012. The organic complexation of iron in the marine environment: a review. Front. Microbiol. **29**.

Gledhill, M., and C. M. van den Berg. 1994. Determination of complexation of iron (III) with natural organic complexing ligands in seawater using cathodic stripping voltammetry. Mar. Chem. **47:** 41-54.

Grill, E. V. 1964. Nutrient regeneration from phytoplankton decomposing in seawater. J. Mar. Res. **22:** 51-69.

Gundersen, K., Michaels, A. 1989. Determination of particulate organic carbon and nitrogen, p. 95-97. Bermuda Biological Station for Research, Inc. Bermuda Atlantic Time-series Study.

Hatta, M., C. I. Measures, J. Wu, S. Roshan, J. N. Fitzsimmons, P. Sedwick, and P. Morton. 2015. An overview of dissolved Fe and Mn distributions during the 2010–2011 US GEOTRACES north Atlantic cruises: GEOTRACES GA03. Deep Sea Res. Part 2 Top. Stud. Oceanogr. **116:** 117-129.

Hawco, N. J., P. J. Lam, J.-M. Lee, D. C. Ohnemus, A. E. Noble, N. J. Wyatt, M. C. Lohan, and M. A. Saito. 2018. Cobalt scavenging in the mesopelagic ocean and its influence on global mass balance: Synthesizing water column and sedimentary fluxes. Mar. Chem. **201:** 151-166.

Hawco, N. J., D. C. Ohnemus, J. A. Resing, B. S. Twining, and M. A. Saito. 2016. A dissolved cobalt plume in the oxygen minimum zone of the eastern tropical South Pacific. Biogeosciences **13:** 5697.

Henderson, G. M., R. F. Anderson, J. Adkins, P. Andersson, E. A. Boyle, G. Cutter, H. d. Baar, A. Eisenhauer, R. Francois, K. Orians, T. Gamo, C. German, W. Jenkins, J. Moffett, C. Jeandel, T. Jickells, S. Krishnaswami, D. Mackey, P. Masque, C. I. Measures, J. K.

Moore, R. P. A. Oschlies, R. S. M. Rutgers van der Loeff, M. Sharma, K. v. Damm, and J. Zhang. 2007. GEOTRACES–An international study of the global marine biogeochemical cycles of trace elements and their isotopes. Chem. Erde-Geochem. **67:** 85-131.

Ho, T. Y., A. Quigg, Z. V. Finkel, A. J. Milligan, K. Wyman, P. G. Falkowski, and F. M. Morel. 2003. The elemental composition of some marine phytoplankton. J. Phycol. **39:** 1145-1159.

Holm-Hansen, O., and B. Riemann. 1978. Chlorophyll a determination: improvements in methodology. Oikos**:** 438-447.

Horner, T. J., R. B. Lee, G. M. Henderson, and R. E. Rickaby. 2013. Nonspecific uptake and homeostasis drive the oceanic cadmium cycle. PNAS **110:** 2500-2505.

Huntsman, S. A., and W. G. Sunda. 1980. The role of trace metals in regulating phytoplankton growth with emphasis on Fe, Mn and Cu [iron, manganese, copper]. Stud. Ecol. USA.

Hurd, D. C. 1972. Factors affecting solution rate of biogenic opal in seawater. Earth Planet Sci. Lett. **15:** 411-417.

Hutchins, D. 1995. Iron and the marine phytoplankton community. Prog. Phycol. Res. **11:** 1-50.

Hutchins, D., and K. Bruland. 1994. Grazer-mediated regeneration and assimilation of Fe, Zn and Mn from planktonic prey. Mar. Ecol. Prog. Ser. **110:** 259-259.

Hutchins, D., C. Hare, R. Weaver, Y. Zhang, G. Firme, G. DiTullio, M. Alm, S. Riseman, J. Maucher, and M. Geesey. 2002. Phytoplankton iron limitation in the Humboldt Current and Peru Upwelling. Limnol. Oceanogr. **47:** 997-1011.

Hutchins, D. A., and K. W. Bruland. 1998. Iron-limited diatom growth and Si: N uptake ratios in a coastal upwelling regime. Nature **393:** 561.

Hutchins, D. A., G. R. DiTullio, and K. W. Bruland. 1993. Iron and regenerated production: Evidence for biological iron recycling in two marine environments. Limnol. Oceanogr. **38:** 1242-1255.

Hutchins, D. A., A. E. Witter, A. Butler, and G. W. Luther. 1999. Competition among marine phytoplankton for different chelated iron species. Nature **400:** 858-861.

Jacquot, J. E., and J. W. Moffett. 2015. Copper distribution and speciation across the International GEOTRACES Section GA03. Deep Sea Res. Part 2 Top. Stud. Oceanogr. **116:** 187-207.

Jakuba, R. W., J. W. Moffett, and S. T. Dyhrman. 2008. Evidence for the linked biogeochemical cycling of zinc, cobalt, and phosphorus in the western North Atlantic Ocean. Global Biogeochem. Cycles **22**.

Jannasch, H. W., B. D. Honeyman, and J. W. Murray. 1996. Marine scavenging: the relative importance of mass transfer and reaction rates. Limnol. Oceanogr. **41:** 82-88.

Jickells, T., Z. An, K. K. Andersen, A. Baker, G. Bergametti, N. Brooks, J. Cao, P. Boyd, R. Duce, and K. Hunter. 2005. Global iron connections between desert dust, ocean biogeochemistry, and climate. Science **308:** 67-71.

Jickells, T., and J. Burton. 1988. Cobalt, copper, manganese and nickel in the Sargasso Sea. Mar. Chem. **23:** 131-144.

John, S. G., and T. M. Conway. 2014. A role for scavenging in the marine biogeochemical cycling of zinc and zinc isotopes. Earth Planet Sci. Lett. **394:** 159-167.

Johnson, K. S., V. Elrod, S. Fitzwater, J. Plant, E. Boyle, B. Bergquist, K. Bruland, A. Aguilar‐Islas, K. Buck, and M. Lohan. 2007. Developing standards for dissolved iron in seawater. Eos, Transactions American Geophysical Union **88:** 131-132.

Johnson, K. S., R. M. Gordon, and K. H. Coale. 1997. What controls dissolved iron concentrations in the world ocean? Mar. Chem. **57:** 137-161.
Johnson, K. S., P. M. Stout, W. M. Berelson, and C. M. Sakamoto-Arnold. 1988. Cobalt and copper distributions in the waters of Santa Monica Basin, California. Nature **332:** 527.
Kamatani, A. 1969. Regeneration of inorganic nutrients from diatom decomposition. Jour. Oceanogr. Soc. Japan **25**.
Kamatani, A. 1982. Dissolution rates of silica from diatoms decomposing at various temperatures. Mar. Biol. **68:** 91-96.
King, A. L., K. N. Buck, and K. A. Barbeau. 2012. Quasi-Lagrangian drifter studies of iron speciation and cycling off Point Conception, California. Mar. Chem. **128:** 1-12.
Kirchman, D. L. 1996. Oceanography-Microbial ferrous wheel. Nature **383:** 303-304.
Knauer, G., J. Martin, and R. Gordon. 1982. Cobalt in north-east Pacific waters. Nature **297:** 49.
Knefelkamp, B., K. Carstens, and K. H. Wiltshire. 2007. Comparison of different filter types on chlorophyll-*a* retention and nutrient measurements. J. Exp. Mar. Biol. Ecol. **345:** 61-70.
Krishnaswami, S., B. Somayajulu, and Y. Chung. 1975. $^{210}Pb/^{226}Ra$ disequilibrium in the Santa Barbara Basin. Earth Planet Sci. Lett. **27:** 388-392.
Kuma, K., J. Nishioka, and K. Matsunaga. 1996. Controls on iron (III) hydroxide solubility in seawater: the influence of pH and natural organic chelators. Limnol. Oceanogr. **41:** 396-407.
Lagerström, M., M. Field, M. Séguret, L. Fischer, S. Hann, and R. Sherrell. 2013. Automated on-line flow-injection ICP-MS determination of trace metals (Mn, Fe, Co, Ni, Cu and Zn) in open ocean seawater: Application to the GEOTRACES program. Mar. Chem. **155:** 71-80.
Landing, W. M., and K. W. Bruland. 1987. The contrasting biogeochemistry of iron and manganese in the Pacific Ocean. Geochim. Cosmochim. Ac. **51:** 29-43.
Lane, T. W., and F. M. Morel. 2000a. A biological function for cadmium in marine diatoms. Proc. Nat. Acad. Sci. **97:** 4627-4631.
---. 2000b. Regulation of carbonic anhydrase expression by zinc, cobalt, and carbon dioxide in the marine diatom *Thalassiosira weissflogii*. Plant Phys. **123:** 345-352.
Lee, B.-G., and N. S. Fisher. 1994. Effects of sinking and zooplankton grazing on the release of elements from planktonic debris. Mar. Ecol. Prog. Ser.**:** 271-281.
Lee, B. G., and N. S. Fisher. 1993. Microbially mediated cobalt oxidation in seawater revealed by radiotracer experiments. Limnol. Oceanogr. **38:** 1593-1602.
Lee, J.-M., E. A. Boyle, Y. Echegoyen-Sanz, J. N. Fitzsimmons, R. Zhang, and R. A. Kayser. 2011. Analysis of trace metals (Cu, Cd, Pb, and Fe) in seawater using single batch nitrilotriacetate resin extraction and isotope dilution inductively coupled plasma mass spectrometry. Anal. Chim. Acta. **686:** 93-101.
Liu, X., and F. J. Millero. 2002. The solubility of iron in seawater. Mar. Chem. **77:** 43-54.
Maldonado, M. T., and N. M. Price. 1999. Utilization of iron bound to strong organic ligands by plankton communities in the subarctic Pacific Ocean. Deep Sea Res. Part 2 Top. Stud. Oceanogr. **46:** 2447-2473.
Marchetti, A., and N. Cassar. 2009. Diatom elemental and morphological changes in response to iron limitation: a brief review with potential paleoceanographic applications. Geobiology **7:** 419-431.
Martin, J. H. 1990. Glacial‑interglacial CO_2 change: The iron hypothesis. Paleoceanography **5:** 1-13.

Martin, J. H., and S. E. Fitzwater. 1988. Iron deficiency limits phytoplankton growth in the north-east Pacific subarctic. Nature **331:** 341.

Martin, J. H., M. Gordon, and S. E. Fitzwater. 1991. The case for iron. Limnol. Oceanogr. **36:** 1793-1802.

Martin, J. H., R. M. Gordon, S. Fitzwater, and W. W. Broenkow. 1989. VERTEX: phytoplankton/iron studies in the Gulf of Alaska. Deep Sea Res. Part 1 Oceanogr. Res. Papers **36:** 649-680.

Martin, J. H., R. M. Gordon, and S. E. Fitzwater. 1990. Iron in Antarctic waters. Nature **3:** 156-158.

Martin, J. H., G. A. Knauer, D. M. Karl, and W. W. Broenkow. 1987. VERTEX: carbon cycling in the northeast Pacific. Deep Sea Res. Part 1 Oceanogr. Res. Pap. **34:** 267-285.

Martínez-Garcia, A., A. Rosell-Melé, S. L. Jaccard, W. Geibert, D. M. Sigman, and G. H. Haug. 2011. Southern Ocean dust–climate coupling over the past four million years. Nature **476:** 312.

Mellett, T., M. T. Brown, P. D. Chappell, C. Duckham, J. N. Fitzsimmons, C. P. Till, R. M. Sherrell, M. T. Maldonado, and K. N. Buck. 2017. The biogeochemical cycling of iron, copper, nickel, cadmium, manganese, cobalt, lead, and scandium in a California Current experimental study. Limnol. Oceanogr.**:** S425-S447.

Menzel, D. W., and J. P. Spaeth. 1962. Occurrence of vitamin b12 in the sargasso sea. Limnol. Oceanogr. **7:** 151-154.

Milne, A., W. Landing, M. Bizimis, and P. Morton. 2010. Determination of Mn, Fe, Co, Ni, Cu, Zn, Cd and Pb in seawater using high resolution magnetic sector inductively coupled mass spectrometry (HR-ICP-MS). Anal. Chim. Acta. **665:** 200-207.

Moffett, J. W. 1995. Temporal and spatial variability of copper complexation by strong chelators in the Sargasso Sea. Deep Sea Res. Part 1 Oceanogr. Res. Papers **42:** 1273-1295.

Moffett, J. W., and C. Dupont. 2007. Cu complexation by organic ligands in the sub-arctic NW Pacific and Bering Sea. Deep Sea Res. Part 1 Oceanogr. Res. Papers **54:** 586-595.

Moffett, J. W., and J. Ho. 1996. Oxidation of cobalt and manganese in seawater via a common microbially catalyzed pathway. Geochim. Cosmochim. Ac. **60:** 3415-3424.

Moore, J., and O. Braucher. 2008. Sedimentary and mineral dust sources of dissolved iron to the world ocean. Biogeosciences **5:** 631-656.

Moore, J. K., S. C. Doney, D. M. Glover, and I. Y. Fung. 2002. Iron cycling and nutrient-limitation patterns in surface waters of the World Ocean. Deep Sea Res. Part 2 Top. Stud. Oceanogr. **49:** 463-507.

Moore, W. S., and J. Dymondt. 1988. Correlation of 210Pb removal with organic carbon fluxes in the Pacific Ocean. Nature **331:** 339.

Morel, F., and N. Price. 2003. The biogeochemical cycles of trace metals in the oceans. Science **300:** 944-947.

Morel, F. M., R. J. Hudson, and N. M. Price. 1991. Limitation of productivity by trace metals in the sea. Limnol. Oceanogr. **36:** 1742-1755.

Noble, A. E., C. H. Lamborg, D. C. Ohnemus, P. J. Lam, T. J. Goepfert, C. I. Measures, C. H. Frame, K. L. Casciotti, G. R. DiTullio, and J. Jennings. 2012. Basin‐scale inputs of cobalt, iron, and manganese from the Benguela‐Angola front to the South Atlantic Ocean. Limnol. Oceanogr. **57:** 989-1010.

Nozaki, Y., K. Turekian, and K. Von Damm. 1980. 210Pb in GEOSECS water profiles from the North Pacific. Earth Planet Sci. Lett. **49:** 393-400.

Park, H., B. Song, and F. M. Morel. 2007. Diversity of the cadmium‑containing carbonic anhydrase in marine diatoms and natural waters. Environ. Microbiol. **9:** 403-413.
Parsons, T. R. 1984. A Manual of Chemical & Biological Methods for Seawater Analysis. Permagon Press.
Peers, G., and N. M. Price. 2004. A role for manganese in superoxide dismutases and growth of iron-deficient diatoms. Limnol. Oceanogr. **49:** 1774-1783.
---. 2006. Copper-containing plastocyanin used for electron transport by an oceanic diatom. Nature **441:** 341.
Peers, G., S. A. Quesnel, and N. M. Price. 2005. Copper requirements for iron acquisition and growth of coastal and oceanic diatoms. Limnol. Oceanogr. **50:** 1149-1158.
Plocke, D. J., C. Levinthal, and B. L. Vallee. 1962. Alkaline phosphatase of *Escherichia coli:* a zinc metalloenzyme. Biochemistry **1:** 373-378.
Poorvin, L., J. M. Rinta-Kanto, D. A. Hutchins, and S. W. Wilhelm. 2004. Viral release of iron and its bioavailability to marine plankton. Limnol. Oceanogr. **49:** 1734-1741.
Poulton, A. J., P. M. Holligan, A. Charalampopoulou, and T. R. Adey. 2017. Coccolithophore ecology in the tropical and subtropical Atlantic Ocean: New perspectives from the Atlantic meridional transect (AMT) programme. Prog. Oceanogr. **158:** 150-170.
Price, N., and F. Morel. 1990. Cadmium and cobalt substitution for zinc in a marine diatom. Nature **344:** 658.
---. 1991. Colimitation of phytoplankton growth by nickel and nitrogen. Limnol. Oceanogr. **36:** 1071-1077.
Qi, H., T. B. Coplen, H. Geilmann, W. A. Brand, and J. K. Böhlke. 2003. Two new organic reference materials for δ13C and δ15N measurements and a new value for the δ13C of NBS 22 oil. Rapid Commun. Mass Spectrom. **17:** 2483-2487.
Rapp, I., C. Schlosser, D. Rusiecka, M. Gledhill, and E. P. Achterberg. 2017. Automated preconcentration of Fe, Zn, Cu, Ni, Cd, Pb, Co, and Mn in seawater with analysis using high-resolution sector field inductively-coupled plasma mass spectrometry. Anal. Chim. Acta. **976:** 1-13.
Raven, J. A., M. C. Evans, and R. E. Korb. 1999. The role of trace metals in photosynthetic electron transport in O2-evolving organisms. Photosynth. Res. **60:** 111-150.
Redfield, A. C. 1934. On the proportions of organic derivatives in sea water and their relation to the composition of plankton. James Johnstone
Rickert, D., M. Schlüter, and K. Wallmann. 2002. Dissolution kinetics of biogenic silica from the water column to the sediments. Geochim. Cosmochim. Ac. **66:** 439-455.
Rue, E. L., and K. W. Bruland. 1995. Complexation of iron (III) by natural organic ligands in the Central North Pacific as determined by a new competitive ligand equilibration/adsorptive cathodic stripping voltammetric method. Mar. Chem. **50:** 117-138.
---. 1997. The role of organic complexation on ambient iron chemistry in the equatorial Pacific Ocean and the response of a mesoscale iron addition experiment. Limnol. Oceanogr. **42:** 901-910.
Saito, M. A., and T. J. Goepfert. 2008. Zinc-cobalt colimitation of *Phaeocystis antarctica*. Limnol. Oceanogr. **53:** 266-275.
Saito, M. A., and J. W. Moffett. 2001. Complexation of cobalt by natural organic ligands in the Sargasso Sea as determined by a new high-sensitivity electrochemical cobalt speciation method suitable for open ocean work. Mar. Chem. **75:** 49-68.

Saito, M. A., J. W. Moffett, S. W. Chisholm, and J. B. Waterbury. 2002. Cobalt limitation and uptake in Prochlorococcus. Limnol. Oceanogr. **47:** 1629-1636.
Saito, M. A., G. Rocap, and J. W. Moffett. 2005. Production of cobalt binding ligands in a Synechococcus feature at the Costa Rica upwelling dome. Limnol. Oceanogr. **50:** 279-290.
Sarmiento, J. á., N. Gruber, M. Brzezinski, and J. Dunne. 2004. High-latitude controls of thermocline nutrients and low latitude biological productivity. Nature **427:** 56.
Sarthou, G., D. Vincent, U. Christaki, I. Obernosterer, K. R. Timmermans, and C. P. Brussaard. 2008. The fate of biogenic iron during a phytoplankton bloom induced by natural fertilisation: Impact of copepod grazing. Deep Sea Res. Part 2 Top. Stud. Oceanogr. **55:** 734-751.
Sato, M., S. Takeda, and K. Furuya. 2007. Iron regeneration and organic iron (III)-binding ligand production during in situ zooplankton grazing experiment. Mar. Chem. **106:** 471-488.
Schoffman, H., H. Lis, Y. Shaked, and N. Keren. 2016. Iron–nutrient interactions within phytoplankton. Front. Plant Sci. **7:** 1223.
Schultes, S., C. Lambert, P. Pondaven, R. Corvaisier, S. Jansen, and O. Ragueneau. 2010. Recycling and uptake of $Si(OH)_4$ when protozoan grazers feed on diatoms. Protist **161:** 288-303.
Sclater, F., E. Boyle, and J. Edmond. 1976. On the marine geochemistry of nickel. Earth Planet Sci. Lett. **31:** 119-128.
Semeniuk, D. M., J. T. Cullen, W. K. Johnson, K. Gagnon, T. J. Ruth, and M. T. Maldonado. 2009. Plankton copper requirements and uptake in the subarctic Northeast Pacific Ocean. Deep Sea Res. Part 1 Oceanogr. Res. Papers **56:** 1130-1142.
Sinoir, M., E. C. Butler, A. R. Bowie, M. Mongin, P. N. Nesterenko, and C. S. Hassler. 2012. Zinc marine biogeochemistry in seawater: a review. Mar. Freshwater Res. **63:** 644-657.
Sohrin, Y., and K. W. Bruland. 2011. Global status of trace elements in the ocean. Trends Anal. Chem. **30:** 1291-1307.
Sohrin, Y., S. Urushihara, S. Nakatsuka, T. Kono, E. Higo, T. Minami, K. Norisuye, and S. Umetani. 2008. Multielemental determination of GEOTRACES key trace metals in seawater by ICPMS after preconcentration using an ethylenediaminetriacetic acid chelating resin. Anal. Chem. **80:** 6267-6273.
Somayajulu, B., and H. Craig. 1976. Particulate and soluble ^{210}Pb activities in the deep sea. Earth Planet Sci. Lett. **32:** 268-276.
Spencer, D. W., D. Robertson, K. K. Turekian, and T. Folsom. 1970. Trace element calibrations and profiles at the GEOSECS test station in the northeast Pacific Ocean. J. Geophys. Res. **75:** 7688-7696.
Stauber, J., and T. Florence. 1990. Mechanism of toxicity of zinc to the marine diatomNitzschia closterium. Mar. Biol. **105:** 519-524.
Strzepek, R., M. Maldonado, J. Higgins, J. Hall, K. Safi, S. Wilhelm, and P. Boyd. 2005. Spinning the "Ferrous Wheel": The importance of the microbial community in an iron budget during the FeCycle experiment. Global Biogeochem. Cycles **19**.
Sunda, W. 2012. Feedback interactions between trace metal nutrients and phytoplankton in the ocean. Front. Microbiol. **3:** 204-226.
Sunda, W. G. 1989. Trace metal interactions with marine phytoplankton. Biol. Oceanogr. **6:** 411-442.

Sunda, W. G., and S. A. Huntsman. 1987. Microbial oxidation of manganese in a North Carolina estuary. Limnol. Oceanogr. **32:** 552-564.
---. 1988. Effect of sunlight on redox cycles of manganese in the southwestern Sargasso Sea. Deep Sea Res. **35:** 1297-1317.
---. 1990. Diel cycles in microbial manganese oxidation and manganese redox speciation in coastal waters of the Bahama Islands. Limnol. Oceanogr. **35:** 325-338.
---. 1994. Photoreduction of manganese oxides in seawater. Mar. Chem. **46:** 133-152.
---. 1995a. Cobalt and zinc interreplacement in marine phytoplankton: biological and geochemical implications. Limnol. Oceanogr. **40:** 1404-1417.
---. 1995b. Regulation of copper concentration in the oceanic nutricline by phytoplankton uptake and regeneration cycles. Limnol. Oceanogr. **40:** 132-137.
Sverdrup, H. U., M. W. Johnson, and R. H. Fleming. 1942. The Oceans: Their physics, chemistry, and general biology. Prentice-Hall New York.
Tagliabue, A., A. R. Bowie, P. W. Boyd, K. N. Buck, K. S. Johnson, and M. A. Saito. 2017. The integral role of iron in ocean biogeochemistry. Nature **543:** 51-59.
Takahashi, Y., A. Manceau, N. Geoffroy, M. A. Marcus, and A. Usui. 2007. Chemical and structural control of the partitioning of Co, Ce, and Pb in marine ferromanganese oxides. Geochim. Cosmochim. Ac. **71:** 984-1008.
Tang, D., and F. M. Morel. 2006. Distinguishing between cellular and Fe-oxide-associated trace elements in phytoplankton. Mar. Chem. **98:** 18-30.
Tani, Y., M. Ohashi, N. Miyata, H. Seyama, K. Iwahori, and M. Soma. 2004. Sorption of Co (II), Ni (II), and Zn (II) on biogenic manganese oxides produced by a Mn-oxidizing fungus, strain KR21-2. J. Environ. Sci. Health A **39:** 2641-2660.
Tebo, B. M., J. R. Bargar, B. G. Clement, G. J. Dick, K. J. Murray, D. Parker, R. Verity, and S. M. Webb. 2004. Biogenic manganese oxides: properties and mechanisms of formation. Annu. Rev. Earth Planet Sci. **32:** 287-328.
Tebo, B. M., K. H. Nealson, S. Emerson, and L. Jacobs. 1984. Microbial mediation of Mn (II) and Co (II) precipitation at the O2/H2S interfaces in two anoxic fjords. Limnol. Oceanogr. **29:** 1247-1258.
Tsuda, A., S. Takeda, H. Saito, J. Nishioka, Y. Nojiri, I. Kudo, H. Kiyosawa, A. Shiomoto, K. Imai, and T. Ono. 2003. A mesoscale iron enrichment in the western subarctic Pacific induces a large centric diatom bloom. Science **300:** 958-961.
Twining, B. S., and S. B. Baines. 2013. The trace metal composition of marine phytoplankton. Ann. Rev. Mar. Sci. **5:** 191-215.
Twining, B. S., S. D. Nodder, A. L. King, D. A. Hutchins, G. R. LeCleir, J. M. DeBruyn, E. W. Maas, S. Vogt, S. W. Wilhelm, and P. W. Boyd. 2014. Differential remineralization of major and trace elements in sinking diatoms. Limnol. Oceanogr. **59:** 689-704.
Ussher, S. J., E. P. Achterberg, and P. J. Worsfold. 2004. Marine biogeochemistry of iron. Environ. Chem. **1:** 67-80.
Van Cappellen, P., S. Dixit, and J. van Beusekom. 2002. Biogenic silica dissolution in the oceans: Reconciling experimental and field‐based dissolution rates. Global Biogeochem. Cycles **16:** 23-21-23-10.
Vance, D., S. H. Little, G. F. de Souza, S. Khatiwala, M. C. Lohan, and R. Middag. 2017. Silicon and zinc biogeochemical cycles coupled through the Southern Ocean. Nat. Geosci. **10:** 202.

Von Brand, T., and N. W. Rakestraw. 1941. Decomposition and regeneration of nitrogenous organic matter in sea water: IV. Interrelationship of various stages; Influence of concentration and nature of particulate matter. Biol. Bull. **81:** 63-69.
Von Brand, T., N. W. Rakestraw, and C. E. Renn. 1937. The experimental decomposition and regeneration of nitrogenous organic matter in sea water. Biol. Bull. **72:** 165-175.
---. 1939. Further experiments on the decomposition and regeneration of nitrogenous organic matter in sea water. Biol. Bull. **77:** 285-296.
Von Brand, T., N. W. Rakestraw, and J. W. Zabor. 1942. Decomposition and regeneration of nitrogenous organic matter in sea water: V. Factors influencing the length of the cycle; observations upon the gaseous and dissolved organic nitrogen Biol. Bull. **83:** 273-282.
Vraspir, J. M., and A. Butler. 2009. Chemistry of marine ligands and siderophores. Annu. Rev. Mar. Sci. **1:** 43.
Werner, R. A., and W. A. Brand. 2001. Referencing strategies and techniques in stable isotope ratio analysis. Rapid Commun. Mass Spectrom. **15:** 501-519.
Werner, R. A., B. A. Bruch, and W. A. Brand. 1999. ConFlo III–an interface for high precision δ13C and δ15N analysis with an extended dynamic range. Rapid Commun. Mass Spectrom. **13:** 1237-1241.
Winder, M., and U. Sommer. 2012. Phytoplankton response to a changing climate. Hydrobiologia **698:** 5-16.
Wolfe-Simon, F., V. Starovoytov, J. R. Reinfelder, O. Schofield, and P. G. Falkowski. 2006. Localization and role of manganese superoxide dismutase in a marine diatom. Plant Phys. **142:** 1701-1709.
Wolfe-Simon, F., D. Grzebyk, O. Schofield, and P. G. Falkowski. 2005. The role and evolution of superoxide dismutases in agae. J. Phycol. **41:** 453-465.
Wu, J., and E. A. Boyle. 1997a. Lead in the western North Atlantic Ocean: completed response to leaded gasoline phaseout. Geochim. Cosmochim. Ac. **61:** 3279-3283.
---. 1997b. Low blank preconcentration technique for the determination of lead, copper, and cadmium in small-volume seawater samples by isotope dilution ICPMS. Anal. Chem. **69:** 2464-2470.
Wyatt, N., A. Milne, E. Woodward, A. Rees, T. Browning, H. Bouman, P. Worsfold, and M. Lohan. 2014. Biogeochemical cycling of dissolved zinc along the GEOTRACES South Atlantic transect GA10 at 40 S. Global Biogeochem. Cycles **28:** 44-56.
Xu, Y., L. Feng, P. D. Jeffrey, Y. Shi, and F. M. Morel. 2008. Structure and metal exchange in the cadmium carbonic anhydrase of marine diatoms. Nature **452:** 56.
Xu, Y., and F. M. Morel. 2013. Cadmium in marine phytoplankton. Met Ions Life Sci. **:** 509-528.
Yee, D., and F. M. Morel. 1996. In vivo substitution of zinc by cobalt in carbonic anhydrase of a marine diatom. Limnol. Oceanogr. **41:** 573-577.
Yoshida, M., K. Kuma, S. Iwade, Y. Isoda, H. Takata, and M. Yamada. 2006. Effect of aging time on the availability of freshly precipitated ferric hydroxide to coastal marine diatoms. Mar. Biol. **149:** 379-392.

APPENDIX A:

SUPPLEMENTAL INFORMATION FOR CHAPTER TWO

Table S1. Composition of the GSe/20 media for *Karenia Brevis*, not including the soil extract amendment. After the cells reached stationary phase, 0.75 L of culture in spent media was added to a carboy of 10 L low nutrient seawater (LNSW) for experiment K1. Calculated contributions of these components to the media and to the carboy for K1 are shown based on the initial media and ignore biological uptake. Note that vitamin B_{12} contains a Co cofactor and therefore contributes to total Co concentration.

		Added concentration	
Form	Component	Gse/20 media	K1 carboy
KNO_3	Nitrate (µmol/L)	100	7
K_2HPO_4	Phosphate (µmol/L)	10	0.7
EDTA $Na_2 \cdot 2H_2O$	EDTA (µmol/L)	5	0.35
H_3BO_3	B (µmol/L)	27.5	1.92
$MnCl_2 \cdot 4H_2O$	Mn (nmol/L)	1000	70
$FeCl_3 \cdot 6H_2O$	Fe (nmol/L)	250	17
$CoCl_2 \cdot 6H_2O$	Co (nmol/L)	30	2.1
$ZnCl_2$	Zn (nmol/L)	120	8.4
-	Se (nmol/L)	0.5	0.035
Cyanocobalamin	Vitamin B_{12} (nmol/L)	37	2.6
Biotin	Vitamin H (nmol/L)	0.2	0.014
Thiamine HCl	Vitamin B_1 (nmol/L)	2	0.14

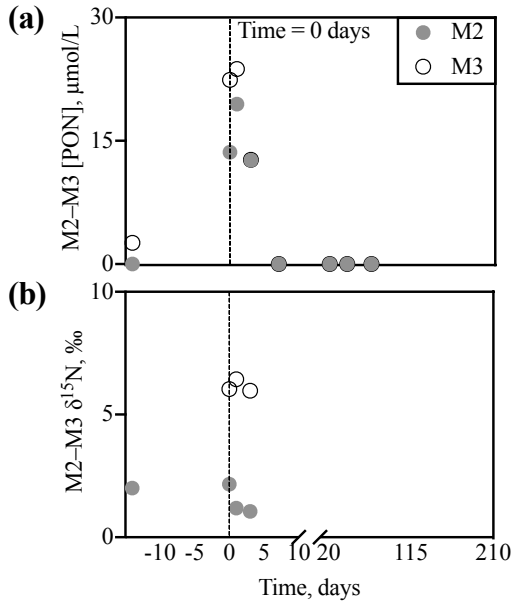

Fig. S1. Particulate organic nitrogen concentration (PON, µM; a) and ^{15}N isotopic composition ($\delta^{15}N$, ‰; b) for mixed assemblages M2 and M3. Stable isotope compositions are normalized to normalized atmospheric air (AT-Air; $\delta^{15}N$) using NIST 8573 and NIST 8574 standards. The dashed line (t = 0 days) represents the start of regeneration; grow-out days are indicated by negative time values. Samples were filtered onto pre-combusted 0.7 µm GF/F glass microfiber filter (Whatman®). Error bars represent the standard deviation of sample replicates when available (see Table S2); no analytical replicates exist because the samples were destroyed during analysis. Samples below the limit of quantification (< LOQ) are plotted as zero for PON, and not plotted for $\delta^{15}N$.

Table S2. Concentrations of chlorophyll *a* (Chl *a*; µg/L), particulate organic carbon (POC; µM), and particulate organic nitrogen (PON; µM) and stable isotope composition for ^{13}C ($\delta^{13}C$, ‰) and ^{15}N ($\delta^{15}N$, ‰) over time for mixed assemblages (M1, M2, M3) and monocultures of *Pseudo-nitzschia dolorosa* (P1) and *Karenia brevis* (K1). Stable isotope compositions are normalized to

normalized to Vienna Pee Dee Belemnite (VPDB; $\delta^{13}C$) and atmospheric air (AT-Air; $\delta^{15}N$) using NIST 8573 and NIST 8574 standards. Day zero represents the start of regeneration; grow-out days for M1, M2, and M3 are indicated by negative time values. Samples were filtered onto 0.7 µm GF/F glass microfiber filter (Whatman®), which were pre-combusted for POC, PON, $\delta^{13}C$, and $\delta^{15}N$ analyses. Analytical replicates were not taken because samples were destroyed during analysis. Averages and standard deviations were calculated from sample replicates when available. If not otherwise specified, n = 1. No data indicates that no data were taken. The "P1 and K1 matrix" sample is representative of the unamended seawater for these incubations and was filtered shipboard. If a sample was below the limit of quantification (LOQ) for one of the replicates of POC or PON (≤ 20 µg/filter) or Chl *a* (≤ 5 raw fluorescence units) , the value is represented by an asterisk (*).

	Time, days	Chl *a*, µg/L	POC, µmol/L	PON, µmol/L	$\delta^{13}C$, NIST 8573/8574 corrected (‰)	$\delta^{15}N$, NIST 8573/8574 corrected (‰)
M1	-13	1.13 ± 0.16 (n = 2)	No data	No data	No data	No data
	0	23.34 ± 2.45 (n = 3)	No data	No data	No data	No data
	1	29.51 ± 5.83 (n = 2)	No data	No data	No data	No data
	3	31.22 ± 1.95 (n = 2)	No data	No data	No data	No data
	6	28.52 (n = 1)	No data	No data	No data	No data
	21	10.96 ± 1.53 (n = 3)	No data	No data	No data	No data
	54	0.63 (n = 1)	No data	No data	No data	No data

	85	1.13 ± 0.25 (n = 4)	No data	No data	No data	No data
	116	0.33 ± 0.03 (n = 2)	No data	No data	No data	No data
	148	0.37 ± 0.00 (n = 2)	No data	No data	No data	No data
M2	-14	0.41 (n = 1)	52.87 (n = 1)	*	-21.57 (n = 1)	2.00 (n = 1)
	0	11.86 (n = 1)	112.39 (n = 1)	13.61 (n = 1)	-18.94 (n = 1)	2.16 (n = 1)
	1	12.44 (n = 1)	145.36 (n = 1)	19.47 (n = 1)	-18.16 (n = 1)	1.19 (n = 1)
	3	4.93 (n = 1)	109.22 (n = 1)	12.63 (n = 1)	-19.44 (n = 1)	1.05 (n = 1)
	7	2.98 (n = 1)	72.64 ± 23.47 (n = 2)	*	-21.37 ± 2.67 (n = 2)	*
	20	*	43.74 (n = 1)	*	-22.36 (n = 1)	*
	40	*	32.28 (n = 1)	*	-25.20 (n = 1)	*
	68	*	28.21 (n = 1)	*	-26.25 (n = 1)	*
	97	*	No data	No data	No data	No data
	124	*	24.11 (n = 1)	*	-26.47 (n = 1)	*
	156	*	22.97 (n = 1)	*	-25.23 (n = 1)	*
	176	*	23.57 (n = 1)	*	-27.72 (n = 1)	*
M3	-14	0.32 (n = 1)	44.57 (n = 1)	2.59 (n = 1)	-21.84 (n = 1)	*
	0	27.00 (n = 1)	219.48 (n = 1)	22.42 (n = 1)	-15.14 (n = 1)	6.04 (n = 1)
	1	23.56 (n = 1)	274.76 (n = 1)	23.73 (n = 1)	No data	6.44 (n = 1)
	3	8.16 (n = 1)	107.73 (n = 1)	12.70 (n = 1)	-15.25 (n = 1)	5.97 (n = 1)
	7	4.41 (n = 1)	65.62 ± 22.21	*	-18.73 ± 1.49 (n = 2)	*

			(n = 2)			
	20	0.81 (n = 1)	32.84 (n = 1)	*	-23.55 (n = 1)	*
	40	*	38.57 (n = 1)	*	-22.55 (n = 1)	*
	68	*	30.06 (n = 1)	*	-25.46 (n = 1)	*
	97	*	No data	No data	No data	No data
	124	*	37.67 (n = 1)	*	-32.46 (n = 1)	*
	156	*	25.14 (n = 1)	*	-26.00 (n = 1)	*
	176	*	16.69 (n = 1)	*	-27.70 (n = 1)	*
P1 and K1 matrix	NA	*	24.97 (n = 1)	*	-24.48 (n = 1)	*
P1	0	9.71 ± 0.77 (n = 2)	76.86 ± 43.64 (n = 2)	*	-23.55 ± 1.65 (n = 2)	*
	1	7.89 ± 0.55 (n = 2)	83.63 ± 62.81 (n = 2)	*	-22.05 ± 2.57 (n = 2)	*
	4	5.08 ± 0.20 (n = 2)	66.09 ± 56.48 (n = 2)	*	-24.37 ± 0.29 (n = 2)	*
	8	2.84 ± 0.06 (n = 2)	75.56 ± 21.56 (n = 2)	*	-26.73 ± 2.96 (n = 2)	*
	20	0.84 ± 0.09 (n = 2)	30.06 ± 4.90 (n = 2)	*	-24.31 ± 0.23 (n = 2)	*
	64	*	26.48 ± 0.76 (n = 2)	*	-25.62 ± 0.78 (n = 2)	*
	89	*	45.94 ± 18.00 (n = 2)	*	-24.32 ± 0.89 (n = 2)	*
	122	*	35.33 (n = 1)	*	-24.57 (n = 1)	*
	151	*	25.42 (n = 1)	*	-27.30 (n = 1)	*
	183	*	20.02 (n = 1)	*	-26.45 (n = 1)	*

K1	0	4.64 ± 0.98 (n = 2)	33.23 (n = 1)	*	-21.47 (n = 1)	*
	1	2.07 ± 1.33 (n = 2)	39.34 (n = 1)	*	-23.47 (n = 1)	*
	3	0.07 (n = 1)	30.59 (n = 1)	*	-22.99 (n = 1)	*
	7	0.09 (n = 1)	38.67 ± 12.37 (n = 2)	*	-23.31 ± 0.26 (n = 2)	*
	22	*	41.67 (n = 1)	*	-24.41 (n = 1)	*
	50	*	39.56 ± 0.13 (n = 2)	*	-26.70 ± 1.87 (n = 2)	*
	86	*	29.68 (n = 1)	*	-25.63 (n = 1)	*
	110	*	27.37 ± 2.02 (n = 2)	*	-25.63 ± 0.55 (n = 2)	*
	144	*	29.09 (n = 1)	*	-26.10 (n = 1)	*
	173	*	26.59 (n = 1)	*	-28.45 (n = 1)	*
	205	*	19.86 (n = 1)	*	-28.53 (n = 1)	*

Table S3. Concentrations (μM) of phosphate, silicate, nitrate + nitrite ("N+N"), nitrite, and ammonium over time for mixed assemblages (M1, M2, M3) and monocultures of *Pseudo-nitzschia dolorosa* (P1) and *Karenia brevis* (K1). Day zero represents the start of regeneration; grow-out days for M1, M2, and M3 are indicated by negative time values. Dissolved fractions for M2, M3, P1, and K1 were obtained by filtration through either a 0.2 μm or 0.4 μm polycarbonate track-etched (PCTE; Whatman®) filter, as indicated. Dissolved fractions for M1 were obtained by filtration through a 0.7 μm GF/F glass microfiber filter (Whatman®). Averages and standard deviations were calculated from analytical replicates on the Lachat Quick8500

QuickChem Flow Injection Analysis system. If not otherwise specified, n = 1. No data indicates that no data were taken. The "P1 and K1 matrix" sample is representative of the unamended seawater for these incubations and was filtered shipboard. Samples below the limit of detection (< LOD) are represented by an asterisk (*). [‡]Sample storage conditions are indicated as follows: (a) all samples frozen, (b) silicate samples refrigerated, (c) silicate and phosphate samples refrigerated, (d) silicate, phosphate, and N+N samples refrigerated. [§]Sample lost during analysis.

	Time, days	Filter size, µm	Storage [‡]	N+N, µM	NO_2, µM	NH_4^+, µM	Si, µM	PO_4^{3-}, µM
M1	-13	0.7	a	34.84	No data	No data	26.93 ± 1.19 (n = 2)	2.33
	-13	0.7	a	35.54	No data	No data	28.46 ± 0.37 (n = 2)	2.47
	0	0.7	a	30.32 ± 0.03 (n = 2)	No data	No data	15.26 ± 0.08 (n = 2)	1.87 ± 0.01 (n = 2)
	0	0.7	a	29.16 ± 0.03 (n = 2)	No data	No data	13.91 ± 0.08 (n = 2)	1.54 ± 0.00 (n = 2)
	0	0.7	a	27.55 ± 0.08 (n = 2)	No data	No data	12.69 ± 0.32 (n = 2)	1.43 ± 0.07 (n = 2)
	1	0.7	a	21.08 ± 0.06 (n = 2)	0.47 ± 0.00 (n = 2)	1.58 ± 0.03 (n = 2)	11.19 ± 0.11 (n = 2)	1.50 ± 0.00 (n = 2)
	1	0.7	a	21.55 ± 0.08 (n = 2)	0.55 ± 0.01 (n = 2)	1.55 ± 0.05 (n = 2)	10.59 ± 0.00 (n = 2)	1.32 ± 0.01 (n = 2)
	3	0.7	a	21.34 ± 0.02 (n = 2)	0.52 ± 0.00 (n = 2)	3.23 ± 0.01 (n = 2)	12.14 ± 0.04 (n = 2)	1.62 ± 0.01 (n = 2)
	3	0.7	a	20.61 ± 0.07 (n = 2)	0.50 ± 0.01 (n = 2)	3.43 ± 0.31 (n = 2)	11.66 ± 0.02 (n = 2)	1.58 ± 0.02 (n = 2)
	6	0.7	a	21.56 ± 0.22	0.47 ± 0.02	6.24 ± 0.02	15.09 ± 0.01	2.04 ± 0.04

				(n = 2)	(n = 2)	(n = 2)	(n = 2)	(n = 2)
	6	0.7	a	20.71 ± 0.05 (n = 2)	0.62 ± 0.04 (n = 2)	6.36 ± 0.02 (n = 2)	15.23 ± 0.04 (n = 2)	2.04 ± 0.01 (n = 2)
	21	0.7	a	17.55 ± 0.01 (n = 2)	0.49 ± 0.03 (n = 2)	6.29 ± 0.08 (n = 2)	16.82 ± 0.08 (n = 2)	1.93 ± 0.02 (n = 2)
	54	0.7	a	21.79 ± 0.01 (n = 2)	0.60 ± 0.00 (n = 2)	6.37 ± 0.17 (n = 2)	27.07 ± 0.64 (n = 2)	2.16 ± 0.00 (n = 2)
	85	0.7	a	§	0.52 ± 0.01 (n = 2)	8.35 ± 0.04 (n = 2)	§	§
	116	0.7	a	22.51 ± 0.01 (n = 2)	0.52 ± 0.00 (n = 2)	15.13 ± 0.06 (n = 2)	28.54 ± 0.01 (n = 2)	2.47 ± 0.00 (n = 2)
	116	0.7	a	21.75 ± 0.02 (n = 2)	0.50 ± 0.03 (n = 2)	13.28 ± 0.04 (n = 2)	28.20 ± 0.14 (n = 2)	2.49 ± 0.00 (n = 2)
	148	0.7	a	21.72 ± 0.07 (n = 2)	0.44 ± 0.02 (n = 2)	9.22 ± 0.08 (n = 2)	28.43 ± 0.01 (n = 2)	2.52 ± 0.00 (n = 2)
	148	0.7	a	19.81 ± 0.00 (n = 2)	0.48 ± 0.01 (n = 2)	11.66 ± 0.17 (n = 2)	25.99 ± 0.23 (n = 2)	2.32 ± 0.02 (n = 2)
M2	-14	0.4	b	43.70 ± 0.88 (n = 3)	0.11 ± 0.04 (n = 3)	*	60.65 ± 0.00 (n = 2)	2.96 ± 0.06 (n = 2)
	0	0.4	c	20.65 ± 0.37 (n = 4)	0.87 ± 0.04 (n = 2)	2.58 ± 0.13 (n = 2)	28.21 ± 0.12 (n = 7)	0.84 ± 0.07 (n = 7)
	1	0.4	b	24.25 ± 0.05 (n = 2)	0.78 ± 0.02 (n = 2)	4.55 ± 0.03 (n = 2)	31.76 ± 0.25 (n = 4)	0.98 ± 0.01 (n = 2)
	3	0.4	b	17.42 ± 0.20 (n = 4)	0.70 ± 0.08 (n = 2)	7.18 ± 0.33 (n = 2)	34.73 ± 0.25 (n = 7)	1.04 ± 0.01 (n = 2)
	7	0.2	b	21.77 ± 0.00 (n = 2)	0.97 ± 0.02 (n = 2)	15.72 ± 0.22 (n = 2)	40.37 ± 0.27 (n = 7)	1.92 ± 0.00 (n = 2)
	20	0.2	b	20.42 ± 0.00 (n = 2)	1.11 ± 0.08 (n = 2)	25.33 ± 1.28 (n = 2)	46.13 ± 0.30 (n = 6)	2.19 ± 0.01 (n = 2)
	40	0.2	b	22.43 ± 0.01	0.93 ± 0.08	25.80 ± 1.57	50.40 ± 0.31	2.71 ± 0.03

				(n = 2)	(n = 2)	(n = 2)	(n = 6)	(n = 2)
	68	0.2	b	17.44 ± 0.10 (n = 2)	0.67 ± 0.04 (n = 2)	19.85 ± 0.44 (n = 2)	52.34 ± 0.32 (n = 6)	2.39 ± 0.00 (n = 2)
	97	0.2	b	36.63 ± 0.81 (n = 2)	*	1.24 ± 0.09 (n = 2)	50.07 ± 0.01 (n = 2)	2.29 ± 0.08 (n = 2)
	124	0.2	b	43.12 ± 0.28 (n = 2)	*	1.13 ± 0.09 (n = 2)	51.29 ± 0.01 (n = 2)	2.80 ± 0.02 (n = 2)
	156	0.2	b	50.68	*	0.80	59.04 ± 0.08 (n = 2)	3.64 ± 0.06 (n = 2)
	176	0.2	b	51.52	*	0.77 ± 0.00 (n = 2)	58.87 ± 0.05 (n = 4)	3.28 ± 0.13 (n = 3)
M3	-14	0.4	b	59.32 ± 0.17 (n = 2)	*	1.27 ± 0.01 (n = 2)	58.28 ± 0.03 (n = 2)	2.74 ± 0.06 (n = 3)
	0	0.4	a	*	*	0.76 ± 0.05 (n = 2)	4.74 ± 0.09 (n = 7)	*
	1	0.4	b	*	*	*	4.40 ± 0.15 (n = 4)	*
	3	0.4	b	*	*	2.33 ± 0.04 (n = 2)	19.87 ± 0.14 (n = 4)	0.19 ± 0.00 (n = 2)
	7	0.2	b	*	*	5.33 ± 0.01 (n = 2)	26.35 ± 0.19 (n = 6)	0.39 ± 0.02 (n = 4)
	20	0.2	b	*	*	25.88 ± 0.78 (n = 2)	44.21 ± 0.28 (n = 6)	1.51 ± 0.01 (n = 2)
	40	0.2	b	*	0.14 ± 0.00 (n = 2)	43.49 ± 3.28 (n = 2)	53.44 ± 0.34 (n = 6)	2.22 ± 0.02 (n = 2)
	68	0.2	b	*	0.17 ± 0.02 (n = 2)	41.59 ± 0.34 (n = 2)	57.40 ± 0.36 (n = 6)	3.04 ± 0.08 (n = 4)
	97	0.2	b	7.12 ± 0.10 (n = 2)	2.43 ± 0.06 (n = 3)	44.45 ± 0.44 (n = 4)	56.38 ± 0.01 (n = 2)	3.05 ± 0.15 (n = 4)
	124	0.2	b	10.83 ± 0.04	3.74 ± 0.09	42.14 ± 0.43	58.08 ± 0.03	3.11 ± 0.32

				(n = 2)	(n = 3)	(n = 4)	(n = 2)	(n = 4)
	156	0.2	b	68.74	53.49 ± 0.20 (n = 2)	0.49 ± 0.08 (n = 2)	63.14 ± 0.13 (n = 2)	4.11 ± 0.35 (n = 2)
	176	0.2	b	75.90	33.85 ± 0.12 (n = 2)	0.61 ± 0.09 (n = 2)	66.98 ± 0.28 (n = 2)	3.76 ± 0.06 (n = 2)
P1 and K1 matrix	NA	NA	d	*	*	*	*	*
P1	0	0.2	a	*	*	0.92 ± 0.23 (n = 4)	*	*
	1	0.2	a	*	0.30 ± 0.01 (n = 4)	*	*	*
	4	0.2	a	*	0.32 ± 0.02 (n = 2)	1.06	*	*
	8	0.2	a	*	0.33 ± 0.02 (n = 3)	1.38 ± 0.14 (n = 4)	*	*
	20	0.2	a	*	0.33 ± 0.01 (n = 5)	1.22 ± 0.08 (n = 4)	2.89 ± 0.64 (n = 8)	0.10 ± 0.02 (n = 6)
	64	0.2	b	*	0.35 ± 0.01 (n = 3)	2.44 ± 0.06 (n = 2)	4.88 ± 0.01 (n = 4)	0.16 ± 0.02 (n = 4)
	89	0.2	b	*	0.36	1.34 ± 0.08 (n = 2)	5.13 ± 0.01 (n = 4)	0.11 ± 0.01 (n = 2)
	122	0.2	b	*	*	2.32 ± 0.03 (n = 2)	4.86 ± 0.00 (n = 2)	0.14 ± 0.02 (n = 4)
	151	0.2	b	*	*	2.62 ± 0.24 (n = 2)	4.96 ± 0.01 (n = 2)	0.16 ± 0.01 (n = 4)
	183	0.2	b	*	*	2.09 ± 0.02 (n = 2)	6.30 ± 0.22 (n = 3)	0.14 ± 0.02 (n = 3)
K1	0	0.2	d	*	*	0.73	3.42 ± 0.11 (n = 2)	*
	1	0.2	d	*	*	0.76 ± 0.02	3.63 ± 0.02	*

						(n = 2)	(n = 2)	
	3	0.2	d	*	*	0.79 ± 0.02 (n = 2)	3.48 ± 0.08 (n = 2)	*
	7	0.2	d	*	*	0.96 ± 0.08 (n = 2)	3.66	0.10 ± 0.01 (n = 2)
	22	0.2	a	*	0.34 ± 0.02 (n = 2)	0.83 ± 0.01 (n = 2)	4.16 ± 0.02 (n = 3)	0.18 ± 0.01 (n = 5)
	50	0.4	b	*	0.33 ± 0.00 (n = 2)	1.14 ± 0.00 (n = 2)	4.19	0.28 ± 0.00 (n = 2)
	86	0.2	b	*	0.36 ± 0.02 (n = 2)	1.01 ± 0.11 (n = 2)	4.42 ± 0.01 (n = 2)	0.26 ± 0.04 (n = 4)
	110	0.2	b	*	0.33 ± 0.02 (n = 2)	1.14 ± 0.04 (n = 2)	4.30 ± 0.03 (n = 4)	0.29 ± 0.01 (n = 3)
	144	0.2	b	*	*	1.97 ± 0.08 (n = 2)	3.85 ± 0.00 (n = 2)	0.29 ± 0.02 (n = 4)
	173	0.2	b	*	*	1.84	3.93 ± 0.01 (n = 2)	0.28 ± 0.02 (n = 3)
	205	0.2	b	*	*	1.27	5.55 ± 0.02 (n = 2)	0.34 ± 0.02 (n = 2)

Table S4. Concentrations of trace metals (nM) manganese (Mn), iron (Fe), cobalt (Co), nickel (Ni), copper (Cu), zinc (Zn), cadmium (Cd), and lead (Pb) over time for mixed assemblages (M1, M2, M3) and monocultures *of Pseudo-nitzschia dolorosa* (P1) and *Karenia brevis* (K1). Day zero represents the start of regeneration; grow-out days for M1, M2, and M3 are indicated by negative time values. Dissolved fractions were obtained by filtration through either a 0.2 µm or 0.4 µm polycarbonate track-etched (PCTE; Whatman®) filter, as indicated. Averages and standard deviations were calculated from analytical replicates on seaFAST (SeaFAST Pico^{TM}). If not otherwise specified, n = 1. All samples were run on the same seaFAST column except M1 -

13 and 0. ^{57}Fe was calculated by subtracting 2.119% natural abundance ^{57}Fe present in Fe measurement. If Fe was below the limit of detection (< LOD), no subtraction was performed. No data indicates that no data were taken. The "P1 and K1 matrix" sample is representative of the unamended seawater for these incubations and was filtered shipboard. Sample < LOD are represented by an asterisk (*).

	Time, days	Filter size, µm	Mn, nM	Fe, nM	^{57}Fe, nM	Co, nM	Ni, nM	Cu, nM	Zn, nM	Cd, nM	Pb, nM
M1	-13	0.2	5.48	3.36	No data	0.194	3.09	2.10	1.69	0.0410	0.0595
	0	0.2	2.02	2.81	No data	0.164	3.06	1.80	0.71	0.0150	0.0342
	1	0.2	1.60 ± 0.05 (n = 2)	0.90 ± 0.02 (n = 2)	No data	0.092 ± 0.005 (n = 2)	2.45 ± 0.08 (n = 2)	1.73 ± 0.09 (n = 2)	15.04 ± 0.61 (n = 2)	0.0070 ± 0.0005 (n = 2)	0.0564 ± 0.0021 (n = 2)
	3	0.2	2.96 ± 0.14 (n = 2)	1.94 ± 0.08 (n = 2)	No data	0.133 ± 0.009 (n = 2)	2.53 ± 0.13 (n = 2)	1.71 ± 0.12 (n = 2)	3.26 ± 0.21 (n = 2)	0.0161 ± 0.0002 (n = 2)	0.0409 ± 0.0017 (n = 2)
	6	0.2	4.28 ± 0.16 (n = 2)	1.99 ± 0.10 (n = 2)	No data	0.168 ± 0.002 (n = 2)	2.80 ± 0.08 (n = 2)	2.01 ± 0.01 (n = 2)	3.63 ± 0.03 (n = 2)	0.0284 ± 0.0010 (n = 2)	0.0435 ± 0.0009 (n = 2)
	21	0.2	3.45 ± 0.04 (n = 2)	1.54 ± 0.03 (n = 2)	No data	0.165 ± 0.004 (n = 2)	2.40 ± 0.02 (n = 2)	1.58 ± 0.01 (n = 2)	2.88 ± 0.07 (n = 2)	0.0296 ± 0.0025 (n = 2)	0.0397 ± 0.0001 (n = 2)
	54	0.2	0.33 ± 0.00 (n = 2)	1.29 ± 0.00 (n = 2)	No data	0.159 ± 0.002 (n = 2)	2.43 ± 0.03 (n = 2)	1.57 ± 0.07 (n = 2)	3.40 ± 0.22 (n = 2)	0.0351 ± 0.0012 (n = 2)	0.0450 ± 0.0007 (n = 2)
	85	0.2	0.52 ± 0.01 (n = 2)	1.83 ± 0.03 (n = 2)	No data	0.163 ± 0.013 (n = 2)	2.44 ± 0.09 (n = 2)	3.23 ± 0.11 (n = 2)	4.87 ± 0.25 (n = 2)	0.0344 ± 0.0003 (n = 2)	0.0440 ± 0.0014 (n = 2)
	116	0.2	0.67 ± 0.02 (n = 2)	7.11 ± 0.15 (n = 2)	No data	0.181 ± 0.001 (n = 2)	3.41 ± 0.01 (n = 2)	1.78 ± 0.05 (n = 2)	3.99 ± 0.13 (n = 2)	0.0365 ± 0.0020 (n = 2)	0.1080 ± 0.0035 (n = 2)
	148	0.2	0.62 ± 0.02 (n = 2)	5.78 ± 0.15 (n = 2)	No data	0.177 ± 0.008 (n = 2)	3.07 ± 0.11 (n = 2)	1.70 ± 0.07 (n = 2)	6.70 ± 0.29 (n = 2)	0.0403 ± 0.0010 (n = 2)	0.0535 ± 0.0028 (n = 2)
M2	-14	0.4	17.85 ± 0.34 (n = 2)	8.66 ± 0.03 (n = 2)	2.41 ± 0.00 (n = 2)	0.249 ± 0.004 (n = 2)	3.48 ± 0.09 (n = 2)	3.30 ± 0.08 (n = 2)	5.39 ± 0.01 (n = 2)	0.0821 ± 0.0059 (n = 2)	0.0276 ± 0.0014 (n = 2)
	0	0.4	8.55 ± 0.02 (n = 2)	3.13 ± 0.10 (n = 2)	0.77 ± 0.02 (n = 2)	0.228 ± 0.002 (n = 2)	3.16 ± 0.00 (n = 2)	2.88 ± 0.06 (n = 2)	3.52 ± 0.05 (n = 2)	0.0260 ± 0.0005 (n = 2)	0.0240 ± 0.0001 (n = 2)

	1	0.4	7.40 ± 0.26 (n = 2)	4.01 ± 0.06 (n = 2)	0.79 ± 0.00 (n = 2)	0.232 ± 0.013 (n = 2)	3.34 ± 0.04 (n = 2)	2.90 ± 0.15 (n = 2)	4.11 ± 0.12 (n = 2)	0.0180 ± 0.0008 (n = 2)	0.0487 ± 0.0058 (n = 2)
	3	0.4	4.23 ± 0.06 (n = 2)	3.43 ± 0.05 (n = 2)	0.79 ± 0.02 (n = 2)	0.233 ± 0.005 (n = 2)	3.06 ± 0.14 (n = 2)	2.81 ± 0.13 (n = 2)	6.66 ± 0.29 (n = 2)	0.0238 ± 0.0011 (n = 2)	0.0359 ± 0.0268 (n = 2)
	7	0.4	1.67 ± 0.01 (n = 2)	4.04 ± 0.08 (n = 2)	0.76 ± 0.00 (n = 2)	0.237 ± 0.004 (n = 2)	2.98 ± 0.03 (n = 2)	2.72 ± 0.06 (n = 2)	3.68 ± 0.04 (n = 2)	0.0525 ± 0.0013 (n = 2)	0.0176 ± 0.0007 (n = 2)
	7	0.2	1.71 ± 0.08 (n = 2)	4.22 ± 0.16 (n = 2)	0.89 ± 0.02 (n = 2)	0.238 ± 0.016 (n = 2)	3.01 ± 0.07 (n = 2)	2.75 ± 0.17 (n = 2)	4.01 ± 0.13 (n = 2)	0.0554 ± 0.0020 (n = 2)	0.0225 ± 0.0010 (n = 2)
	20	0.2	0.56 ± 0.01 (n = 2)	2.47 ± 0.07 (n = 2)	0.59 ± 0.01 (n = 2)	0.237 ± 0..008 (n = 2)	2.84 ± 0.09 (n = 2)	2.56 ± 0.14 (n = 2)	7.10 ± 0.12 (n = 2)	0.0723 ± 0.0076 (n = 2)	0.0203 ± 0.0023 (n = 2)
	40	0.2	0.44 ± 0.02 (n = 4)	2.58 ± 0.18 (n = 4)	0.65 ± 0.13 (n = 4)	0.241 ± 0.016 (n = 4)	2.85 ± 0.18 (n = 4)	2.57 ± 0.10 (n = 4)	7.38 ± 0.42 (n = 4)	0.0764 ± 0.0042 (n = 4)	0.0126 ± 0.0013 (n = 4)
	68	0.2	0.32 ± 0.01 (n = 2)	1.80 ± 0.03 (n = 2)	0.41 ± 0.01 (n = 2)	0.227 ± 0.002 (n = 2)	2.79 ± 0.09 (n = 2)	2.60 ± 0.16 (n = 2)	15.41 ± 0.63 (n = 2)	0.0854 ± 0.0031 (n = 2)	0.0138 ± 0.0002 (n = 2)
	97	0.2	0.21 ± 0.02 (n = 4)	1.68 ± 0.17 (n = 4)	0.43 ± 0.07 (n = 4)	0.241 ± 0.029 (n = 4)	2.87 ± 0.12 (n = 4)	2.38 ± 0.16 (n = 2)	6.36 ± 0.41 (n = 4)	0.0825 ± 0.0064 (n = 4)	0.0118 ± 0.0015 (n = 4)
	124	0.2	0.30 ± 0.02 (n = 2)	1.74 ± 0.06 (n = 2)	0.37 ± 0.02 (n = 2)	0.233 ± 0.009 (n =2)	2.89 ± 0.11 (n = 2)	2.53 ± 0.16 (n = 2)	17.13 ± 1.03 (n = 2)	0.0806 ± 0.0008 (n = 2)	0.0165 ± 0.0005 (n = 2)
	156	0.2	0.61 ± 0.01 (n = 2)	4.20 ± 0.32 (n = 2)	0.81 ± 0.01 (n = 2)	0.219 ± 0.005 (n =2)	3.38 ± 0.00 (n = 2)	2.85 ± 0.04 (n = 2)	14.44 ± 0.27 (n = 2)	0.0737 ± 0.0029 (n = 2)	0.0137 ± 0.0016 (n = 2)
	176	0.2	0.27 ± 0.01 (n = 2)	3.56 ± 0.89 (n = 2)	0.75 ± 0.00 (n = 2)	0.211 ± 0.003 (n =2)	3.43 ± 0.00 (n = 2)	3.36 ± 0.43 (n = 2)	7.76 ± 0.05 (n = 2)	0.0741 ± 0.0030 (n = 2)	0.0101 ± 0.0000 (n = 2)
M3	-14	0.4	18.39 ± 0.05 (n = 2)	13.41 ± 0.19 (n = 2)	2.96 ± 0.05 (n = 2)	0.256 ± 0.001 (n =2)	3.54 ± 0.05 (n = 2)	3.46 ± 0.07 (n = 2)	2.61 ± 0.02 (n = 2)	0.0808 ± 0.0019 (n = 2)	0.0345 ± 0.0013 (n = 2)
	0	0.4	6.30 ± 0.21 (n = 2)	2.45 ± 0.03 (n = 2)	0.46 ± 0.01 (n = 2)	0.233 ± 0.007 (n =2)	3.37 ± 0.12 (n = 2)	2.73 ± 0.12 (n = 2)	1.91 ± 0.03 (n = 2)	0.0103 ± 0.0029 (n = 2)	0.0176 ± 0.0012 (n = 2)
	1	0.4	8.53 ± 0.15 (n = 2)	3.01 ± 0.07 (n = 2)	0.54 ± 0.01 (n = 2)	0.234 ± 0.006 (n =2)	3.59 ± 0.06 (n = 2)	2.49 ± 0.06 (n = 2)	3.79 ± 0.04 (n = 2)	0.0075 ± 0.0008 (n = 2)	0.0274 ± 0.0018 (n = 2)
	3	0.4	10.75 ± 0.16 (n = 2)	2.87 ± 0.04 (n = 2)	0.54 ± 0.00 (n = 2)	0.241 ± 0.013 (n =2)	3.40 ± 0.06 (n = 2)	2.48 ± 0.05 (n = 2)	9.51 ± 0.08 (n = 2)	0.0128 ± 0.0003 (n = 2)	0.0211 ± 0.0007 (n = 2)
	7	0.4	4.83 ± 0.15 (n = 2)	2.99 ± 0.05 (n = 2)	0.54 ± 0.01 (n = 2)	0.240 ± 0.013 (n =2)	3.45 ± 0.10 (n = 2)	2.44 ± 0.11 (n = 2)	5.39 ± 0.85 (n = 2)	0.0151 ± 0.0022 (n = 2)	0.0189 ± 0.0005 (n = 2)
	7	0.2	4.96 ± 0.24 (n = 2)	2.47 ± 0.06 (n = 2)	0.57 ± 0.00 (n = 2)	0.240 ± 0.019 (n =2)	3.46 ± 0.15 (n = 2)	2.43 ± 0.09 (n = 2)	4.12 ± 0.14 (n = 2)	0.0120 ± 0.0011 (n = 2)	0.0133 ± 0.0003 (n = 2)

	20	0.2	1.31 ± 0.07 (n = 2)	1.81 ± 0.06 (n = 2)	0.41 ± 0.02 (n = 2)	0.244 ± 0.010 (n =2)	3.27 ± 0.14 (n = 2)	2.21 ± 0.12 (n = 2)	1.80 ± 0.08 (n = 2)	0.0515 ± 0.0059 (n = 2)	0.0158 ± 0.0012 (n = 2)
	40	0.2	0.54 ± 0.01 (n = 2)	1.90 ± 0.05 (n = 2)	0.41 ± 0.01 (n = 2)	0.257 ± 0.001 (n =2)	3.33 ± 0.11 (n = 2)	2.20 ± 0.14 (n = 2)	5.97 ± 0.28 (n = 2)	0.0657 ± 0.0044 (n = 2)	0.0132 ± 0.0013 (n = 2)
	68	0.2	1.94 ± 0.09 (n = 2)	5.25 ± 0.19 (n = 2)	0.73 ± 0.03 (n = 2)	0.261 ± 0.010 (n =2)	3.48 ± 0.14 (n = 2)	2.61 ± 0.15 (n = 2)	12.09 ± 0.63 (n = 2)	0.0760 ± 0.0030 (n = 2)	0.0172 ± 0.0015 (n = 2)
	97	0.2	0.75 ± 0.01 (n = 2)	4.67 ± 0.04 (n = 2)	0.94 ± 0.01 (n = 2)	0.260 ± 0.005 (n =2)	3.66 ± 0.02 (n = 2)	3.09 ± 0.13 (n = 2)	6.98 ± 0.17 (n = 2)	0.0471 ± 0.0053 (n = 2)	0.0170 ± 0.0102 (n = 2)
	124	0.2	0.73 ± 0.01 (n = 2)	6.01 ± 0.11 (n = 2)	0.97 ± 0.03 (n = 2)	0.273 ± 0.012 (n =2)	3.64 ± 0.18 (n = 2)	3.31 ± 0.18 (n = 2)	16.69 ± 0.87 (n = 2)	0.0865 ± 0.0059 (n = 2)	0.0107 ± 0.0003 (n = 2)
	156	0.2	0.39 ± 0.00 (n = 2)	4.46 ± 0.12 (n = 2)	1.13 ± 0.00 (n = 2)	0.276 ± 0.026 (n =2)	3.59 ± 0.06 (n = 2)	3.33 ± 0.00 (n = 2)	7.88 ± 0.02 (n = 2)	0.0777 ± 0.0001 (n = 2)	0.0083 ± 0.0005 (n = 2)
	176	0.2	0.27 ± 0.00 (n = 2)	5.04 ± 0.14 (n = 2)	1.11 ± 0.01 (n = 2)	0.253 ± 0.006 (n =2)	3.52 ± 0.02 (n = 2)	3.32 ± 0.04 (n = 2)	6.77 ± 0.19 (n = 2)	0.0737 ± 0.0010 (n = 2)	0.0068 ± 0.0002 (n = 2)
P1 and K1 mat-rix	NA	NA	1.51 ± 0.03 (n = 2)	0.33 ± 0.00 (n = 2)	No data	0.042 ± 0.001 (n =2)	2.14 ± 0.02 (n = 2)	1.80 ± 0.04 (n = 2)	1.30 ± 0.04 (n = 2)	0.0008 ± 0.0013 (n = 2)	0.0140 ± 0.0002 (n = 2)
P1	0	0.2	4.03 ± 0.09 (n = 2)	8.21 ± 0.15 (n = 2)	No data	0.066 ± 0.004 (n =2)	2.24 ± 0.03 (n = 2)	2.15 ± 0.06 (n = 2)	9.58 ± 0.40 (n = 2)	0.0044 ± 0.0006 (n = 2)	0.0219 ± 0.0012 (n = 2)
	0	0.2	3.79 ± 0.18 (n = 2)	7.93 ± 0.45 (n = 2)	No data	0.064 ± 0.005 (n =2)	2.15 ± 0.08 (n = 2)	2.02 ± 0.04 (n = 2)	9.24 ± 0.31 (n = 2)	0.0035 ± 0.0017 (n = 2)	0.0700 ± 0.0045 (n = 2)
	1	0.2	4.27 ± 0.27 (n = 2)	8.93 ± 0.43 (n = 2)	No data	0.068 ± 0.004 (n =2)	2.24 ± 0.17 (n = 2)	1.93 ± 0.18 (n = 2)	9.58 ± 0.75 (n = 2)	0.0114 ± 0.0007 (n = 2)	0.0288 ± 0.0038 (n = 2)
	1	0.2	4.28 ± 0.05 (n = 2)	9.88 ± 1.36 (n = 2)	No data	0.069 ± 0.002 (n =2)	2.37 ± 0.07 (n = 2)	2.04 ± 0.05 (n = 2)	11.14 ± 0.61 (n = 2)	0.0083 ± 0.0012 (n = 2)	0.0237 ± 0.0008 (n = 2)
	4	0.2	4.26 ± 0.21 (n = 2)	5.69 ± 0.15 (n = 2)	No data	0.068 ± 0.008 (n =2)	2.14 ± 0.10 (n = 2)	1.80 ± 0.12 (n = 2)	12.52 ± 0.72 (n = 2)	0.0181 ± 0.0011 (n = 2)	0.0293 ± 0.0020 (n = 2)
	4	0.2	4.29 ± 0.24 (n = 2)	6.48 ± 0.33 (n = 2)	No data	0.070 ± 0.001 (n =2)	2.13 ± 0.084 (n = 2)	1.79 ± 0.11 (n = 2)	8.44 ± 0.58 (n = 2)	0.0152 ± 0.0016 (n = 2)	0.0229 ± 0.0017 (n = 2)
	8	0.2	4.57 ± 0.25 (n = 2)	4.50 ± 0.27 (n = 2)	No data	0.071 ± 0.007 (n =2)	2.16 ± 0.15 (n = 2)	1.83 ± 0.15 (n = 2)	9.47 ± 0.73 (n = 2)	0.0064 ± 0.0006 (n = 2)	0.0130 ± 0.0011 (n = 2)
	8	0.2	4.34 ± 0.12 (n = 2)	4.30 ± 0.10 (n = 2)	No data	0.071 ± 0.002 (n =2)	2.04 ± 0.09 (n = 2)	1.77 ± 0.06 (n = 2)	11.49 ± 0.56 (n = 2)	0.0065 ± 0.0011 (n = 2)	0.01867 ± 0.0005 (n = 2)
	20	0.2	4.58 ± 0.05 (n = 2)	2.58 ± 0.02 (n = 2)	No data	0.075 ± 0.000 (n =2)	2.11 ± 0.03 (n = 2)	1.72 ± 0.02 (n = 2)	14.41 ± 0.00 (n = 2)	0.0089 ± 0.0017 (n = 2)	0.0068 ± 0.0005 (n = 2)

	20	0.2	4.48 ± 0.10 (n = 2)	2.48 ± 0.03 (n = 2)	No data	0.073 ± 0.001 (n =2)	2.08 ± 0.07 (n = 2)	1.65 ± 0.06 (n = 2)	11.73 ± 0.20 (n = 2)	0.0087 ± 0.0010 (n = 2)	0.0056 ± 0.0003 (n = 2)
	64	0.2	0.50 ± 0.01 (n = 2)	2.42 ± 0.09 (n = 2)	No data	0.069 ± 0.002 (n =2)	2.15 ± 0.06 (n = 2)	1.57 ± 0.06 (n = 2)	21.55 ± 0.09 (n = 2)	0.0340 ± 0.0007 (n = 2)	0.0129 ± 0.0001 (n = 2)
	89	0.2	0.25 ± 0.01 (n = 2)	1.47 ± 0.03 (n = 2)	No data	0.065 ± 0.004 (n =2)	2.02 ± 0.11 (n = 2)	1.38 ± 0.05 (n = 2)	12.74 ± 0.13 (n = 2)	0.0295 ± 0.0007 (n = 2)	0.0058 ± 0.0001 (n = 2)
	122	0.2	0.28 ± 0.00 (n = 2)	1.85 ± 0.00 (n = 2)	No data	0.061 ± 0.0001 (n =2)	2.09 ± 0.04 (n = 2)	1.45 ± 0.00 (n = 2)	18.49 ± 0.46 (n = 2)	0.0320 ± 0.0023 (n = 2)	0.0081 ± 0.0002 (n = 2)
	151	0.2	0.43 ± 0.04 (n = 4)	1.73 ± 0.21 (n = 4)	No data	0.060 ± 0.005 (n = 4)	2.08 ± 0.21 (n = 4)	1.36 ± 0.15 (n = 2)	19.05 ± 1.87 (n = 4)	0.0290 ± 0.0055 (n = 4)	0.0074 ± 0.0015 (n = 4)
	183	0.2	0.59 ± 0.05 (n = 2)	1.67	No data	0.060 ± 0.007 (n =2)	1.98 ± 0.16 (n = 2)	1.31 ± 0.10 (n = 2)	25.51 ± 2.33 (n = 2)	0.0325 ± 0.0038 (n = 2)	0.0062 ± 0.0011 (n = 2)
K1	0	0.2	22.97 ± 0.71 (n = 2)	0.44 ± 0.02 (n = 2)	No data	0.600 ± 0.025 (n =2)	2.57 ± 0.09 (n = 2)	4.53 ± 0.10 (n = 2)	9.22 ± 0.12 (n = 2)	0.0089 ± 0.0016 (n = 2)	0.1431 ± 0.0058 (n = 2)
	1	0.2	22.91 ± 0.39 (n = 2)	0.48 ± 0.02 (n = 2)	No data	0.592 ± 0.014 (n =2)	2.54 ± 0.05 (n = 2)	4.49 ± 0.11 (n = 2)	9.60 ± 0.03 (n = 2)	0.0405 ± 0.0035 (n = 2)	0.0378 ± 0.0041 (n = 2)
	3	0.2	19.39 ± 1.29 (n = 4)	0.48 ± 0.32 (n = 4)	No data	0.575 ± 0.041 (n = 2)	2.41 ± 0.21 (n = 4)	4.90 ± 0.43 (n = 2)	9.88 ± 0.85 (n = 4)	0.0960 ± 0.0090 (n = 4)	0.0441 ± 0.0070 (n = 4)
	7	0.2	7.49 ± 0.05 (n = 2)	0.48 ± 0.00 (n = 2)	No data	0.603 ± 0.009 (n =2)	2.53 ± 0.00 (n = 2)	4.40 ± 0.13 (n = 2)	14.65 ± 0.03 (n = 2)	0.1609 ± 0.0040 (n = 2)	0.0445 ± 0.0011 (n = 2)
	22	0.2	0.96 ± 0.01 (n = 2)	0.62 ± 0.03 (n = 2)	No data	0.579 ± 0.014 (n =2)	2.41 ± 0.02 (n = 2)	3.63 ± 0.06 (n = 2)	16.22 ± 0.24 (n = 2)	0.1775 ± 0.0057 (n = 2)	0.0627 ± 0.0008 (n = 2)
	50	0.4	0.23 ± 0.00 (n = 2)	0.76 ± 0.01 (n = 2)	No data	0.548 ± 0.009 (n =2)	2.56 ± 0.07 (n = 2)	3.72 ± 0.09 (n = 2)	20.33 ± 0.45 (n = 2)	0.3419 ± 0.0064 (n = 2)	0.0788 ± 0.0016 (n = 2)
	86	0.2	0.43 ± 0.01 (n = 2)	0.81 ± 0.02 (n = 2)	No data	0.524 ± 0.013 (n =2)	2.58 ± 0.03 (n = 2)	3.66 ± 0.07 (n = 2)	28.55 ± 0.55 (n = 2)	0.3392 ± 0.0002 (n = 2)	0.0797 ± 0.0019 (n = 2)
	110	0.2	0.74 ± 0.02 (n = 2)	0.76 ± 0.00 (n = 2)	No data	0.504 ± 0.001 (n =2)	2.55 ± 0.06 (n = 2)	3.85 ± 0.15 (n = 2)	25.23 ± 0.30 (n = 2)	0.3424 ± 0.0035 (n = 2)	0.0789 ± 0.0014 (n = 2)
	144	0.2	3.07 ± 0.05 (n = 2)	1.50 ± 0.05 (n = 2)	No data	0.489 ± 0.014 (n =2)	2.65 ± 0.11 (n = 2)	4.13 ± 0.14 (n = 2)	21.76 ± 0.20 (n = 2)	0.3675 ± 0.0022 (n = 2)	0.0840 ± 0.0037 (n = 2)
	173	0.2	1.86 ± 0.07 (n = 2)	1.22 ± 0.02 (n = 2)	No data	0.500 ± 0.015 (n =2)	2.75 ± 0.09 (n = 2)	4.41 ± 0.19 (n = 2)	27.90 ± 0.84 (n = 2)	0.3777 ± 0.0120 (n = 2)	0.0878 ± 0.0043 (n = 2)
	205	0.2	4.73 ± 0.16 (n = 2)	1.57 ± 0.33 (n = 2)	No data	0.622 ± 0.167 (n =2)	2.66 ± 0.01 (n = 2)	4.42 ± 0.15 (n = 2)	37.13 ± 1.07 (n = 2)	0.3592 ± 0.0110 (n = 2)	0.0971 ± 0.0008 (n = 2)

APPENDIX B:

DATA NOT USED FOR CHAPTER TWO

Appendix B outlines the methods and data collected for leachable particulate trace metals, cell counts, and 16S rRNA gene analysis. Leachable particulate samples were collected and analyzed for 0.2 – 3.0 and > 3.0 μm particles. However, due to expired hydroxylamine hydrochloride reagent, the recovery was not accurate and is not included in the body of this thesis. The samples for 16S rRNA and cell counts were also collected at selected time points, but have not yet been analyzed as a result of missing T_0 time points, cost, and timing.

Methods

Leachable particulate trace metals

Samples for leachable particulate trace metals were comprised of the 3 μm and 0.2 or 0.4 μm PCTE (Whatman®) filters used for the dissolved trace metal filtering (see Chapter 2 Methods). The filters were folded into $1/8^{th}$ pie shapes in acid-cleaned 1.5 mL snap-cap vials and stored at -20 °C. Labile metals were leached using a previously-described method (Berger et al. 2008). Briefly, 1 mL of a solution of 4.4 M glacial acetic acid (Fisher, TMG) and 0.02 M hydroxylamine hydrochloride (Acros, 99+%) in Milli-Q (> 18.2 MΩ cm) was added to the vials, and filters were leached in a water bath for 10 minutes at 90 ± 5 °C, followed by 110 min at 35 ± 5 °C, as measured by a glass thermometer. The leachate was then transferred to acid-cleaned quartz beakers, filters were quadruple-rinsed with 0.5 mL Milli-Q (> 18.2 MΩ cm), and liquid was evaporated at 120 °C after two 100 μL additions of triple-distilled concentrated HNO_3. The

residue was dissolved in 5% triple-distilled HNO_3 with 10 ppb In and Rh and stored in 8 or 15 mL acid-cleaned LDPE bottles. Each set of leaches (~ 30 samples) was accompanied by a minimum of one 0.2 μm and one 3 μm filter blank, which underwent the identical leaching procedure without any seawater filtered through them.

A Thermo Element XR ICP-MS was used to measure ^{55}Mn, ^{56}Fe, ^{57}Fe, ^{59}Co, ^{60}Ni, ^{63}Cu, ^{65}Zn, ^{110}Cd, ^{111}Cd, and ^{208}Pb as described above for Total dissolved trace metals. Concentrations in the leachate were determined by standard addition: counts normalized to the In internal standard were divided by the elution acid calibration curve. Filter blank concentrations and total nanomoles per filter (Table A1) were averaged for each filter size. Limits of detection in leachates were assessed based on three times the standard deviation of the filter blank concentrations. The initial seawater concentrations were then determined by subtracting the appropriate-size filter blank concentration and dividing the value by the magnitude of concentration determined by the filtered and leached volumes.

Additional biological parameters

Bacterial counts

Unfiltered seawater was collected in 3 mL cryovials, fixed with a 25% gluteraldehyde solution (60 μL each), flash-frozen, and stored at -80 °C.

Bacterial diversity

Samples for 16S rRNA gene sequencing were collected onto 3 and 0.2 μm PCTE filters by vacuum filtration. The filters were saved in 3 mL cryovials, flash-frozen, and stored at -80 °C.

Results

Results for leachable particulate trace metals below. No results have been obtained yet for the bacterial samples.

Table S5. Leachable particulate trace metal averages and standard deviations for 0.2 µm and 3 µm filter blanks. Total nmol/filter or pmol/filter was determined by converting the measured concentration to total nmol or pmol in the leachate.

	Mn (nmol)	Fe (nmol)	Co (pmol)	Ni (nmol)	Cu (nmol)	Zn (nmol)	Cd (pmol)	Pb (pmol)
Filter blank, 3 µm	0.0015 ± 0.0004 (n=15)	0.09 ± 0.05 (n = 15)	0.2 ± 0.2 (n = 15)	0.021 ± 0.009 (n = 15)	0.005 ± 0.001 (n = 14)	0.19 ± 0.04 (n = 15)	0.03 ± 0.03 (n = 15)	0.33 ± 0.09 (n = 15)
Filter blank, 0.2 µm	0.0016 ± 0.0004 (n = 15)	0.06 ± 0.02 (n = 15)	0.19 ± 0.07 (n = 15)	0.013 ± 0.004 (n = 15)	0.005 ± 0.002 (n = 15)	0.15 ± 0.04 (n = 15)	0.06 ± 0.08 (n = 15)	0.4 ± 0.3 (n = 14)

Table S6. Small and large leachable particulate fractions of manganese (Mn), iron (Fe), cobalt (Co), nickel (Ni), copper (Cu), zinc (Zn), cadmium (Cd), and lead (Pb) (nM) over time for mixed assemblages (M1, M2, M3) and monocultures of *Pseudo-nitzschia dolorosa* (P1) and *Karenia brevis* (K1). Day zero represents the start of regeneration; grow-out days for M1, M2, and M3 are indicated by negative time values. Small and large leachable fractions were operationally defined as being 0.2– or 0.4 – 3 µm and > 3 µm, respectively, as specified. ^{57}Fe was calculated by subtracting 2.119% natural abundance ^{57}Fe present in Fe measurement. If Fe was below the limit of detection (< LOD), no subtraction was performed. No data indicates that no data were taken. Samples < LOD are represented by an asterisk (*).

	Time, days	Filter size, µm	Mn, nM	Fe, nM	^{57}Fe, nM	Co, nM	Ni, nM	Cu, nM	Zn, nM	Cd, nM	Pb, nM
M1	-13	0.2	0.0327	0.65	No data	0.0003	0.002	0.011	-0.02	0.4749	1.8771
	0	0.2	0.1517	0.25	No data	0.0005	0.007	0.007	*	0.5660	1.5049
	0	0.2	0.0884	0.11	No data	0.0004	0.002	0.005	*	0.6458	1.2975
	1	0.2	0.0376	0.10	No data	0.0008	0.016	0.018	0.08	0.5311	*
	3	0.2	0.0259	0.08	No data	0.0006	0.013	0.012	0.00	0.2632	*
	6	0.2	0.0081	0.06	No data	0.0003	-0.003	0.011	0.05	0.5819	*
	21	0.2	0.0733	0.17	No data	0.0007	0.019	0.027	0.09	*	*
	54	0.2	0.0979	0.05	No data	0.0005	0.005	0.008	-0.01	0.4845	1.7648
	85	0.2	0.0334	0.03	No data	0.0001	0.008	0.007	0.30	*	*

	116	0.2	0.0425	1.38	No data	0.0062	0.181	0.016	0.19	0.5020	1.7779
	148	0.2	0.0331	1.51	No data	0.0034	0.082	0.065	0.14	*	6.2937
	174	0.2	0.0047	1.18	No data	-0.0001	*	0.069	*	*	*
M2	-14	3	1.6154	15.23	1.17	0.0085	*	0.062	5.03	0.0042	0.0189
	0	3	2.4270	1.90	0.37	0.0109	0.049	0.084	3.29	0.0256	0.0075
	1	3	0.1705	*	0.07	*	*	0.023	0.24	0.0018	*
	3	3	5.5101	16.90	1.81	0.0206	0.164	0.165	5.34	0.0328	0.0170
	7	3	10.4874	29.14	3.27	0.0233	0.291	0.213	6.30	0.0213	0.0294
	20	3	1.3613	2.54	0.39	0.0029	*	0.102	0.86	0.0020	0.0025
	40	3	0.5635	1.39	0.20	0.0015	*	0.041	0.29	0.0015	0.0008
	68	3	0.2922	0.89	0.14	0.0015	*	0.060	0.46	0.0012	0.0002
	97	3	0.1680	*	0.08	*	*	0.019	1.73	0.0008	0.0001
	124	3	0.5491	1.89	0.24	0.0021	*	0.045	1.41	0.0016	0.0044
M2	-14	0.4	0.5562	2.75	0.50	0.0011	*	0.021	0.01	0.0018	0.0027
	0	0.4	0.0596	0.08	0.04	0.0010	*	0.009	0.17	0.0012	*
	1	0.4	6.7813	15.74	2.20	0.0302	0.245	0.286	6.79	0.0501	0.0214
	3	0.4	0.6545	0.47	0.08	0.0012	*	0.024	0.12	0.0024	*
	7	0.2	0.2228	0.35	0.07	0.0010	*	*	1.50	0.0010	*
	20	0.2	0.0569	2.45	0.08	0.0016	*	0.021	0.12	*	*
	40	0.2	0.0398	0.27	0.07	0.0008	*	0.035	0.14	*	*
	68	0.2	0.0239	0.14	0.05	0.0004	*	0.016	0.08	0.0008	*
	97	0.2	0.0219	*	0.03	*	*	*	0.24	0.0013	*
	124	0.2	0.0319	*	0.02	0.0007	*	0.161	0.30	0.0021	*
M3	-14	3	0.8491	7.65	0.64	0.0041	*	0.027	0.36	0.0036	0.0081
	0	3	5.3201	3.05	0.61	0.0174	0.052	0.254	1.27	0.0367	0.0125
	1	3	3.9569	2.46	0.54	0.0169	*	0.253	1.40	0.0342	0.0128
	3	3	0.6939	0.77	0.19	0.0055	*	0.056	1.10	0.0046	0.0013
	7	3	0.3505	0.60	0.22	*	*	0.027	0.21	0.0031	*
	7	3	1.8922	1.31	0.26	0.0038	*	0.075	0.93	0.0100	0.0028
	20	3	1.9377	1.19	0.26	0.0020	*	0.057	0.17	0.0048	0.0015
	40	3	0.4979	0.95	0.10	0.0020	*	0.030	0.22	0.0027	0.0003
	68	3	1.1951	2.47	0.46	*	*	0.073	0.03	0.0023	0.0010
	97	3	0.5686	1.69	0.29	*	*	0.041	0.60	0.0025	0.0016
	124	3	0.5378	2.19	0.32	0.0013	*	0.019	0.94	0.0017	0.0012
M3	-14	0.4	1.4006	21.56	1.15	0.0114	0.022	0.080	2.06	0.0031	0.0193
	0	0.4	0.1363	0.13	0.05	0.0015	*	0.021	0.18	0.0013	0.0039
	1	0.4	0.2754	5.58	0.07	0.0029	*	0.102	2.46	0.0015	*
	3	0.4	0.0783	0.28	0.06	0.0008	*	0.014	0.18	0.0006	*
	7	0.4	0.1328	0.40	0.07	0.0020	*	0.027	0.13	*	*
	7	0.2	0.1594	0.29	0.08	0.0010	*	0.027	0.23	0.0012	*
	20	0.2	0.0628	*	0.03	0.0012	*	*	0.29	0.0010	*
	40	0.2	0.0165	*	0.01	0.0010	*	0.015	0.44	0.0009	*
	68	0.2	0.1325	*	0.04	0.0005	*	*	0.41	0.0042	*
	97	0.2	0.1610	0.08	0.05	0.0006	*	*	0.20	0.0147	*

	124	0.2	0.1678	0.27	0.07	0.0008	*	0.014	0.63	0.0047	*
P1	0	3	0.7089	108.51	No data	0.0093	*	0.178	0.65	0.0010	0.0080
	0	3	0.7411	116.53	No data	0.0096	*	0.164	0.35	0.0011	0.0064
	1	3	0.5310	94.81	No data	0.0073	*	0.196	1.33	0.0022	0.0088
	4	3	0.2914	62.88	No data	0.0043	*	0.148	1.02	0.0025	0.0147
	8	3	0.1494	54.81	No data	0.0021	*	0.087	0.25	0.0003	0.0048
	20	3	0.1776	54.85	No data	0.0017	*	0.084	0.48	0.0004	0.0045
	64	3	1.6605	3.81	No data	0.0034	*	0.066	0.06	0.0003	0.0021
	89	3	0.7105	1.82	No data	0.0037	*	0.142	-0.09	0.0003	0.0006
	122	3	0.4606	5.71	No data	0.0018	*	0.039	0.06	0.0002	0.0013
	151	3	0.2617	14.78	No data	0.0011	*	0.037	0.29	0.0007	0.0026
P1 and K1 matrix	N/A	3	0.8066	0.19	No data	0.0075	*	0.059	0.66	0.0007	0.0002
	NA	0.2	0.0572	*	No data	0.0003	*	0.017	*	*	*
P1	0	0.2	0.0086	1.05	No data	0.0001	*	0.237	-0.02	*	*
	0	0.2	0.0186	1.83	No data	0.0002	*	0.093	0.19	*	*
	1	0.2	0.0182	2.86	No data	0.0002	*	0.089	0.29	*	0.0082
	4	0.2	0.0227	2.85	No data	0.0010	0.004	0.083	0.13	*	*
	8	0.2	0.0195	2.18	No data	0.0003	*	0.064	0.45	*	*
	20	0.2	0.0516	1.26	No data	0.0006	*	0.056	0.16	0.0012	*
	64	0.2	0.1432	0.54	No data	0.0015	*	0.032	0.57	*	*
	89	0.2	0.0857	0.13	No data	0.0006	*	*	0.86	*	*
	122	0.2	0.0713	0.42	No data	0.0004	*	0.028	0.55	*	*
	151	0.2	0.0241	0.16	No data	0.0002	*	0.019	0.42	*	*
K1	0	3	0.4914	*	No data	0.0040	*	0.032	0.19	0.0004	0.0005
	1	3	0.6145	*	No data	0.0048	*	0.048	0.18	0.0022	*
	3	3	1.8662	*	No data	0.0057	*	0.049	0.21	0.0017	0.0007
	7	3	9.0984	*	No data	0.0097	*	0.133	0.01	0.0102	0.0015
	22	3	0.6928	*	No data	0.0034	*	0.095	0.01	0.0034	-0.0002
	50	3	1.0048	*	No data	0.0081	*	0.048	0.77	0.0015	-0.0003
	86	3	0.2254	*	No data	0.0020	*	0.036	-0.04	0.0009	0.0001
	110	3	0.1875	*	No data	0.0024	*	0.038	3.19	0.0017	-0.0002
	144	3	0.7603	*	No data	0.0015	*	0.040	-0.23	0.0007	0.0005
	173	3	1.0956	1.97	No data	0.0027	*	0.033	0.60	0.0005	0.0011
K1	0	0.2	0.3936	0.34	No data	0.0029	*	0.060	0.17	*	*
	1	0.2	0.3239	0.66	No data	0.0016	*	0.032	-0.10	*	*
	3	0.2	0.3784	0.05	No data	0.0021	*	0.055	2.05	0.0020	*
	7	0.2	1.5164	*	No data	0.0031	*	0.120	0.95	0.0036	*
	22	0.2	6.6075	0.42	No data	0.0153	*	0.123	1.50	0.0017	*
	50	0.4	0.1296	*	No data	0.0040	*	0.087	0.37	*	*
	86	0.2	0.2909	0.39	No data	0.0017	*	0.104	0.60	0.0010	*
	110	0.2	0.0657	1.11	No data	0.0024	*	0.098	1.38	0.0014	*
	144	0.2	0.2345	*	No data	0.0004	*	0.044	1.24	*	*
	173	0.2	0.7962	*	No data	0.0021	*	0.039	0.41	;*	*

APPENDIX C:

FAIR USE WORKSHEETS

Appendix C explains how figures 1.1, 1.2, and 1.3 fall under Fair Use.

INSTRUCTIONS

Check all boxes that apply, and keep a copy of this form for your records. If you have questions, please contact the USF General Counsel or your USF Tampa Library Copyright Librarian.

Name: Adrienne Hollister Date: 3-27-19

Class or Project: Master's Thesis

Title of Copyrighted Work: (1) Morel and Price, 2003. (2) Sunda, 2012. (3) Von Brand et al, 1937.

Note: Three works were used. The answers are the same for all.

PURPOSE AND CHARACTER OF THE USE

Likely Supports Fair Use	Likely Does Not Support Fair Use
■ Educational ☐ Teaching (including multiple copies for classroom use) ■ Research or Scholarship ☐ Criticism, Parody, News Reporting or Comment ☐ Transformative Use (your new work relies on and adds new expression, meaning, or message to the original work) ☐ Restricted Access (to students or other appropriate group) ☐ Nonprofit	☐ Commercial ☐ Entertainment ☐ Bad-faith behavior ☐ Denying credit to original author ☐ Non-transformative or exact copy ☐ Made accessible on Web or to public ☐ Profit-generating use

Overall, the purpose and character of your use ■supports fair use or ☐does not support fair use.

NATURE OF THE COPYRIGHTED MATERIAL

Likely Supports Fair Use	Likely Does Not Support Fair Use
■ Factual or nonfiction ■ Important to favored educational objectives ■ Published work	☐ Creative or fiction ☐ Consumable (workbooks, tests) ☐ Unpublished

Overall, the nature of the copyrighted material ■supports fair use or ☐does not support fair use.

AMOUNT AND SUBSTANTIALITY OF MATERIAL USED IN RELATION TO WHOLE

Likely Supports Fair Use	Likely Does Not Support Fair Use
■ Small amount (using only the amount necessary to accomplish the purpose) ☐ Amount is important to favored socially beneficial objective (i.e. educational objectives) ☐Lower quality from original (ex. Lower resolution or bitrate photos, video, and audio)	☐ Large portion or whole work ☐ Portion used is qualitatively substantial (i.e. it is the 'heart of the work') ☐Similar or exact quality of original work

Overall, the amount and substantiality of material used in relation to the whole ■supports fair use or ☐does not support fair use.

EFFECT ON THE MARKET FOR ORIGINAL

Likely Supports Fair Use	Likely Does Not Support Fair Use
■ No significant effect on the market or potential market for the original ☐ No similar product marketed by the copyright holder ☐ You own a lawfully acquired copy of the material ☐ The copyright holder is unidentifiable ☐ Lack of licensing mechanism for the material	☐ Replaces sale of copyrighted work ☐ Significantly impairs market or potential market for the work ☐ Numerous copies or repeated, long-term use ☐ Made accessible on Web or to public ☐ Affordable and reasonably available permissions or licensing

Overall, the effect on the market for the original ■supports fair use or ☐does not support fair use.

CONCLUSION

The combined purpose and character of the use, nature of the copyrighted material, amount and substantiality of material used in relation to the whole and the effect on the market for the original

■likely supports fair use or ☐likely does not support fair use.

Note: Should your use of copyrighted material not support fair use, you may still be able to locate and request permissions from the copyright holder. For help on this, please feel free to contact your Copyright Librarian.

This worksheet has been adapted from:

Cornell University's Checklist for Conducting A Fair use Analysis Before Using Copyrighted Materials: https://copyright.cornell.edu/policies/docs/Fair_Use_Checklist.pdf

Crews, Kenneth D. (2008) Fair use Checklist. Columbia University Libraries Copyright Advisory Office. http://copyright.columbia.edu/copyright/files/2009/10/fairusechecklist.pdf

Smith, Kevin; Macklin, Lisa A.; Gilliland, Anne. A Framework for Analyzing any Copyright Problem. Retrieved from: https://d396qusza40orc.cloudfront.net/cfel/Reading%20Docs/A%20Framework%20for%20Analyzing%20any%20Copyright%20Problem.pdf

LeEtta Schmidt, lmschmidt@usf.edu and Drew Smith dsmith@usf.edu
Reviewed by USF General Counsel 08/11/2015